



VILNIUS UNIVERSITY
LIFE SCIENCES CENTER

Karolina Limanovskaja

Rapid Manufacturing of 3D Organoid Scaffolds Using Femtosecond Laser

Master's thesis

Molecular biotechnology study program

Thesis supervisor

Dr. Linas Jonušauskas

Thesis completed at

UAB, Vital3D Technologies

Vilnius 2024

Table of Contents

Introduction	3
1. Literature review.....	5
1.1. Challenges of bioprinted organs	5
1.2. 2D and 3D cell cultures	6
1.3. Organoids.....	11
1.4. Additive biofabrication	12
1.5. 2 photon polymerization	14
1.6. Towards beam shaping solutions	18
2. Materials and Methods.....	22
2.1. Phase mask generation.....	22
2.2. Z-scan setup	23
2.3. 2PP 3D Printing setup	24
2.4. 3D structure printing, development and characterization	24
2.5. 3D structure characterization	26
2.6. Data Analysis	28
3. Results	29
3.1. Phase mask width correlation with the polymerized area of material.....	29
3.2. Intensity distribution analysis and optimisation	30
3.3. Microstructure fabrication.....	32
3.4. Voxel characterization with 2PP	33
3.4.1. 1 px phase mask.....	34
3.4.2. 10 px phase mask.....	35
3.4.3. 50 px phase mask.....	36
3.4.4. 100 px phase mask.....	37
3.4.5. 200 px phase mask.....	38
3.5. Scaffold printing for cell seeding	39
4. Discussion.....	40
Conclusions	48
Supplementary.....	49
References	50
Abstract (in English).....	83
Abstract (in Lithuanian).....	84
Author's personal contribution.....	85

Introduction

Global demand for transplantable tissues and organs puts a heavy strain on the medical system as the demand greatly outweighs the supply. Roughly 17 people die every day waiting for an organ, graft or tissue, even in countries with donation programs (*Organ Donation Statistics | Organdonor.Gov*, 2024). Faced with this deficit, the potential of 3D bioprinted organs has taken the spotlight as a possible way of resolving this problem (A. Lee et al., 2019). First through organoid-based disease models to push more extensive treatment option development and knowledge about organ development and, ultimately moving toward fully functional bioprinted organs and tissues (Y. S. Zhang et al., 2016; Urciuolo et al., 2023). 3D cell culture development presents itself as a first step in understanding the necessary steps in the workflow leading to how bionic tissues and organs should be produced (Fu et al., 2023).

Currently cellular scaffolds are considered as invaluable tools in 3D culture engineering and development by providing a micro-environment that mimics natural physiology, facilitates cell adhesion, migration, differentiation and long-term viability (Martínez-Espuga et al., 2023). Biofabrication can be used in manufacturing cellular scaffolds by printing various biocompatible or biomimetic materials (Levato et al., 2021). Later this can transition to bioprinting by mixing cells into the printing process. However, most manufacturing methods struggle to deliver scaffolds that are simultaneously biomimetic, reproducible and clinically scalable. Hydrogel suspensions are highly cytocompatible but lack porosity and mechanical strength (Marks et al., 2012). Electrospun meshes achieve nanofiber architecture but suffer from solvent toxicity and poor mass transport (Wilson et al., 2022). Stereolithography, which offers layer-by-layer fabrication, can pattern centimeter-scale objects, though falling short at resolution, barely achieving 10 μm and having long print times. Extrusion bioprinting, while versatile, exposes cells to severe shear and thermal stresses, limiting viability and structural fidelity (Kumar & Kim, 2020).

2 photon polymerization (2PP) offers a different approach to biofabrication and bioprinting. Non-linear absorption at the focal point of a sharp focusing lens confines polymer cross-linking to a voxel smaller than the diffraction limit, enabling free-form architectures with sub-micrometer features (Jonušauskas et al., 2018; Ežerskytė et al., 2022). Crucially, as a nozzle-free process 2PP has the potential to eliminate the mechanical and chemical stressors, which inherently would boost biocompatibility and adaptability of this technology. Additionally, 2PP uses either visible or infrared radiation, also eliminating UV-related damage to cell DNA. Together with integrated spatial light modulation (SLM) 2PP becomes a highly tunable tool for rapid manufacturing of various biocompatible constructs (Vitkūnaitė et al., 2024). Among numerous ways to improve the throughput of the 2PP recently proposed horizontal voxel

elongation seems to strike the best balance between simplicity, applicability and flexibility, especially in the context of the biological applications.

The key for SLM operation is what is called a phase mask. The phase mask is normally a gray-scale image where shades of grey denote how much the phase of the incident light will be retarded. Then, after the phase is modulated, the wavefront would diffract in a way to create the desired intensity distribution in the far field (i.e. infinitely far away) or in the focal plane of the focusing optic (Shirshneva-Vashchenko et al., 2023). Overall, phase mask generation is a rather complicated process. At its simplest level it can be imagined as a two-dimensional Fourier transform. Because of that, only a limited amount of the most basic intensity distributions can be calculated deterministically. For anything more advanced or proprietary Gerchberg-Saxton algorithm is used. The main issue with it is that in its basic form, it does not account for intensity distribution before and after the focal plane. Additionally, because it is an iterative approximate calculation method, the precision of the intensity distribution calculations depends on the number of iterations.

So far, for uses in 2PP phase masks are generated using software provided by the vendor of SLM (HOLOEYE). While it generally works, it is a “black box” solution with unclear tunability potential. Therefore, before developing more sophisticated solutions for phase mask generation, we need more understanding of what exactly can be achieved using current software and what are the primary limitations. This thesis situates itself at the intersection of laser physics, materials science and regenerative biology to demonstrate how 2PP with integrated SLM can be used in rapid manufacturing. There are two main lines of work in this study: experimental investigation of intensity distributions with the Z-scan and application of acquired best phase masks for 3D printing.

The aim of this study is to analyze the current capabilities and limitations of phase mask generation while using the “HOLOEYE” software and use the best performing for 3D organoid scaffold printing. Therefore, the tasks are approached as follows:

- 1) Test how intensity distribution depends on the width of the line in the initial image from which the horizontally elongated voxel is generated. Measure it along the optical axis.
- 2) Characterize voxel parameters after applying the generated phase masks for 2PP printing.
- 3) Use generated phase masks for organoid scaffold printing.

1. Literature review

1.1. Challenges of bioprinted organs

The first successfully transplanted organ was the kidney. The surgery took place in 1959 in United States of America, Louisiana. The case marked the first successful transplant between individuals who were not genetically identical. The donor and recipient were fraternal twin brothers (Murray et al., 1962). The early days of transplantation focused on kidneys. However by the late 1960s and early 1970s organs like liver, heart and lungs were successfully transplanted (Hardy et al., 1964; Barnard, 1967; Starzl & Demetris, 1990). As the transplantation procedure was being researched and applied as a lifesaving treatment option, doctors faced many challenges from understanding how the immune system influences the procedure by navigating the way of organ collection and donation. Despite the continues development of organ transplantation methodology there's still an array of challenges that hinder further progress, viable donor shortage being one of them. Roughly 17 people die every day from a lack of organs for transplantation (*Organ Donation Statistics* | *Organdonor.Gov*, 2024).

To battle the constant challenge of organ shortage, tissue regeneration as well as bioprinting begin to emerge. 3D bioprinting describes a process in which cells are combined with other biomaterials as printing inks and used to print complex 3D structures that would recreate the biological function of *in vivo* tissues (A. Lee et al., 2019). The main goal of developing 3D printing technology in organ reconstruction is to print fully functional bionic tissues in the direction of multi-organ reconstruction. Significant progress has been made in recent years achieving printing with live cells (S. H. Lee et al., 2023). However, there are still many challenges present when moving towards printing fully functional organs. Many technologies although showing promising results in initial studies do not provide longevity in their bioprinted tissues whether due to low cell viability caused by a stressful printing process, usage of harmful solvents in bioinks or the dependance of the printing process on UV light which is a direct carcinogen (Moncal et al., 2019; Z. Zheng et al., 2021). Currently no technology has been able to demonstrate the printing of a fully functional solid organ that would be usable for tissue reconstruction or transplantation. On the other hand, the emergence of 3D printed skin grafts (Fu et al., 2023), miniature liver (Jaksa et al., 2023) and heart models (Y. S. Zhang et al., 2016) confirm the possibility of 3D printed organs while pioneering the field of bioprinting.

In order to move forward in this field challenges like vascularization, multi-tissue printing, overall printing throughput, cellular viability, immune response and mechanical tissue structure engineering need to be resolved. 3D cell culture engineering poses itself as a starting step in 3D bioprinting. Structures like

organoids and spheroids provide valuable insight on cell differentiation, proliferation, viability and generally what is needed for further tissue maturation and development (Mun et al., 2019; Rolver et al., 2019; Urciuolo et al., 2023). It is crucial to understand cellular behavior when modeling the bioprinting process as it ensures that the developed technology can be aligned with the specific needs of printed organs.

1.2. 2D and 3D cell cultures

In the past most studies on cellular behaviors in mammalian cells were either carried out *in vivo*, in mice or *in vitro* within two-dimensional (2D) cell cultures (Rederer et al., 2023). Response to different stimuli, gene expression or biochemical signaling pathways are a few examples of topics that 2D cell cultures were used to research (Saleem et al., 2002). For these studies cells were grown in 2D and attached to polystyrene utensils or flat adherent surfaces (Kleinman et al., 2003; Ishiguro et al., 2023). During the attachment process cells would form monolayer aggregates which then would be studied under varying conditions. Historically, this type of system has been used by scientists since the early 1900s, specifically in co-culturing of cellular heterogeneity and in oncological research in order to evaluate the efficacy of chemical compounds (Habanjar et al., 2021). Despite the advantages of mouse models and 2D cell cultures used in research, both systems presented significant shortcomings when it came to working with them. Maintenance of transgenic mouse models and *in vivo* studies have high costs, are time consuming and present an array of ethical issues within their usage. At the same time conventional two-dimensional, *in vitro*, cell cultures are well established, cost effective and much easier to handle (Rederer et al., 2023). Unfortunately, 2D cell culture models cannot reproduce the necessary cellular microenvironment that is needed for tissue formation including intra- and cell-cell interactions with different communication pathways. This in turn causes results gathered from working with 2D cell cultures to be less translatable when working on drug response studies, disease modelling or cellular behavior research (Vidyasekar et al., 2016; Lin et al., 2020; Martínez-Espuga et al., 2023; Rederer et al., 2023). Additionally due to characteristics of 2D cell culture environment it has been observed that cell proliferation and differentiation is also affected, further distorted the generated structures characteristics when compared to natural tissues (Duval et al., 2017; Jeibouei et al., 2022; Salinas Vera et al., 2022; Vitkūnaitė et al., 2024).

Evidently three-dimensional (3D) cell culture models are more physiologically relevant than 2D cell models (Mun et al., 2019; Kerslake et al., 2023). 3D cell models revolutionized research, allowing the creation of an *in vivo*-like tissues using an *in vitro* environment, which is more complex and physiologically relevant than traditional monolayer cultures (Table 1) (Kerslake et al., 2023). The

development of organoid and spheroid models capable of long-term expansion with competent tissue functionality may provide a versatile and valuable platform for physiologically and pathologically relevant tissue studies (Mun et al., 2019).

Table 1 Differences between 2D and 3D cell culture systems (Kerslake et al., 2023).

2D Cell culture	3D Cell culture
Cells grown in monolayers – biologically simple	Cells form differentiated aggregates, spheroids, or organoids – biologically complex
Gene and protein expression differ in vivo	Gene expression closely mimics in-vivo
Uniform exposure to chemical stimuli; drugs often appear effective	Nonuniform growth results in toxicity profiles and diffusion gradients closely related to in vivo
Long-term cell cultures can develop genetic drift	Growth is typically short-term, minimizing genetic drift
Oxygen diffusion is uniform and higher than many in vivo structures, thus augmenting mitochondrial function and reactive oxygen production	Oxygen distribution varies and hypoxic cores are evident, mimicking in vivo variations of many complexes
Cheaper, less complex and easily recapitulated in lab	Required additional nutrients, biological scaffolding, are more expensive and time consuming
Established protocols	Limited established protocols

3D cell cultures can be divided into scaffold-based and scaffold-free systems. Usually scaffold-free approaches include hanging drop cultures, liquid suspensions, usage of non-adhesive wells, rotating well vessels or magnetic levitation (Boyer et al., 2018; Vu et al., 2021). The mentioned methodologies usually result in cell culture forming spherical aggregates also called spheroids or organoids depending on the properties of the cell culture. The main characteristic differentiating organoids from spheroids in 3D cell cultures is the differentiation properties of the used cell lines (Wehrli et al., 2024). Cell aggregates that are formed from a single cell line, especially immortalized or cancer cell lines are called spheroids. Meanwhile organoids are generated from stem cells or primary cells isolated from specific tissue. Mature organoids consist of several cell types (Bonanini et al., 2022). Scaffold-free 3D cell culture models offer significant advantages and are generally better suited for research than 2D cell cultures (Mun et al., 2019).

However, challenges related to size, shape and integrity arise when forming scaffold-free cell cultures. Additionally, the extracellular matrix (ECM), which is crucial for cell aggregate formation, in scaffold-free spheroid models is influenced by different cell lines and outside stimuli that occurs as

numerous variations of cell culture generation protocols (Figure 1) (Dissanayaka et al., 2014). Therefore, there are noticeable differences when comparing generated cultures as it is difficult to maintain stable, unchanging conditions (de Araújo et al., 2024). Additional shortcomings of scaffold-free cell culture include: the time-consuming protocols of spheroid generation and harvest; lack of control over size, shape, and cell density; low-throughput type assays; the requirement for special equipment; the need to transfer the generated co-culture into specific environments dependent on assays (Lin et al., 2020). The need for transferring of the generated co-cultures especially disrupts spheroid or organoid generation as cell cultures become prone to the loss of integrity. This especially applies to cells that have poor cell-cell adhesion (Berens et al., 2015; Shoval et al., 2017). Such drawbacks need to be addressed to achieve more uniform cellular structures that bring researchers even closer to true tissue models (Figure 1).

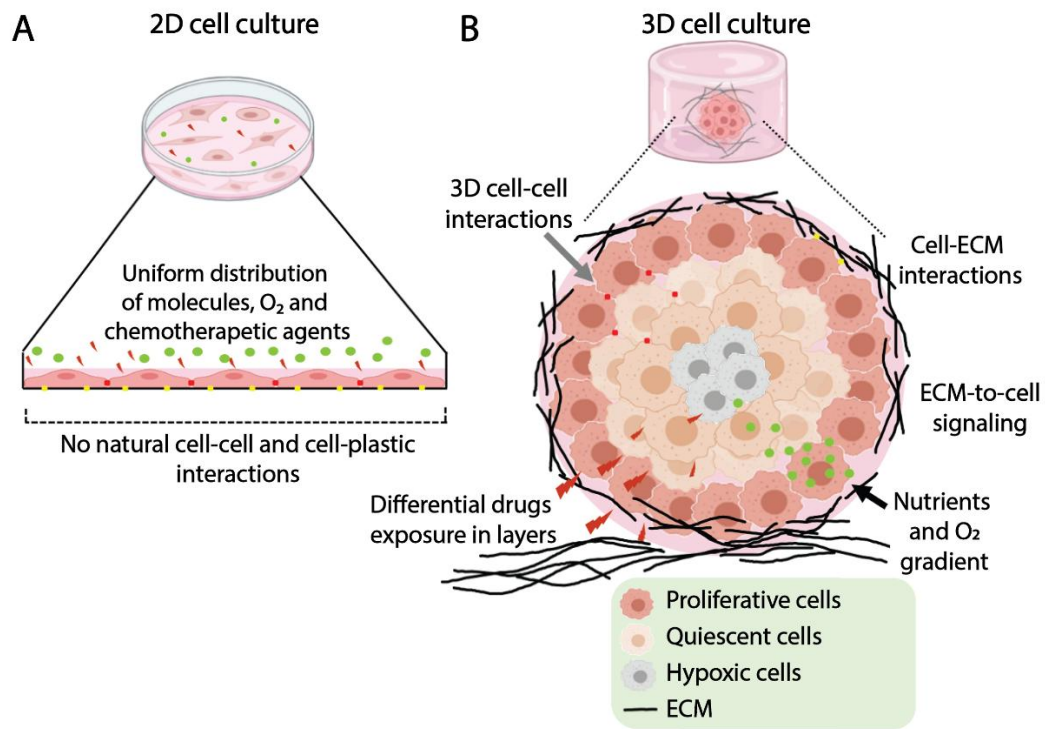


Figure 1 Illustration represents the main differences between 2D and 3D cell cultures. A - 2D cell cultures where cells are grown in a mono layer. B - 3D cell culture where cells aggregate into an organoid with multiple outside factors influencing the culture development. Proliferative cells – cells that are actively going through cell division. Quiescent cells - cells that have stepped out of the active cell. Hypoxic cells – cells that are experiencing oxygen concentrations below the level they normally need for optimal metabolism and survival. ECM - extracellular matrix. (Salinas Vera et al., 2022).

Multiple studies emphasize the importance of cell microenvironment for maintaining and regulating essential cell behaviors like stemness, differentiation and migration by providing support which has a significant effect on gene expression (Fanhchaksai et al., 2016; Cheng et al., 2024; Havel &

Griswold, 2024). The integration of a supportive structure, like a scaffold, creates a necessary environment for 3D cellular attachment, proliferation and differentiation as it closely mimics the extracellular environment of live tissues. Scaffolds provide a role of mimicking tissue-tissue, cell-cell or cell-ECM interactions and chemical gradients that are normally present within a living system (Campuzano & Pelling, 2019). Additionally, scaffolds can be covered with bioactive compounds, regulating the cellular behavior, as well as having biodegradable properties meaning that the protein polymers would be absorbed by the body over time allowing for tissue remodeling and integration (Colangelo et al., 2020; Dong et al., 2022). This property not only allows for the development of accurate cell culture but also creates an opportunity to use cellular scaffolds for live tissue regeneration *in vivo*. Depending on the used scaffold material the structure provides benefits like customizability allowing precise control over scaffold properties tailoring them specifically for the used cell culture, consistency in shape and stability, porosity and permeability, biocompatibility overall preserving tissue specific characteristics (Abdul Samat et al., 2023). Materials used for scaffold generation can be generally classified into natural or synthetic later branching out into groups like polymers, hydrogels, decellularized tissue and hybrid organic-inorganic polymers (Sokocevic et al., 2013; Hendrikx et al., 2016; J. Zhang et al., 2022). Materials like cellulose, chitin/chitosan, alginate, recombinant silk, polylactic acid (PLA), polycaprolactone (PCL), provide low costs, consistent and tunable scaffolds which can be applied for cell culture generation (Colangelo et al., 2020; P. Li et al., 2021; X. Liu et al., 2023; Suryavanshi et al., 2023). However, with many advantages there are a number of disadvantages usually related to the scaffold material and its fabrication process (Table 2).

Table 2 Different types of 3D scaffolds typically used for cell culture generation. Table adapted from Habanjar et al., 2021.

3D Scaffold Fabrication Method	Scaffold Properties	Advantages	Disadvantages
Suspended Hydrogel Solution (Marks et al., 2012; Habanjar et al., 2021; Nerger et al., 2024)	A dense network of fibers suspended in a chemical solution. Properties of fibers heavily depend on the manufacturing process.	Easily accessible and applicable. High levels of cell viability. Well established user protocols.	Not porous. High risk of poor cell and nutrient distribution. Poorly controlled architecture – low reproducibility. Poor mechanical properties.

Continuation of Table 3 Different types of 3D scaffolds typically used for cell culture generation. Table adapted from Habanjar et al., 2021.

3D Scaffold Fabrication Method	Scaffold Properties	Advantages	Disadvantages
Electrospinning (W. Liu et al., 2016; Wilson et al., 2022; Piscitelli et al., 2024)	Dense and tight array of fibers, nano – micro scale. Generated by applying a high-voltage electric field which causes an eruption of the polymer from the tip of the needle. During the process the solvent evaporated leaving a dried-fiber scaffold.	Wide range of achievable size/diameter in architecture. High cell viability.	Requirement for harmful solvents. High price of solvents. Dence fiber networks cause poor cell and nutrient distribution. Variability in architecture batch to batch – low reproducibility.
Lyophilization (Habanjar et al., 2021; Anderson & Segura, 2022)	Homogenous suspension of collagen with acid. Developed through heat treatment for the sublimation of ice crystals under vacuum to the defined freezing point before returning to 0 °C.	Wide generation range in terms of pore sizes. Highly porous. Inexpensive. High cell viability.	Difficult freezing process. High variability in architecture batch to batch – low reproducibility. Poor mechanical properties.
Stereolithography (Zhu et al., 2016; Kumar & Kim, 2020)	Printed layer-by-layer, usually from a UV curable material.	Capable of producing scaffolds mm - cm in size. Highly reproducible. It can be combined with hydrogels or electrospinning. High cell differentiation rate and adhesion. Imitation of complex in vivo architecture.	High cost. Low resolution. Slow process.

Engineering of 3D cell cultures depends on a few points: specific properties of the cell, 3D microenvironment imitating the natural ECM, scaffold-based biomaterials, signaling molecules and cell culture that can support tissue development (Kerslake et al., 2023). To create a platform that would allow us to generate reproducible tissue models suited for disease modeling, drug testing and fundamental research it is essential to optimize as many components as possible. Currently there are little to no

technical options to generate nearly identical scaffolds perfectly tailored for cell growth. Nevertheless, by evolving the currently present stereolithography scaffold generation process we can move close to being able to efficiently generate perfectly optimized constructs specifically tailored for 3D cell culture generation.

1.3. Organoids

Organoids are defined as 3D cell cultures that are grown *in vitro* from various cell sources including: adult stem cells (ASCs), collected directly from biopsies of different tissues, pluripotent stem cells (PSCs) like embryonic (ESCs) or induced (iPSC) stem cells obtained by reprogramming differentiated cells (S. Wang et al., 2019; Silva et al., 2021; Geurts et al., 2023). Placed in an *in vitro* environment the mentioned cells tend to self-organize and differentiate into functional cell types, mimicking the structures and functions of an organ *in vitro* (Figure 2).

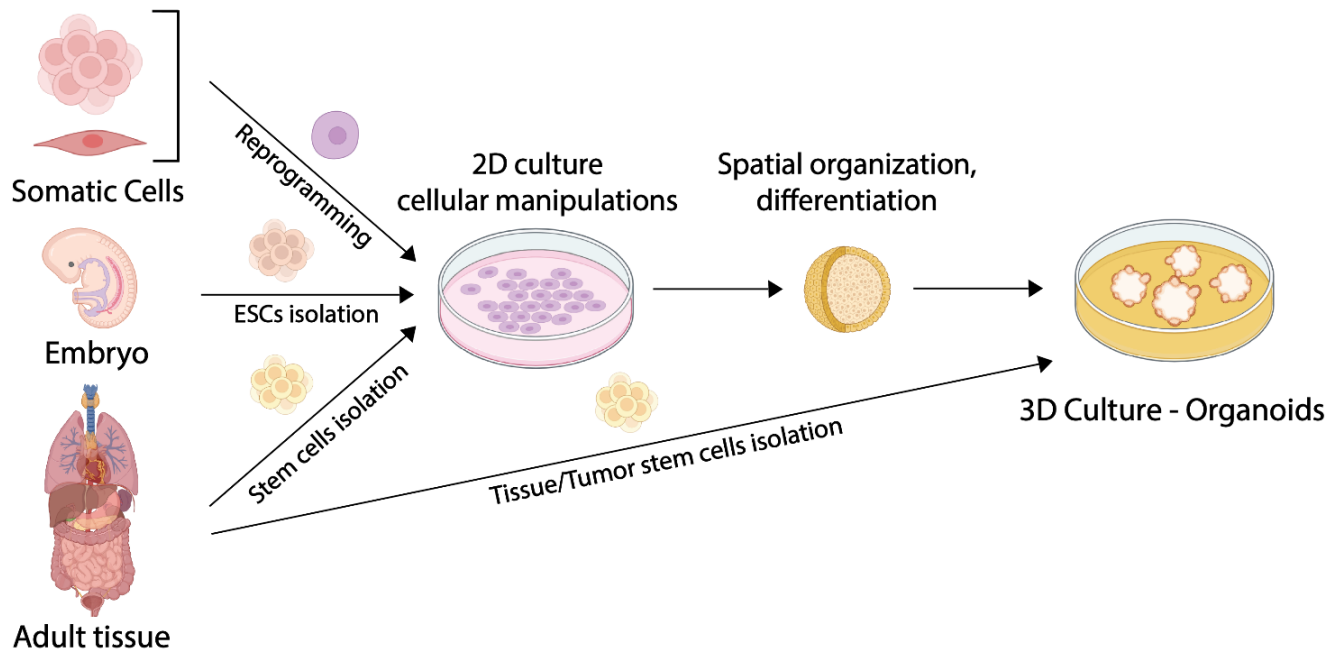


Figure 2 Schematic illustration of main cell courses for organoid cell culture generation. Cells are isolated from embryonic or adult stem cells or derived from reprogramming of somatic cells. Under specific conditions the prepared cells aggregate into 3D structures - organoids (Aqeilan, 2020).

The key objective for an organoid is to resemble some morphological, functional, and transcriptomic features of human organs. Usually, such 3D cell cultures are engineered to harbor specific disease-causing mutations or are grown directly from patient cells in order to provide insights into the progression of the disease (Cowan et al., 2020; Lewis-Israeli et al., 2021). One of the first discoveries in organoid research occurred in 1987 when it was observed that breast epithelial cells can form complex 3D cultures which appeared to be able to form ducts and secrete milk proteins (M. L. Li et al., 1987).

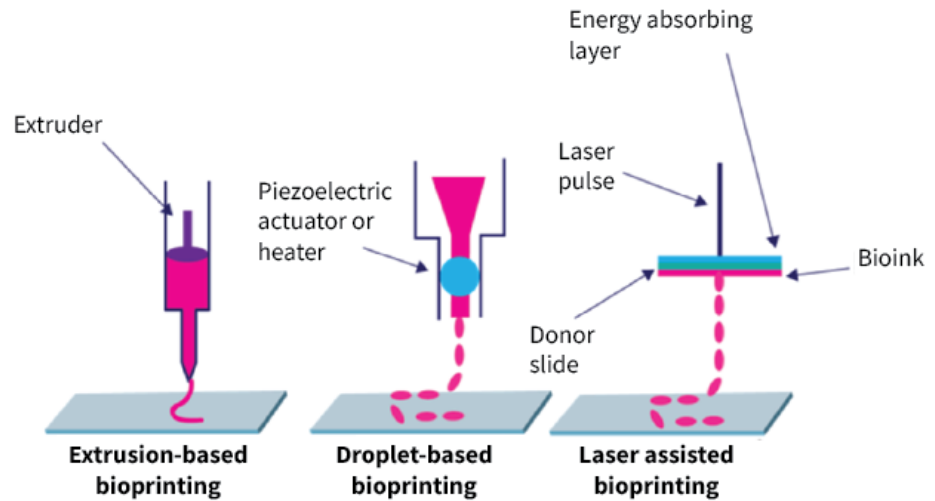
Organoid research pointed scientists to move from 2D onto 3D cell cultures as they offered more complexity and accuracy when comparing cellular behavior of naturally occurring tissues with widely used 2D cell cultures (Mun et al., 2019). Nowadays various protocols have been developed in order to generate a variety of organoids including gastrointestinal (Gerli et al., 2024), tongue (Vincent-Chong & Seshadri, 2020), liver (Shinozawa et al., 2021), pancreatic (Chen et al., 2024), brain (Hu et al., 2025), retinal (Norrie et al., 2021), kidney (Nerger et al., 2024) and other types of organoids. As protocols evolve and improve organoids are becoming one of the main cell-culture tools in biomedical studies.

A vast number of tissue types, the expansion and modification capacity, and the physical 3D architecture turn organoids into a powerful new technology for many biological and clinical applications. Precision and regenerative medicine, drug testing, disease modeling, development and gene editing studies are amongst many application fields that organoids can aid in (Corrò et al., 2020). Neurodevelopmental disorder research has significantly advanced by employing organoids as they can replicate early brain development and generate diverse cell types found *in vivo*. For example single-cell brain organoid screenings help identify developmental ques in diseases like autism (C. Li et al., 2023). Additionally organoid research help understand tumorigenesis that rise from hepatitis B virus infections which are modeled directly from patient cells (De Crignis et al., 2021). In addition to that organoids can also be used to model direct disease progression when discussing treatment options for patients offering drug-toxicity screenings and patient specific drug development whilst screening for disease-specific drug vulnerabilities (Calandrini & Drost, 2022).

1.4. Additive biofabrication

Additive manufacturing (AM) technology is a fabrication method introduced into the field of engineering for solid model fabrication based on a computer file (Gibson et al., 2021). This technology defines a process of joining materials to make objects from 3D models, fabricating it layer by layer. This technology can also be referred to as additive fabrication, additive process, direct digital manufacturing, rapid prototyping, rapid manufacturing, 3D printing, ect. (Alammar et al., 2022). Biofabrication is defined by a number of techniques which produce 2D or 3D structures from materials like living cells, proteins, biomaterials and molecules (Ino et al., 2020). AM combined with biofabrication develops into a number of strategies for additive biofabrication including droplet, extrusion, light and laser assisted bioprinting (Moncal et al., 2019; Roversi et al., 2022; Kunwar et al., 2024). Every mentioned approach

has a different working principle with its associated advantages and disadvantages which mostly affect cell processing, the resolution of the printed structures and the material portfolio (Figure 3).



Achievable resolution:	Hundreds of μm	Hundreds of μm	Single cells
Print throughput:	High	High	Slow
Materials:	Cell laden pastes	Cell laden liquids	Various

Figure 3 Schematics of the 3 most popular 3D bioprinting technologies: extrusion-based, droplet-based and laser-assisted / LIFT.

Extrusion based biofabrication relies on selectively dispensing the used material through a nozzle, much like simple bioprinters that are used to work with plastics and other materials (Moncal et al., 2019). Extrusion of the material through a nozzle allows to generate 3D structures with feature size of about $100 \mu\text{m} - 1 \text{ cm}$, the technology allows for the deposition of more physically relevant cell densities, however the entire process is usually incredibly damaging to the cells due to the used heat and mechanical stress (Hooper et al., 2024).

Droplet-based bioprinting describes a printing technique in which cell-containing material droplets are selectively ejected to form a 3D structure drop by drop. With this technology you can usually achieve a resolution of $10 \mu\text{m} - 300 \mu\text{m}$ (Ji et al., 2019). The process itself has a high printing throughput and uses cell-laden liquid materials. However, this methodology cannot reach physiologically relevant cell densities (reaching about $< 10^6$ cells/ml) or large enough tissue sizes. Typically achieved thickness of the 3D constructs does not exceed 3 cm (Kotlarz et al., 2022).

Laser-based biofabrication which includes two photon polymerization, projection micro stereolithography and volumetric printing utilizes the principle of selective solidification of a cell containing hydrogel by applying light as an energy source (Vidler et al., 2024). This technology offers an advantage over droplet and extrusion based biofabrication as it is not limited by sheer mechanical stress and can allow the manufacturing of constructs that are cm in size with incorporated features reaching only a few microns (Levato et al., 2021). However, this technology faces challenges related to the low throughput and reliance on UV in certain fabrication methodologies (Huh et al., 2021; Hooper et al., 2024). Laser-based biofabrication is a sub type of light-based biofabrication, which employs a selective application of a pulsed laser to an absorbent layer, containing a cell-laden hydrogel ink, that promotes the transfer of a cell-hydrogel droplets to a receiver substrate, droplet by droplet generating a 3D structure (Gruene et al., 2011). Yet this method can only generate structures 10 μm – 300 μm in size and is a generally slow process and in certain methodologies uses UV light for polymer curing (Roversi et al., 2022).

Additive biofabrication is directly linked to bioprinting as it allows the *in vitro* fabrication of biological constructs with precise combinations of cells and biomaterials. The complimentary digital manufacturing processes additionally provides a future perspective for biological structures to be shaped into the geometry of the target tissue or organ (Castilho et al., 2020). Generally, there are three main points that bioprinting technology needs to address to be able to print biological tissues. The technology must print 3D structures in size range from μm to cm, materials used for bioprinting need to be biocompatible or bioactive and finally, the printing time should be short to maintain cell viability and be economically feasible. Currently there is no single additive biofabrication technology that would satisfy all the criteria mentioned.

1.5. 2 photon polymerization

Out of all optical 3D printing techniques, 2 photon polymerization (2PP) stands out as an excellent tool for producing various 3D structures with sub- μm precision (Jonušauskas et al., 2018). It positions 2PP as a quite promising technology adaptable for bioprinting applications. 2PP works by focusing a femtosecond laser is on a photoactive material (pre-polymer), where a high-intensity ($\sim\text{TW}/\text{cm}^2$) area is created in the focal volume. This induces nonlinear absorption in the focal point, resulting in cross-linking of pre-polymer (Ovsianikov et al., 2010). Because the process is nonlinear and has an

intensity threshold, material around the focal volume is not affected, allowing to construct structure point-by-point one volume pixel (voxel) at the time (Figure 4) (Keiser, 2021).

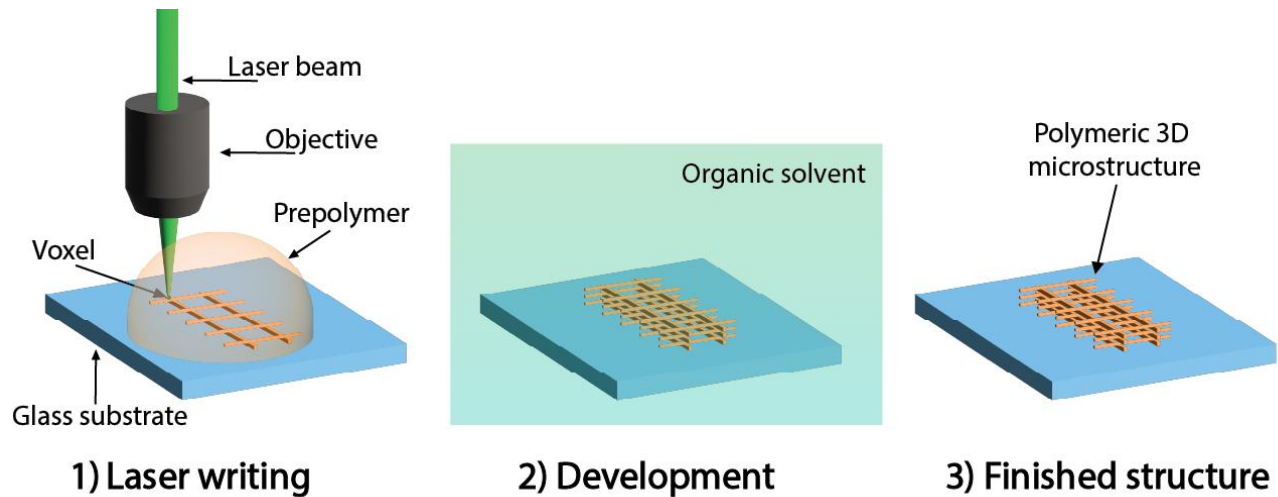


Figure 4 General principle of 2PP style 3D printing. A focused femtosecond laser pulse induces localized polymerization in a photosensitive material. After the printing process the polymerized structure is developed in an organic solution and then air dried or cured depending on the protocol.

Depending on material properties, laser system peculiarities, and focusing optics volume pixel can be as small as several hundred nm (L. Zheng et al., 2019). In regular 2PP systems, this feature size can be tuned by changing the numerical aperture (NA) of the focusing objective by 2-3 orders of magnitude (Jonušauskas et al., 2019). Additionally, there are virtually no limitations to the 3D geometry, other than the resolution of the process. It can be applied in numerous ways to enhance the throughput of the printing process. Before printing, the model must be sliced into layers and each layer hatches with its fill pattern. Increasing layer thickness and hatch spacing expedites fabrication but may reduce mechanical strength and dimensional fidelity. Employing voxel elongation mitigates these limitations, enabling higher production speeds while maintaining structural robustness and geometric accuracy (Figure 5).

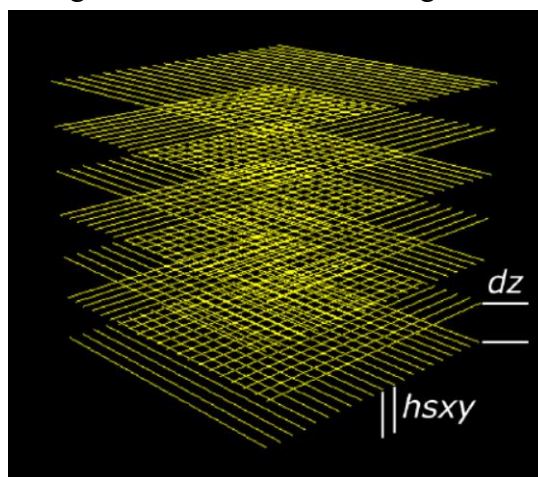


Figure 5 Model visualizing slicing and hatching. “dz” - represents slicing. “hsxy” – represents hatching.

Overall, 2PP is a very versatile tool for additive microfabrication. 2PP-produced structures can have very smooth surfaces, with RMS being less than 10 nm (Jonušauskas et al., 2019; L. Zheng et al., 2019). One of the areas where 2PP was explored by many groups is 3D biofabrication (Ovsianikov et al., 2010; Tytgat et al., 2020; Weisgrab et al., 2020). Here, bioprinting differentiates as a technology where cell-laden bio-ink is used for structuring and biofabrication produces objects needed for biomedicine, yet cells are introduced to it after the manufacturing process. In biofabrication, 2PP was used to produce various scaffolds, that were used for cell cultivation (Remuzzi et al., 2020), cell-material interaction investigation (Richter et al., 2017), and even for pre-clinical uses (Mačiulaitis et al., 2015). Architectures of such structures also differed heavily, from simple square pores all the way to complex, shape-shifting structures (Danilevicius et al., 2015; J. Liu et al., 2023). As a result, there is already substantial understanding and general knowledge about the biocompatibility of many 2PP processable materials. This also includes various hydrogels like polyethylene glycol diacrylate - PEG-DA and gelatin methacryloyl – GelMA, biopolymers, and even naturally derived photopolymers (Barner-Kowollik et al., 2017; Merkininkaitė et al., 2019).

At the moment, 2PP is well-established in the field of 3D biofabrication (Nguyen & Narayan, 2017). All this knowledge forms an excellent base to evolve 2PP from purely biofabrication to bioprinting. Additionally, 2PP uses either green or infrared light for structuring, which is substantially better than UV in terms of residual effects on cells present in bio-inks (Nieto et al., 2020). Next, as 2PP is an intensity-driven process, if the bio-ink formulation polymerization threshold is substantially lower than the laser-induced damage threshold of cell polymers and / or water, the light should have no effect on cells. Finally, it was shown that 2PP is an inherently cold process, excluding even this pathway for process-cell interaction during printing (Mueller et al., 2013). All of this, together with the capability of printing μm -sized 3D features makes it an excellent underlying technology for 3D bioprinting, as it was already shown to adhere to two out of three main requirements for an ideal 3D bioprinting technology - sufficient resolution and relevant material selection.

However, this technology still faces issues regarding its throughput. Theoretically, 2PP can be scaled up by changing the numerical aperture of focusing optics. Then the voxel size scales according to the Gaussian focusing laws (Jonušauskas et al., 2019). Nevertheless, scaling is highly anisotropic, as voxel height increases a lot faster than the width. Thus, not only resolution is lost, but it is lost in such a way that after $\text{NA} < 0.3$ 2PP basically becomes a 2D structuring technique with voxels becoming 50-70 μm height, which mimics stereolithography methodology (Danilevicius et al., 2012). It was attempted to at least partially remedy anisotropic scaling by dynamic NA tuning using laser beam

diameter manipulations, but even then, results were limited (Vařák et al., 2020). Therefore, 2PP is limited to structures in the range of a few mm, with the sweet spot still being in sub-mm manufacturing. For bioprinting, it means that 2PP in its current state can be used for academic experimentation but lacks true scalability to become an attractive commercial solution. Thus, some substantial development in this area is needed. The created solution should somehow preserve the high-resolution capability of 2PP but also should enable on-demand structured volume increase towards filling in large volumes.

The most popular way to increase 2PP throughput is continuous improvement to linear translation velocity of the scanning system. Current commercial 2PP systems can achieve linear translation velocity of well more than 1 m/s. Yet it faces problems and limitations tied to it. The first one is related to pulsed laser usage in 2PP. Generally, the repetition rate of lasers used in 2PP roughly varies from 200 kHz for amplified systems to 100 MHz for lower power oscillators (Fischer et al., 2013). At low velocities (below 1 mm/s) repetition rate of the laser pulse in 2PP is not relevant, because pulse overlap is in the range of single-digit nm, even for amplified system (Malinauskas et al., 2010). However, when translation velocity reaches and bypass 1 cm/s limit the distance between single pulses during scanning can reach tens, or in some more extreme cases, hundreds of nm which in turn can cause architectural disruptions in the 3D structure (Figure 6) (Qi et al., 2004).

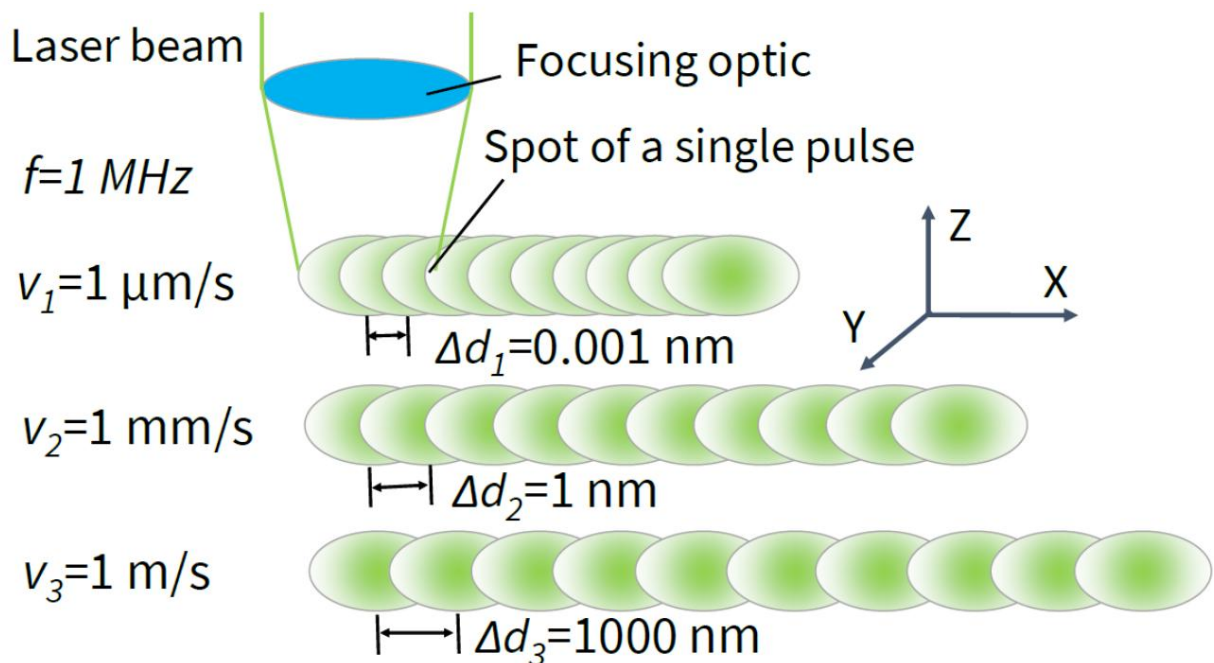


Figure 6 Visualization explaining why increase in translation velocity (v_1 , v_2 and v_3) can lead to increase in intra-pulse distance (δ_1 , δ_2 , δ_3) at fixed repetition rate f .

As a result, there is a hard upper limit to how much the throughput of 2PP can be increased just by continuously improving linear translation velocity via application of more and more advanced scanning units.

Materials used for fabrication also play a big role in the printing process (Kalirajan et al., 2021). If the used material has low two photon absorption cross section and the photopolymerization reaction is in itself not very efficient an increase in translation velocity is not an option, as inherently longer exposure times are needed to form cross-linked polymer matrix (Ežerskytė et al., 2022). This is an important consideration in the context of bioprinting, because in a lot of cases various biomaterials have substantially worse polymerization properties in comparison to synthetic photopolymers (Yu et al., 2020). For this reason, it is obvious that continuous translation velocity increase might not be the way to go in increasing 2PP throughput in the context of biofabrication and bioprinting.

1.6. Towards beam shaping solutions

Light is quite a malleable tool, and other beam profiles than Gaussian can be used for 2PP. This means that laser beam shaping (LBS) can be a solution needed to push 2PP from sub-mm manufacturing to true multi cm capability. Beam shaping is a process of getting the desired intensity distribution of the incident beam (Kim & Choi, 2024). It can be realized in multiple different ways, using static elements such as special refractive lenses (like axions), diffractive optical elements (DOE), or active means, such as dynamic mirror devices (DMD) or spatial light modulator (SLM) (El-Tamer et al., 2020). Choice in how to induce LBS depends on exact application and tolerance on how complex optical chain can be. One of the main drawbacks of LBS is the severe increase in the complexity and sensitivity of the optical chain (Sivarajah, 2023). Thus, to justify the application of LBS, the increase in functionality must be dramatic.

Among ways to induce LBS, SLM has some distinct advantages in comparison to DMD, such as higher base efficiency and the possibility to directly influence the phase of the incident laser beam (Turtaev et al., 2017). As a result, the key for SLM operation is what is called a phase mask. The phase mask is normally a gray-scale image where shades of grey denote how much the phase of the incident light will be retarded. For some intensity distributions, it can be calculated deterministically, but for most cases, iterative approximate methods are used, such as the Gerchberg-Saxton algorithm. Then, after the phase is modulated, such beam would diffract to the desired intensity distribution in the “far field” (i.e. infinitely far away) or in the focal plane of the focusing optic placed after SLM in the optical path

(Shirshneva-Vashchenko et al., 2023). Beam shaping allows a lot more sophisticated laser beam manipulation for material processing.

However, all of them have some kind of drawback limiting their widespread usage. For instance, multi-focal point printing increases throughput by the number of focal points formed but also reduces the effective working field to the distance between focal points (Gittard et al., 2011). It is acceptable for highly periodic structures (Maibohm et al., 2020) or for mass production of very small (\sim tens of μm) particles (Kiefer et al., 2024), but not for big, irregular structures. Using SLM to scan structure in 3D was also demonstrated, with the advantage of avoiding the usage of any moving components for the structuring process (Vizsnyiczai et al., 2014). The drawback is the relatively low speed due to the refresh rate of standard commercial SLMs being in the range of tens of Hz (normally 30, 60, or 120 Hz). Printing the entire layer by single exposure was also demonstrated, making 2PP rather like DLP (Yang et al., 2014). Nevertheless, it requires rather high laser power to maintain the intensity needed for polymerization, which might optically damage the SLM itself. Alternatively, the amount of photoinitiator in the material can be increased to sufficiently increase the material sensitivity so even lower intensity can induce crosslinking, however it can have a negative impact on the biocompatibility of the bio-ink (Kawasaki & Sendo, 2021).

To solve the challenge of throughout the beam shaping solution in question should result in a methodology that does not reduce and is not limited at all by the working field of the focusing optic (Jonušauskas et al., 2018). Also, to make sure that additives in bio-ink, such as photoinitiators, are kept to the minimum, the process should not struggle to maintain the required intensity in the focal point (\sim TW/cm²) with available commercial femtosecond laser system average powers (up to few W) (Huh et al., 2021; Kawasaki & Sendo, 2021). Additionally, it should not impede the inherent procession of the 2PP process, allowing smooth switching between high-resolution structuring and high throughput printing (Vitkūnaitė et al., 2024). Last, it should be compatible with already existing printing strategies enabling rapid merging of the process with the already existing software base. Also, it should not limit 3D geometry.

To adhere to these main criteria an SLM-based technique that exploits on-demand voxel elongation was developed. The general premise of the technology is the capability to expand a voxel in one direction without affecting the voxel size in the other direction and its height. Then the volume of structure that does not require precision can be filled in at a high volume/time rate. For more precise parts beam shaping can be turned off and structuring can be performed using a standard high-resolution focal point. This way

it is possible to produce cm-scale objects while maintaining μm -level precision/feature size. There are multiple advantages of using such a solution for the up-scaling of 2PP. First, because the voxel is expanded only in one direction, the volume in which intensity needs to be sufficient for cross-linking increases a lot less than in the layer-by-layer case, allowing to use of less power and/or less photoinitiator. This can be done with μm -level precision, so it has no negative impact on printing resolution. It is important to note that while continuous voxel is the simplest case, more complex intensity distributions can be achieved. For instance, if the structure to be printed has some kind of periodicity, a dashed voxel can be formed, allowing the drawing of several features of the structure at once, further increasing the manufacturing throughput. Alternatively, ring-shaped distribution makes it possible to print vasculature in one translation. All these distributions can be easily rotated in the horizontal plane. Full rotation in 3D is also possible, but more sophisticated calculation algorithms are needed. As the developed technology gives rise to a new way of bioprinting challenges regarding the uniformity of the mentioned brushed still need to be solved (Figure 7).

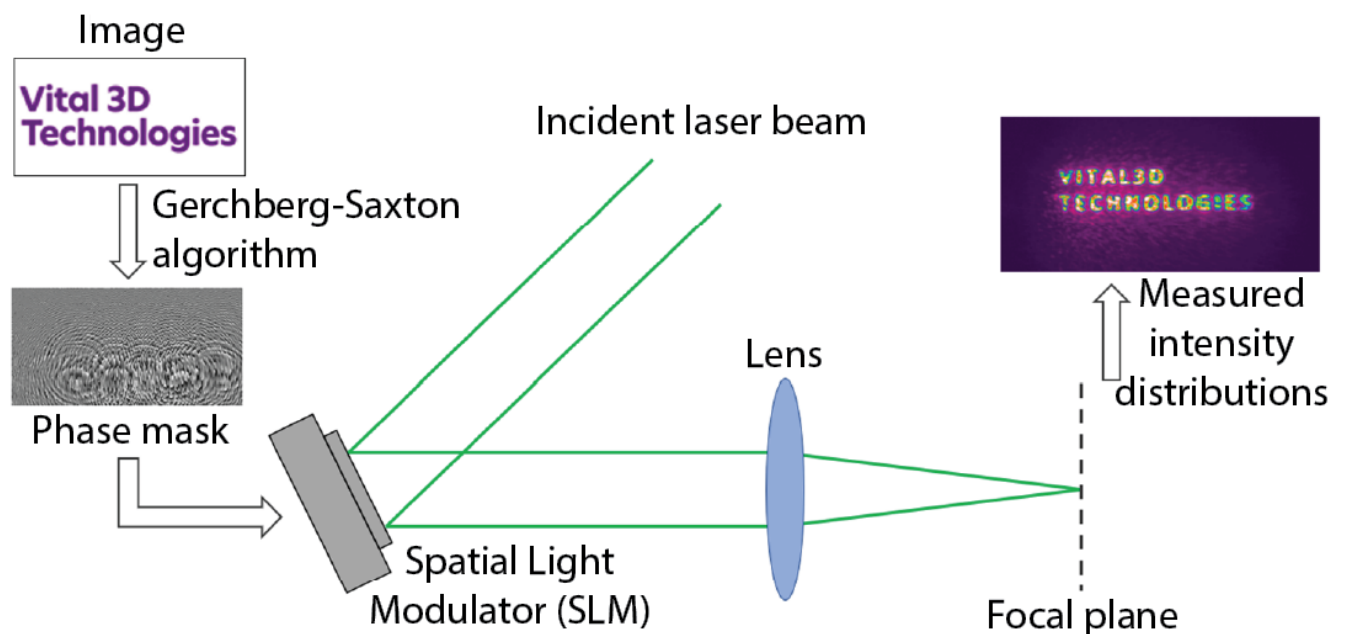


Figure 7 Principle of beam shaping using SLM.

So far, all phase masks used for voxel elongation are generated using software provided by the vendor of SLM (HOLOEYE). Although, functional this solution for LBS works with seemingly very little tunability and capability to influence the outcome of phase mask generation, thus greatly influencing the biofabrication process. Therefore, before developing more solutions for tissue printing a deeper understanding of phase mask generation must be achieved.

Spatial light modulation offers a host of advantages for high-resolution biofabrication—and ultimately bioprinting—when combined with two-photon polymerization. Yet before this potential can be fully realized, the generation of accurate phase masks, the critical intermediary between light modulation and printed geometry, must be thoroughly understood, optimized, and translated into the printing workflow. In this work phase mask generation and voxel characterization will be carried out in order to optimize an organoid scaffold printing process.

2. Materials and Methods

2.1. Phase mask generation

A precursor mask can be generated using any graphics editing software. Image dimensions - 1920×1080 pixels (px). The image entails an entirely black canvas with a line of white or gray-scale pixels positioned in the middle of the canvas. The line represents desired intensity distribution in the focal plane of focusing optic. The created image is exported from the software as a portable network graphic (PNG) file and then is processed by HOLOEYE SLM software to create a functional phase mask (Figure 8).

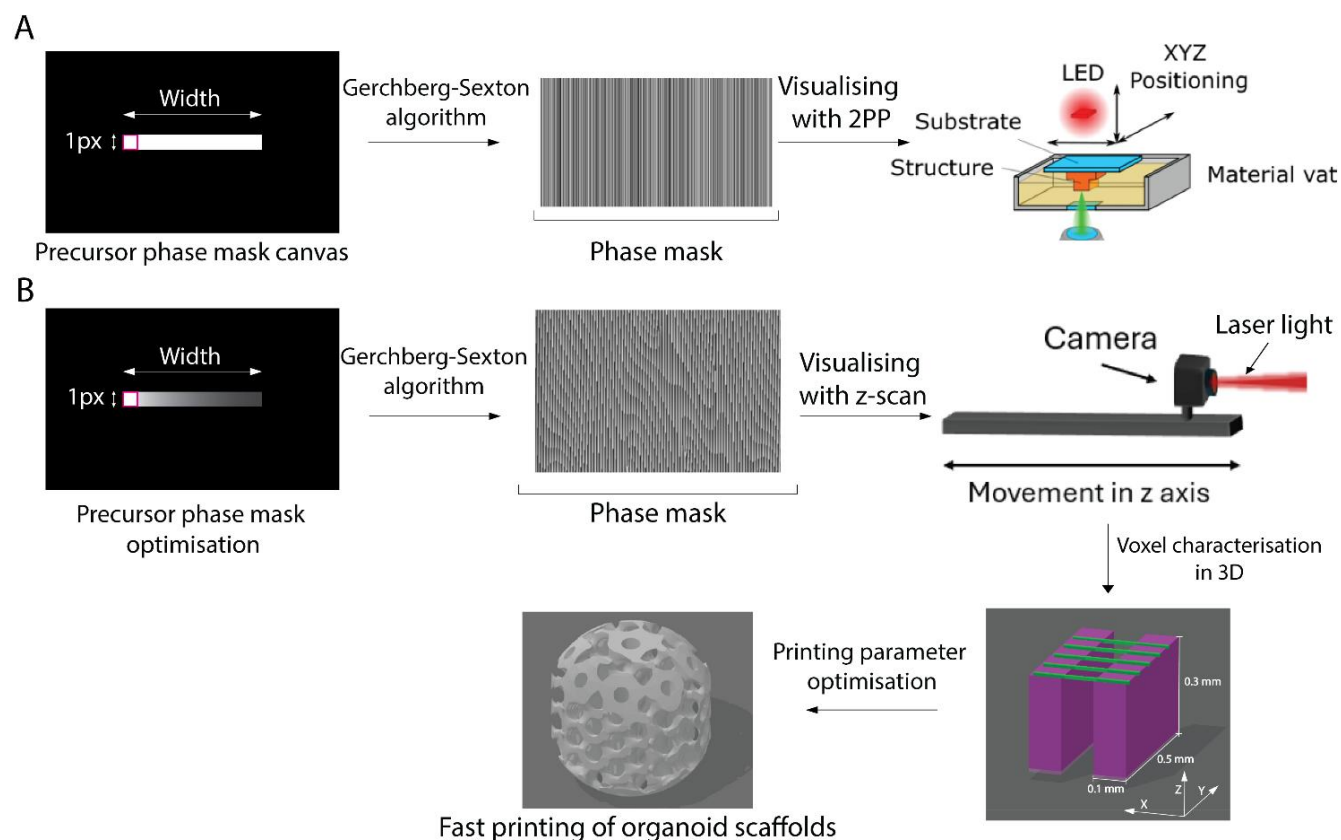


Figure 8 Schematic representation of the study methodology. A – Visualization of phase mask generation and application in 2PP. B – Visualization of phase mask generation and voxel parameter characterization in 3D space. The width of the precursor phase mask represents the number of pixels used in one phase mask.

The resulting voxels were then visualized *in situ* with real-time imaging sub-system built into used 2PP setup to determine the correlation between the width of the line in the precursor image and the polymerized width of the line in the 2PP setup. After, the precursor images of chosen phase masks were modified and visualized with the Z-scan. The intensity distribution visualized with the z-scan allowed to determine which pixels of the precursor image need to be darkened to optimize the phase masks. When

the optimization was completed the generated phase masks were used to characterize voxel in 3D space by resolution bridge method. This allowed to determine the best parameters for organoid scaffold printing (Figure 8).

2.2. Z-scan setup

The light source used in the experimental systems is a femtosecond laser “LightWire” (EKSPLA, Vilnius, Lithuania) which emits 133 fs pulses at 50 MHz repetition rate and wavelength of 1032 nm. The light is directed into the power attenuator “LPA” (Optogama, Vilnius, Lithuania), and a 3× fixed ratio beam expander (Optogama, Vilnius, Lithuania). These components ensure that the laser beam completely fills out the apertures of the SLM and objective lens. SLM used in the setup is PLUTO-2.1 (Holoeye, Berlin, Germany) with a matrix size of 1920×1080 pixels. After the SLM two lenses forming a 4F system follow, with the iris being placed in the focal plane acting as a spatial filter. In front of the camera there is another lens focusing on the camera, with a focal length of 200 mm. After, a charge-coupled device (CCD) camera (Ophir® SP920, Vilnius, Lithuania) is placed for system and beam shaping diagnostics. The camera is stationed on a moving axis allowing to image the resulting intensity in the Z axis (NRT100, Thorlabs, Germany). For phase mask analysis the camera moves in Z axis and makes stops every 2 mm. During the brief stops the camera creates an image visualizing the shape of the laser beam. When the camera reaches the end coordinate of the moving Z axis the images get compiled in the data analysis software to create a 3D projection of the shape of the voxel (Figure 9).

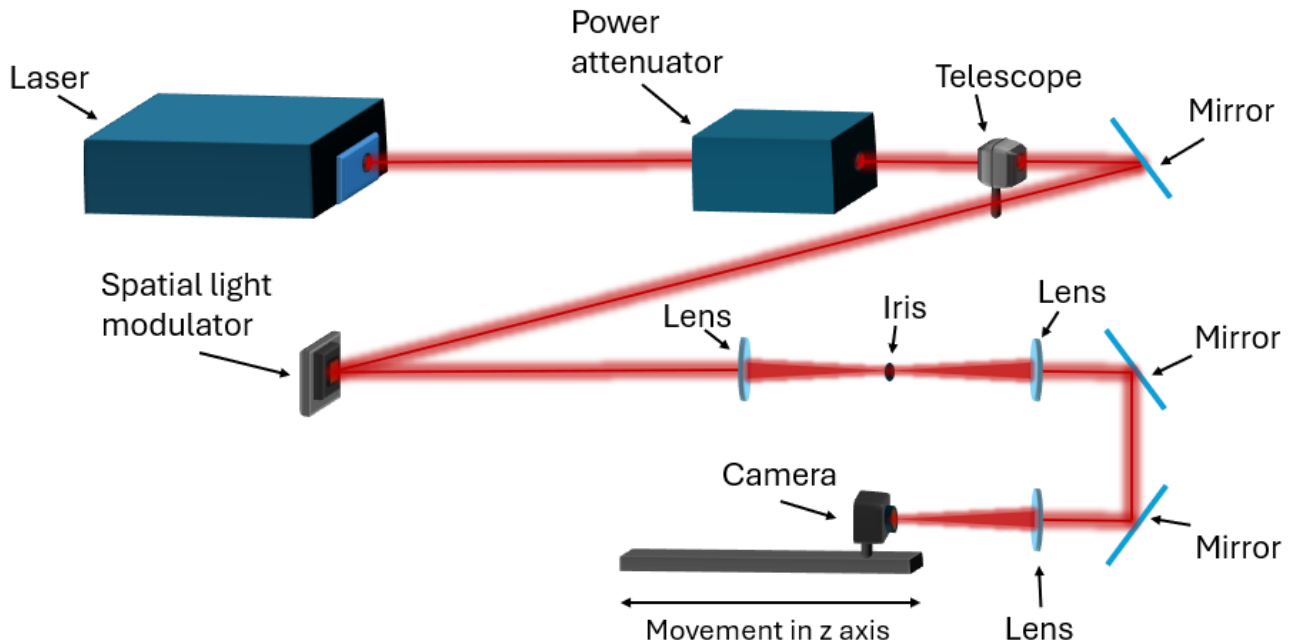


Figure 9 Schematics of the Z-scan setup optical chain.

2.3. 2PP 3D Printing setup

The optical chain guides the laser beam towards the material vat where the 2PP printing takes place. The light source in experimental systems is a femtosecond laser “Biolit 2” (Litilit, Vilnius, Lithuania) emitting 80 fs pulses at 40 MHz repetition rate. II harmonic crystal follows, converting fundamental wavelength of 1045 nm to 522 nm radiation needed for printing. Then the light is directed to the power attenuator “LPA” (Optogama, Vilnius, Lithuania), polarization rotor “MRO” (Optogama, Vilnius, Lithuania), and 3× beam expander – telescope (Optogama, Vilnius, Lithuania). The beam is expanded to fill the full apertures of the SLM and objective lens. SLM used in the setup is Leto (HOLOEYE, Berlin, Germany) with a matrix size of 1920×1080 pixels.

Two lenses forming a 4F system follow, with the iris being placed in the focal plane acting as a spatial filter. The dichroic mirror then directs the laser beam to the objective lens which focuses it on the sample. The printing setup also has an integrated light-emitting diode (LED), lens, and complementary metal oxide semiconductor (CMOS) camera (Levenhuk, Prague, Czech Republic), which allows monitoring of the printing process in real time (Figure 10).

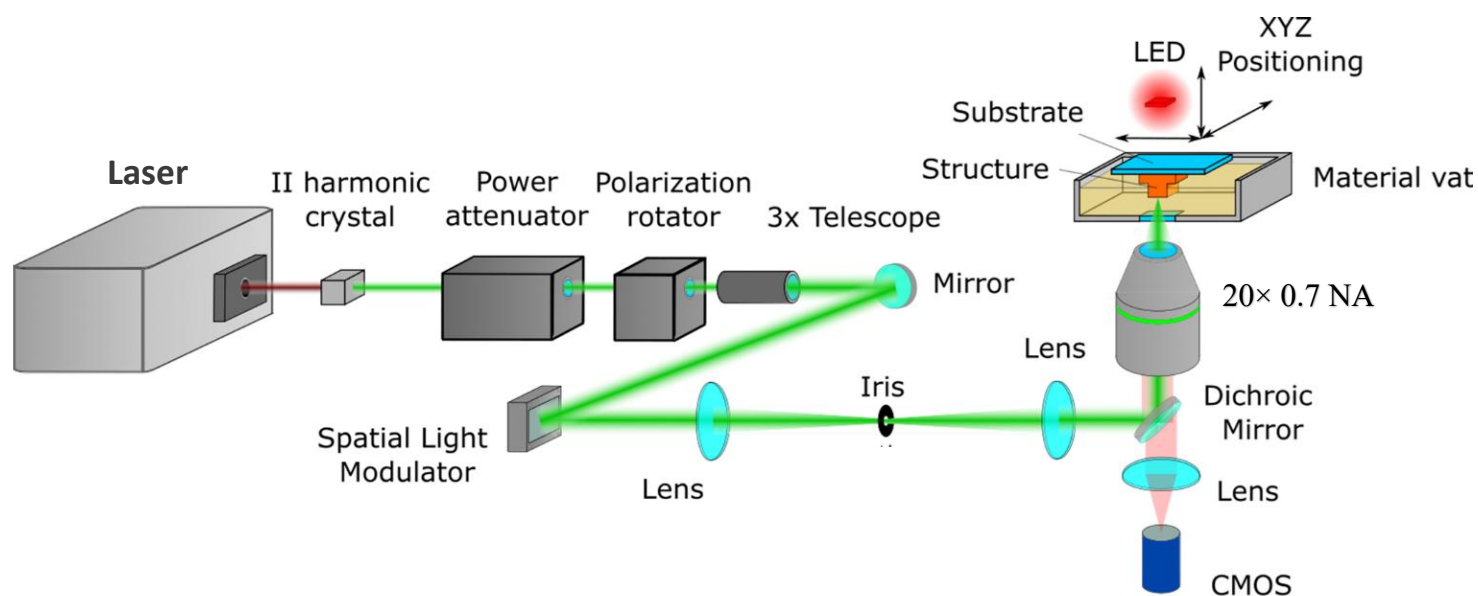


Figure 10 2PP 3D printing setup, that was used for experimental voxel characterization and organoid scaffold printing.

2.4. 3D structure printing, development and characterization

The glass substrate used for 3D structure fabrication is prepared by first slicing the microscopy slides (631-1550, Avantor, Pennsylvania, U.S.) into squares with $25 \times 25 \times 1$ mm dimensions. Then, the glass slides are cleaned by sonication for 1 h at 37 °C) in a MilliQ water solution with 1.5 wt % Alconox powdered detergent. After, the glass slides are thoroughly rinsed in excess MilliQ water, followed by

rinsing in excess ethanol (95 %). Slides are transferred to a sanitizing solution of 300 mL ethanol (95 %), 15 mL of silane compound (3-trimethoxysilyl-propyl-methacrylate; Sigma-Aldrich, St. Louis, MO), and 10 mL diluted acetic acid (10 %). Slides are allowed to react for 12–24 h in the solution at room temperature. After they are rinsed in excess ethanol (95 %) followed by excess MilliQ water. When the process is complete the slides are baked on a stove at 60 °C for 5–12 h. If not used immediately the glass slides can be stored for up to 2 months protected from light at 4 °C.

PEDGA (Mn 700, Sigma Aldrich, Burlington, MA, USA) is warmed in a 40 °C bath to lower its viscosity. Then in an amber vial 1 wt % of the photoinitiator 2-Hydroxy-4'-(2-hydroxyethyl)-2-methylpropiophenone (Irgacure 2959, Sigma Aldrich) is added. The vial is capped and vortexed for 1-2 min. If the crystals remained the solution was sonicated in a closed vial in a lukewarm (~30 °C) bath for 5 min or stirred with a magnetic bar until clear. After preparation the material was stored at 4 °C, in a tinted vial protected from light. Shelf life is ~3 months unopened. If the solution turned yellow or its viscosity increased, it was discarded as expired. Before initiating the printing process, the material used for printing is brought to room temperature and poured into the material vat. The glass substrate prepared for the printing is placed into a sample holder. The glass substrate is then submerged into the material vat and positioned in 3D space by using mechanical stages, i.e., the sample holder is moved in relation to the focal point (Figure 11). The structure then is fabricated layer-by-layer in XY plane and extracted out of the vat in Z direction after each layer is completed.

3D models for scaffold printing or resolution printing experiments were generated with AutodeskFusion 360 (<https://www.autodesk.com/in/products/fusion-360/free-trial>) and, with Microsoft 3D Builder (<https://apps.microsoft.com/detail/9wzdncrfj3t6?hl=en-us&gl=PH>).

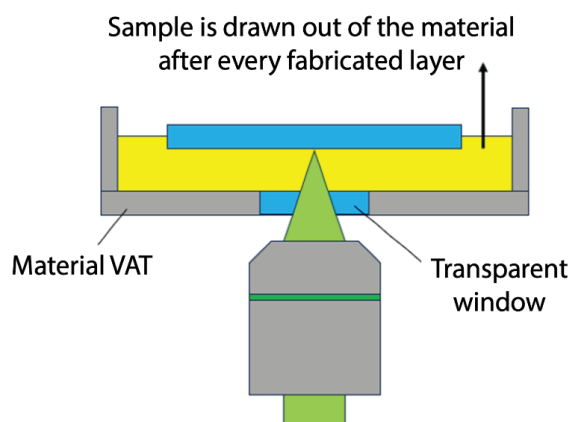


Figure 11 Visualization of the sample holder and the material vat.

After the printing process is completed, the printed structure is removed together with the glass substrate and submerged completely into 99.8 % isopropanol (1096341011, Sigman ALDRICH Co., Germany) solution for 20 min. Then the structure is air dried for 10 min at room temperature. When dried the printed structures were viewed with a light microscope MRCL700 3D Imager Pro (Microqubic AG, Zug, Switzerland). The morphology of the 3D-printed structures was characterized using a scanning electron microscope (SEM TM-3000, Hitachi, Chiyoda, Tokyo). The samples are not additionally prepared for SEM.

2.5. 3D structure characterization

After visualizing the shape of the voxel with Z-scan, a standard technique of resolution bridge printing applied in 2PP for voxel shape characterization was used to define the voxels in 3D space (Jonušauskas et al., 2016). Figure 12 shows the structure which was used to define the voxel shape. It consisted of 2 pillars and 5 lines placed on top of them, which allows to measure the parameters of voxels in X, Y and Z planes.

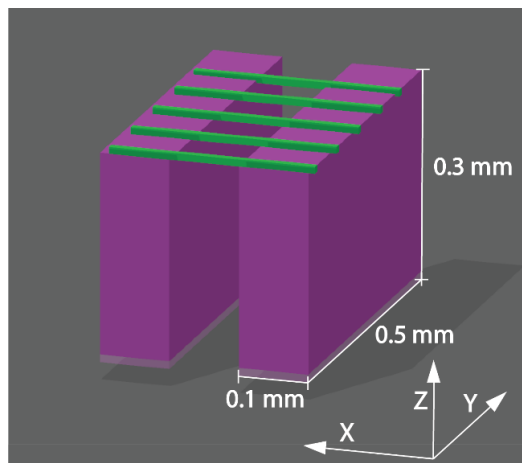


Figure 12 Visualization represents resolution bridges.

Since the printed structures would be visualized with SEM TM-3000 which has no built-in way to rotate or otherwise manipulate the sample. The resolution bridges needed to be fabricated at the edge of the glass substrate to ensure the best accuracy for measurements. In order to measure the size of the voxel in Z axis the fabricated samples would be placed on a 45° stand, therefore these structures were placed 5 in a row alongside the corner of the glass substrate. Each resolution bridge was stationed 0.5 mm from the edge of the glass substrate and 0.3 mm apart from each other (Figure 13).

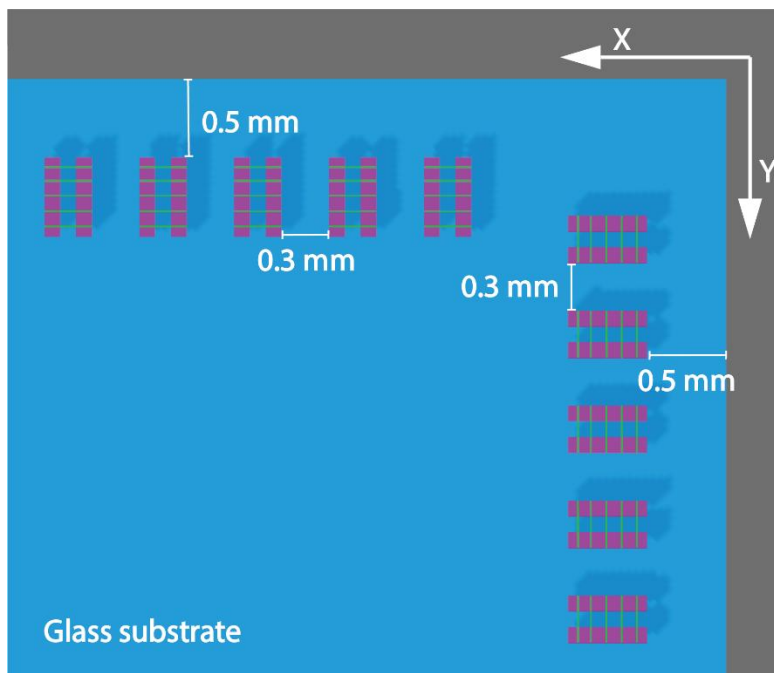


Figure 13 Schematic representing the printing of resolution bridges.

To measure the voxel in X and Y planes the fabricated lines were analyzed visualizing them from above the structure. During phase mask generation the width of the line was expanded only in one direction, therefore during printing lines fabricated alongside X plane might have different parameters when compared to lines printed in Y plane (Figure 14).

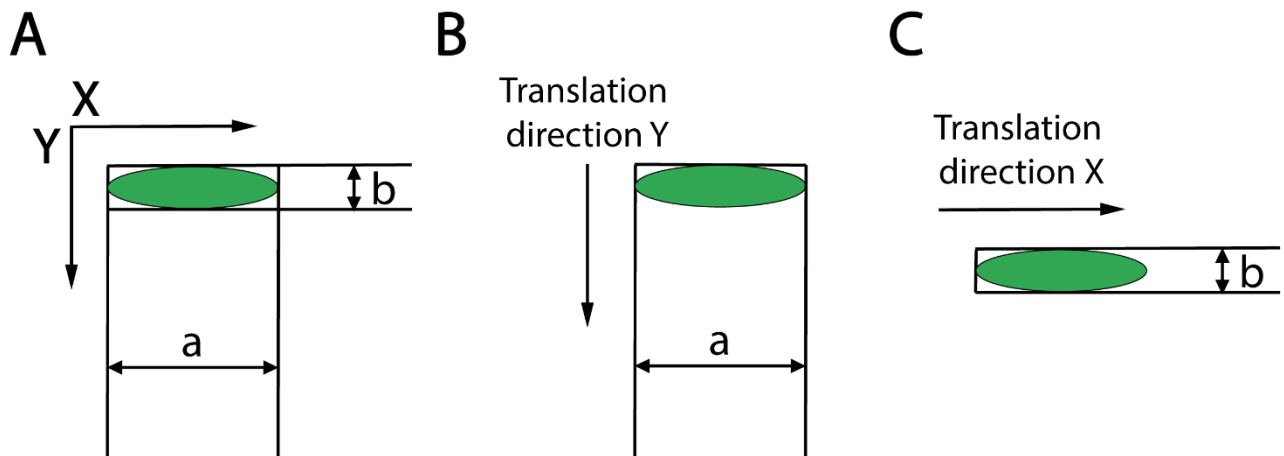


Figure 14 Illustration represents the different width of the polymerized area in X or Y plane. A – general shape of voxel and movement axes. B – Translational direction of the voxel movement in Y axis. C – translational movement of the voxel in X axis. “a” – represents the polymerized width of the line when the laser moves in Y axis. “b” – represents the polymerized width when the laser moves in X axis.

The 3D model presented in Figure 15 was used as a scaffold for spheroid culture development. The scaffold embodies a spherical shape with various hollow channels to facilitate cell attachment, growth

and proliferation. The second model dimensions are 1 mm in XYZ axis together with 100 μm pores placed through the spheroidal structure.

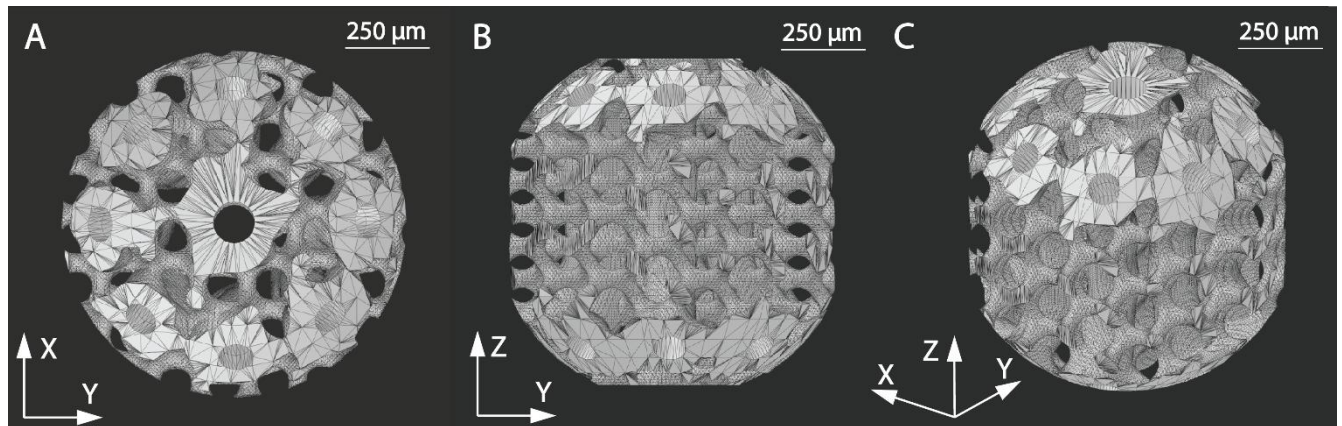


Figure 15 3D model of a spheroidal structure used for cell seeding. A – visualisation of the scaffold in XY plane. B – visualisation of the scaffold in ZY plane. C – Visualisation of the scaffold in 3D space.

2.6. Data Analysis

ImageJ (<https://imagej.net/ij/>) was used to analyze the images captured by the SEM microscope. Microsoft Excel (<https://www.microsoft.com/en-us/microsoft-365/excel>) was used to analyze data. Graphs were plotted using GraphPad Prism version 8.0.0 for Windows, GraphPad Software, San Diego, California USA, (<https://www.graphpad.com/>).

3. Results

3.1. Phase mask width correlation with the polymerized area of material

31 phase masks were generated with dimensions of 1 px in the Y axis and 10 px in the X axis. Each phase mask was increased by 10 px in the X axis until it reached 300 px. All pixels in this experiment were exclusively white. An additional phase mask with dimensions of 1 px in the X axis and 1 px in the Y axis was generated. This phase mask was used as a base line for voxel modifications. The generated masks were first analyzed during a printing experiment with the setup described in section 2.5. During the experiment the generated phase masks were uploaded to the SLM software one by one, changing them before every separate measurement starting from the 1 px phase mask and moving on until the 300 px phase mask. The experiment visualized how the number of pixels in a phase mask precursor translates to μm during the actual printing process (Figure 16). The experiment was carried out by analyzing what area of the pre-polymer is polymerized after 1 s or 10 s of exposure to laser light. The polymerization reaction was determined experimentally by increasing the power of the laser from 1 mW until the polymerized area became visible *in situ* in real time as an image through the built-in camera.

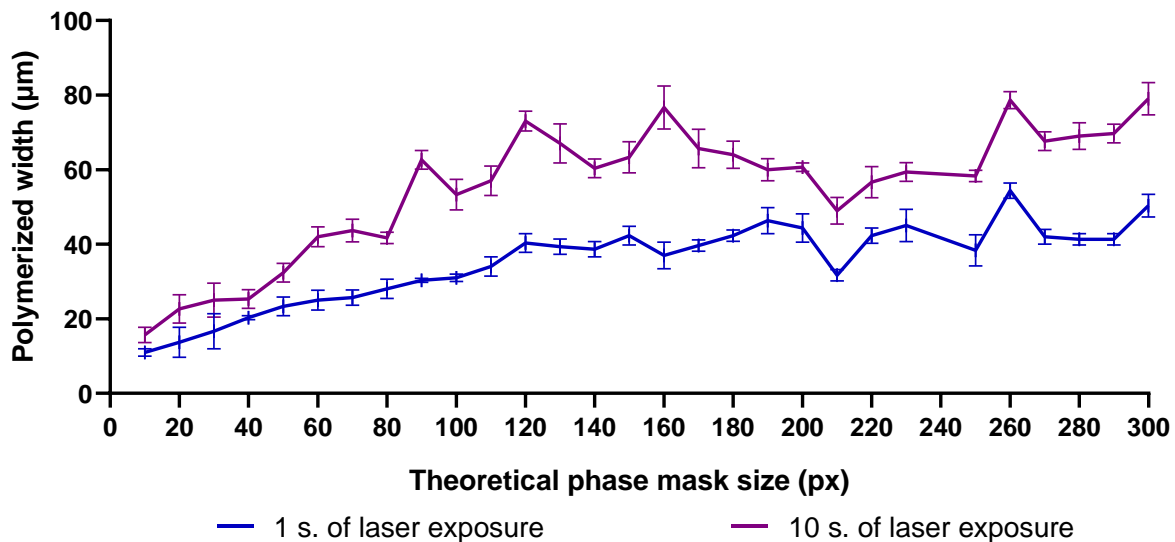


Figure 16 Polymerized width vs. Phase-Mask Size at 1 s and 10 s Laser Exposure.

The graph visualized in Figure 15 allowed to determine that overall, for both conditions, the polymerized width expands as the brush size increases. However, the curves of the graph beyond 120 px saturates in comparison with the steeper increase of polymerized area of brushes sizes from 1 to 120 px. This trend suggests a practical upper limit where widening the beam provides little extra polymerized width. Additionally, the 10 s exposure time consistently provides greater modifications width than the 1

s exposure. 10 s of exposure generates a larger polymerized area by about 15 – 25 μm . According to this graph, 5 phase masks were chosen for further analysis and optimization: 1 px, 10 px, 50 px, 100 px and 200 px, as they represent range where pixel width increase also results in significant modification widening and one value from the middle of the range where without optimization it has seemingly saturated. 1 px phase mask represented the baseline for all further measurements. 10 px and 50 px points were chosen as representations of masks with rapidly increasing polymerized lines. 100 px phase mask was chosen as a point before the flattening of the curve and 200 px were chosen as a representative of the measurements after. We did not choose any phase masks beyond 200 px, because the wider phase masks require more power output during fabrication, which may not be practical.

3.2. Intensity distribution analysis and optimisation

The first iteration of phase masks were generated from a black canvas with exclusively white pixels forming either a single dot or a line. The measurements were carried out with the Z-scan, that generated intensity distributions for the masks. This allowed us to determine the baseline for the phase masks and how they could be modified (Figure 17).



Figure 17 Visualising the intensity distributions. A – 1 px phase mask. B – 10 px phase mask.

Z-scan imaging of 1 px and 10 px phase masks revealed the shape of a baseline voxel. Along the Z-scan, CCD sensor is positioned on the center of the focal plane. This can be explained by how close

resulting intensity distribution is to what would be acquired using regular non-beam shaped Gaussian laser beam. Therefore, any modifications made to 1 px or 10 px precursor image of the phase mask is redundant. So, their version of phase masks were used in further experiments.

Figure 17 visualises the side by side comparison of unoptimised and optimised phase masks. The visualisation of 50 px, 100 px and 200 px intensity distributions before modification prove that the phase mask generation is a non-deterministic calculation model that often results in ununiform intensity distributions with many random peaks. These are considered to be defects and need to be corrected in order to create an intensity distribution with ideally eliminated or at least minimizes random intensity peaks in Z direction, towards more uniform distribution. This can be done by taking the white line that was drawn originally and attempting to darken the pixels that form the unwanted peaks in a finished version of a phase mask. An optimised version of 50 px, 100 px and 200 px models are visualised in Figure 18.

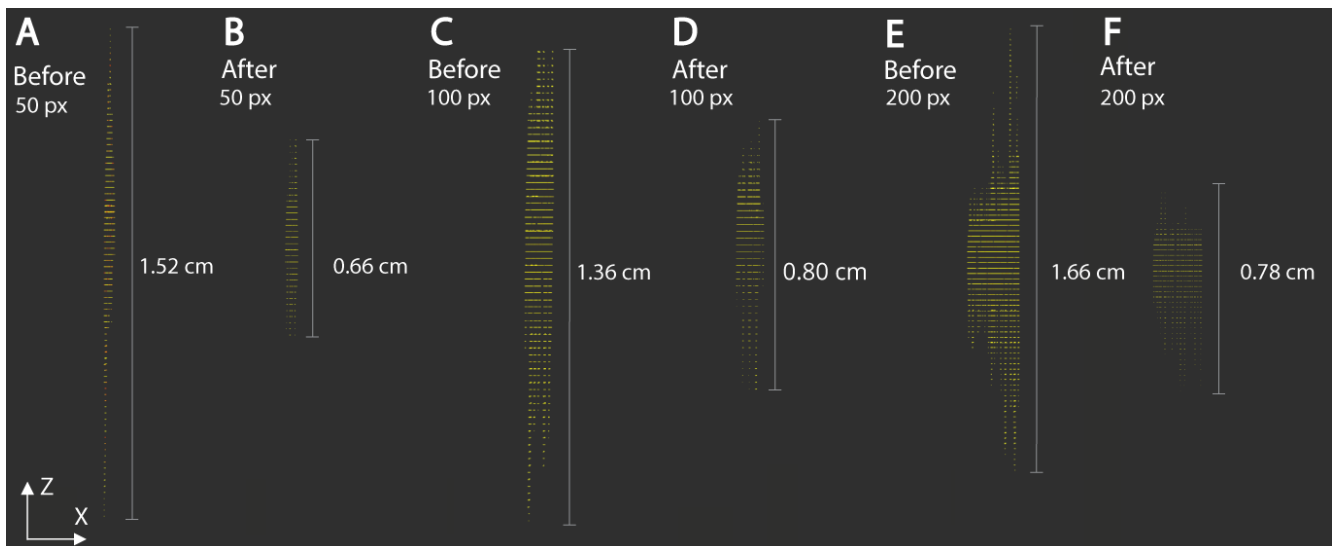


Figure 18 Comparison of intensity distribution of phase masks before and after optimisation. A – 50 px phase mask before optimisation. B – 50 px phase mask after optimisation. C – 100 px phase mask before optimisation. D – 100 px phase mask after optimisation. E – 200 px phase mask before optimisation. F – 200 px phase mask after optimisation.

The optimised phase masks visualised with the Z-scan in Figure 17 were used in further voxel shape characterisation in 3D.

3.3. Microstructure fabrication

1 px, 10 px, 50 px, 100 px and 200 px phase masks were used to generate the resolution bridges in section 2.5 for voxel shape characterisation in 3D space. Figures 19 – 23 illustrate resolution bridges printed by applying the generated phase masks - 1 px, 10 px, 50 px, 100 px, 200 px respectively. For each resolution bridge 3 images are presented illustrating the shape of the voxel in X, Y and Z axes. Resolution bridges illustrating the fabricated lines in X and Y axes were visualised directly above the printed structures. Voxel parameters in Z axis were visualised by taking the printed samples and tilting the printed structure by 45°.

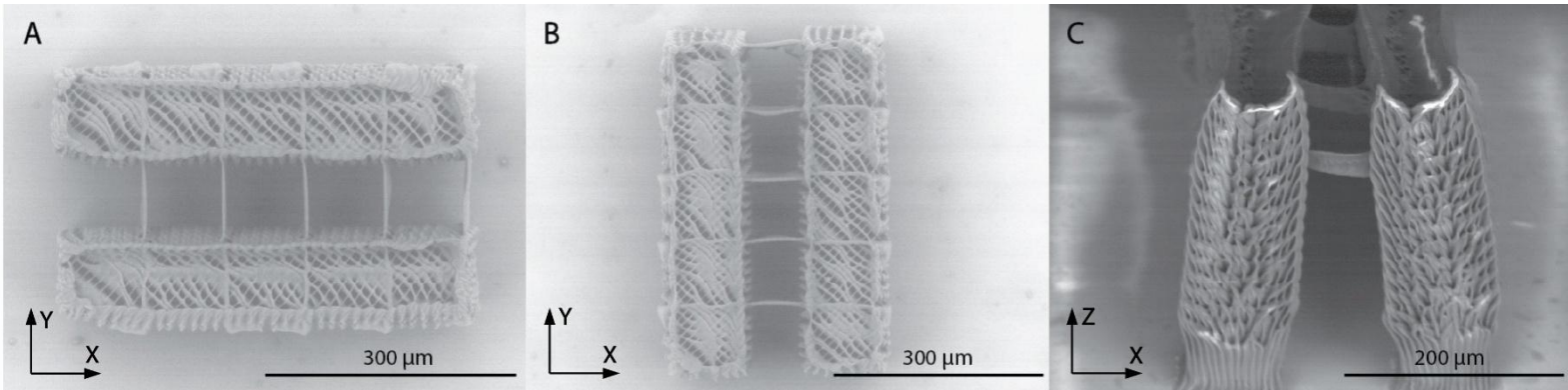


Figure 19 Resolution bridges fabricated with 1 px phase mask. A – resolution bridge for Y axis measurements. B – resolution bridge for X axis measurements. C – resolution bridge for Z axis measurement.

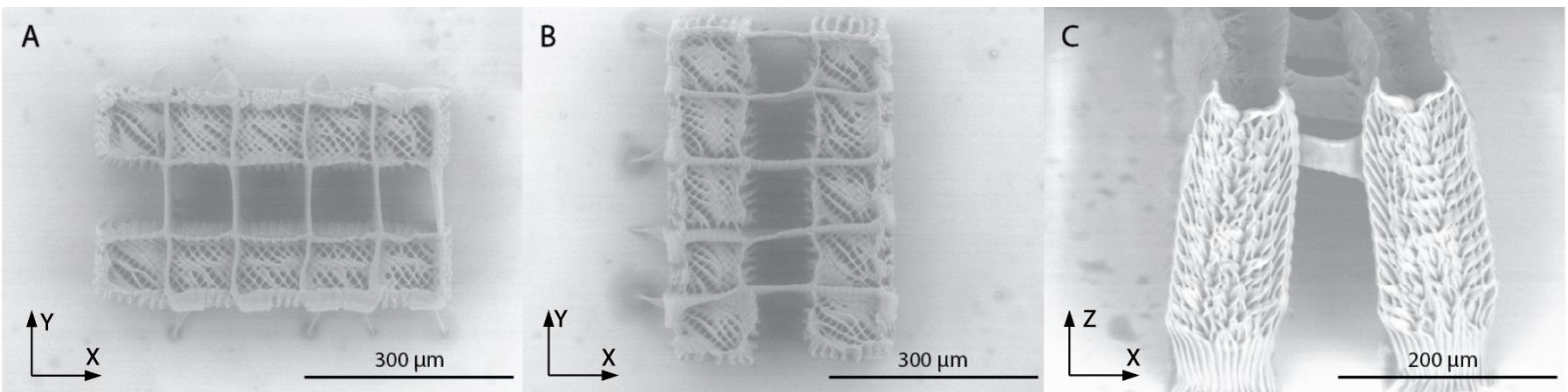


Figure 20 Resolution bridges fabricated with 10 px phase mask. A – resolution bridge for Y axis measurements. B – resolution bridge for X axis measurements. C – resolution bridge for Z axis measurement.

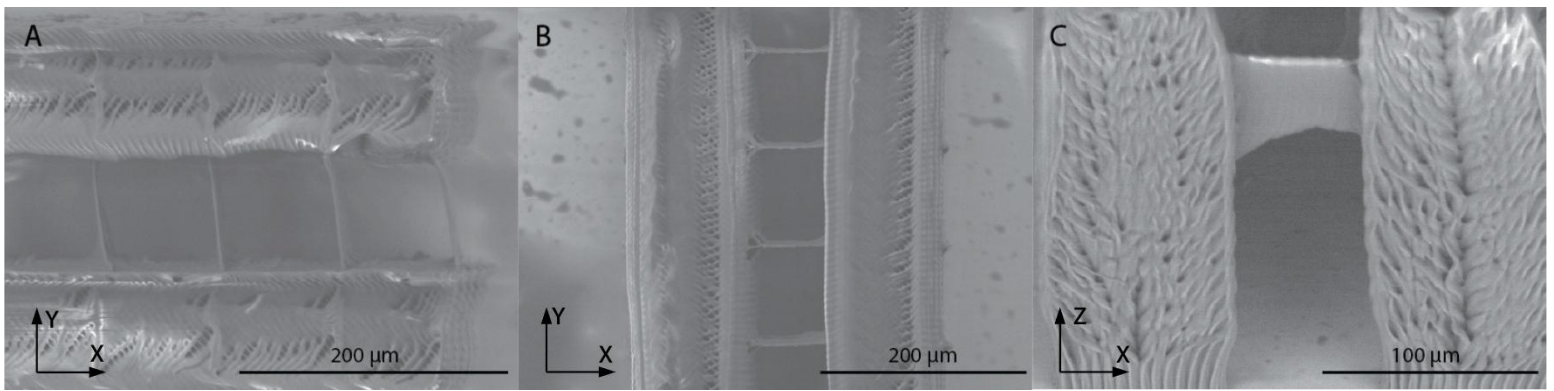


Figure 21 Resolution bridges fabricated with 50 px phase mask. A – resolution bridge for Y axis measurements. B – resolution bridge for X axis measurements. C – resolution bridge for Z axis measurement.

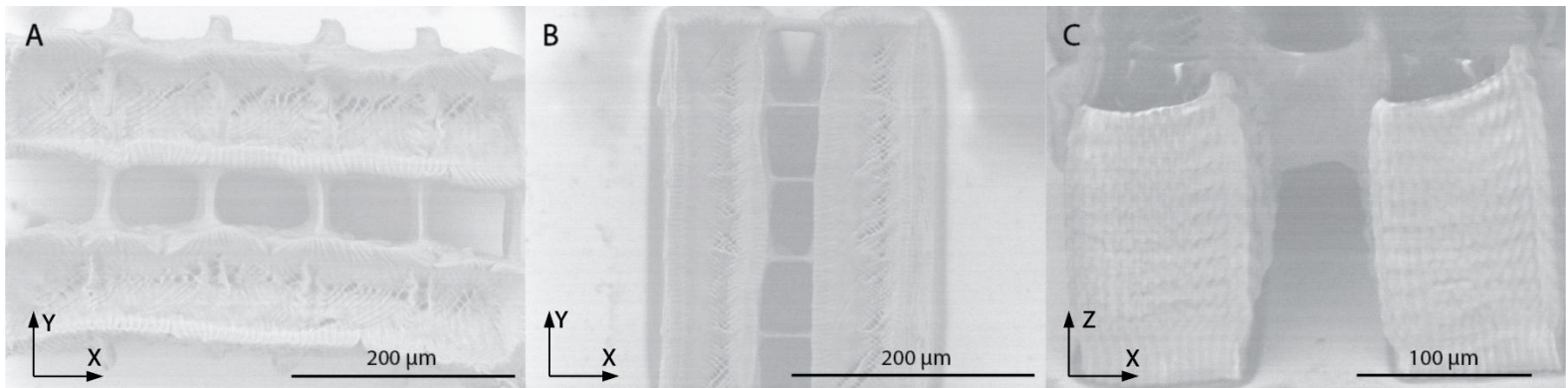


Figure 22 Resolution bridges fabricated with 100 px phase mask. A – resolution bridge for Y axis measurements. B – resolution bridge for X axis measurements. C – resolution bridge for Z axis measurement.

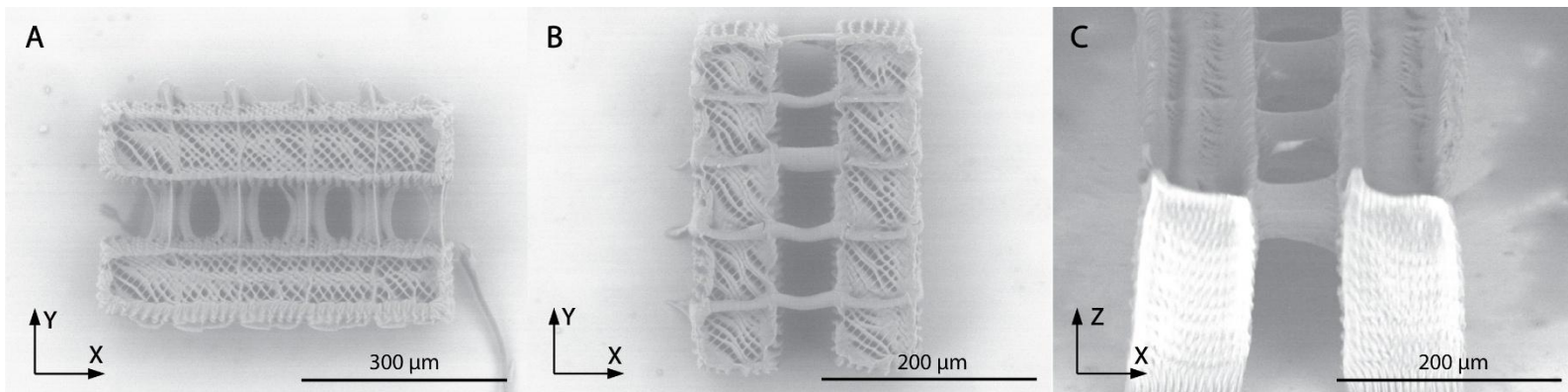


Figure 23 Resolution bridges fabricated with 200 px phase mask. A – resolution bridge for Y axis measurements. B – resolution bridge for X axis measurements. C – resolution bridge for Z axis measurement.

3.4. Voxel characterization with 2PP

For one point on the graph 3-5 lines that were visualized with the SEM, measured and averaged. Additionally, voxel analysis for each phase mask consisted of measuring 5 sets of resolution bridges with different fabrication power settings. The range of laser power used for each phase mask analysis was

determined experimentally by fabricating the microstructures starting with the lowest power setting of 1 mW and gradually increasing it until stable resolution bridges were fabricated.

3.4.1. 1 px phase mask

Figure 24 represents voxel parameters generated from a 1 px phase mask. The graph represents the changes in the voxel parameters as the amount of laser power is increased for printing structures. Voxel generated with 1 px phase mask was characterised by printing the microstructures while increasing the used laser power from 2.5 mW to 4.5 mW.

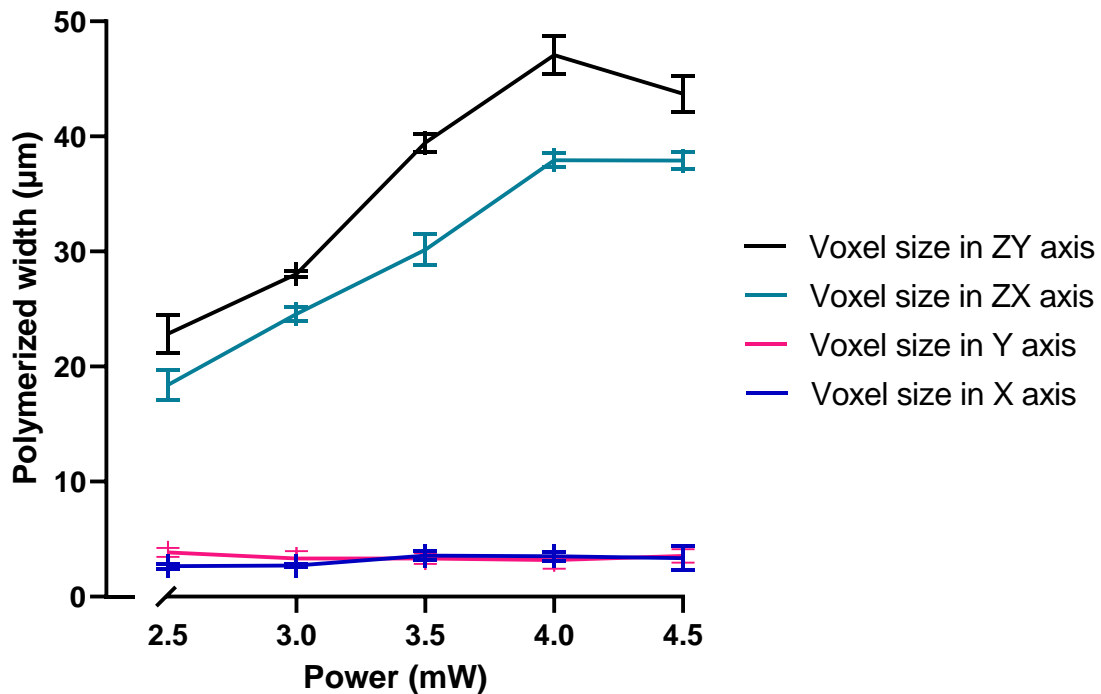


Figure 24 Characteristics of the voxel generated with the 1 px phase mask. The black line represents measurements in ZY axis. Teal line represents measurements in ZX axis. Pink like represents measurements in Y axis. Blue line represents measurements in X axis. Error bars represent the standart deviation of the measurements.

The measurements show that there are no observable difference between the lines generated in X and Y axes. The smallest measurement was observes in the X axis – $2.63 \mu\text{m} \pm 0.24 \mu\text{m}$. The biggest measurement was observed in Y axis – $3.83 \mu\text{m} \pm 0.41 \mu\text{m}$. Voxel expansion in Z axis was observed to be about 10 times greater than the width of the lines measured in X and Y axes. The hight of the voxel observed in the ZY axis configuration resolution bridges reached $47.06 \mu\text{m} \pm 1.67 \mu\text{m}$, while the height of voxel in the ZX axis reached only $37.93 \mu\text{m} \pm 0.61 \mu\text{m}$. in height at their maximum. Measurements in

Z axis present a trend that the voxel expands while the amount of power used for fabrication is increased. We do not observe this trend in X and Y axis measurements within margin of error.

3.4.2. 10 px phase mask

Figure 25 represents measurements taken from resolution bridges printed with a 10 px phase mask. In the graph we can see how the observable voxel parameters change depending on the amount of laser power used for microstructure generation. The lines on each resolution bridge were generated under laser powers spanning from 4.0 mW to 6.0 mW.

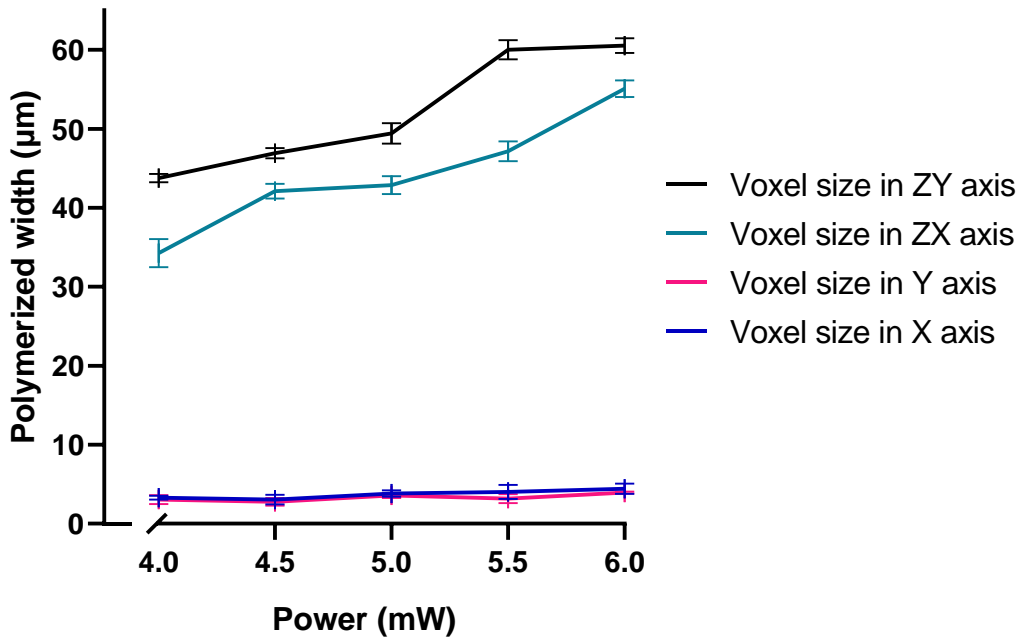


Figure 25 Characteristics of the voxel generated with the 10 px phase mask. Black and teal lines represent measurements in Z axis (black – ZY, teal – ZX). Blue line represents measurements in X axis while pink represents the Y axis. Error bars indicate the standard deviation of the measurements.

The graph visualises that there are no observable differences between X and Y axes. Even with the increase of laser power used for microstructure generation the width of the voxel remains relatively the same. The maximum width for both X and Y axes is $4.41 \mu\text{m} \pm 0.64 \mu\text{m}$ and the minimal observed width is $2.77 \mu\text{m} \pm 0.47 \mu\text{m}$. In case of measurements of the Z axis we can observe an increase in voxel length correlating with the increased laser power used for microstructure generation. Overall the voxel expands from $34.24 \mu\text{m} \pm 1.80 \mu\text{m}$ to $55.07 \mu\text{m} \pm 1.05 \mu\text{m}$ observed in the ZX axis and from $43.75 \mu\text{m} \pm 0.52 \mu\text{m}$ in the ZY axis.

3.4.3. 50 px phase mask

Figure 26 illustrates the data gathered from measurements of microstructures printed with the optimized 50 px phase mask. The graph presents a trend of rapidly increasing length of the voxel as the used laser power increases. We do not observe such an increase in width while observing changes in X and Y axes. Laser power was set from 4.0 mW to 6.0 mW to fabricate the lines on the resolution bridges.

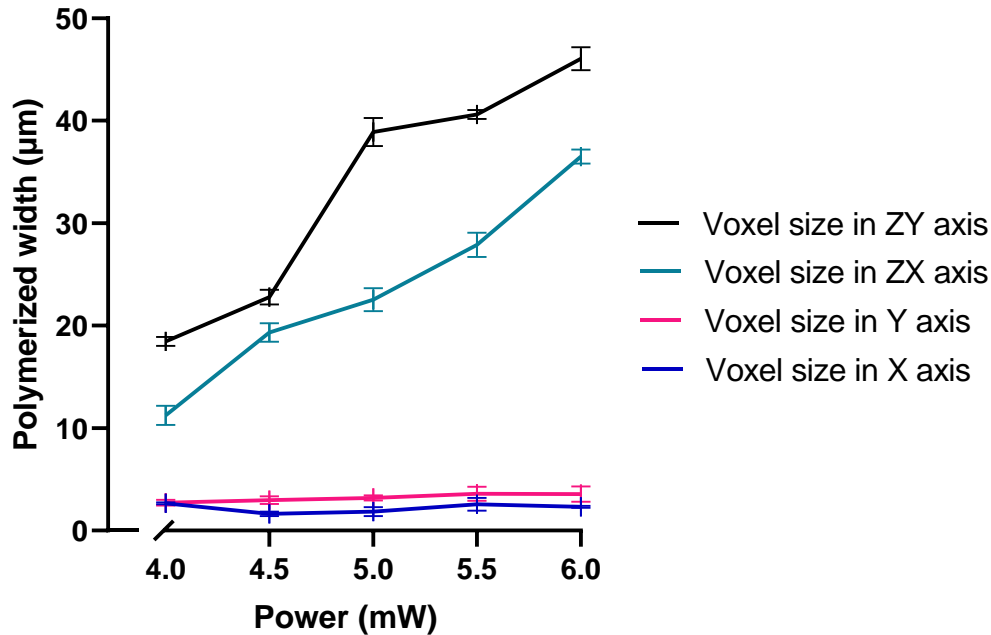


Figure 26 Voxel parameters generated with a 50 px phase mask. Black and teal lines accordingly represent measurements in ZY and ZX axes. Blue and pink lines represent the X and Y axes accordingly. Error bars indicate the standard deviation of the measurements.

X and Y axes remain relatively consistent with their measured widths even after increasing the fabrication power. The polymerized line has a greater width in the Y axis when compared with the X axis. The lowest value observed in X axis reached $1.62 \mu\text{m} \pm 0.22 \mu\text{m}$, while the highest observed value was $2.66 \mu\text{m} \pm 0.08 \mu\text{m}$. The width of the Y axis remained relatively consistent as well with the lowest measurement reaching $2.73 \mu\text{m} \pm 0.31 \mu\text{m}$ and the highest measurement reaching $3.59 \mu\text{m} \pm 0.68 \mu\text{m}$. ZX and ZY values rapidly increase as the fabrication power increases. The voxel reaches its maximum at $46.04 \mu\text{m} \pm 1.14 \mu\text{m}$ in ZY measurements at the same time the minimal value of ZY was measured to be $18.47 \mu\text{m} \pm 0.43 \mu\text{m}$. ZX values also exhibit rapid growth with increasing power. The minimal value was measured to be $11.25 \mu\text{m} \pm 0.95 \mu\text{m}$ and the maximal value was measured to be $36.49 \mu\text{m} \pm 0.67 \mu\text{m}$.

3.4.4. 100 px phase mask

Figure 27 represents the data gathered by measuring the resolution bridges printed with a phase mask which contained a 100 px gray-scale line drawn on a black canvas. Overall, the graph reveals how voxel parameters change by increasing the laser power for fabricating the resolution bridges. The lines on the resolution bridges were fabricated in a power range of 12.0 mW – 14.0 mW.

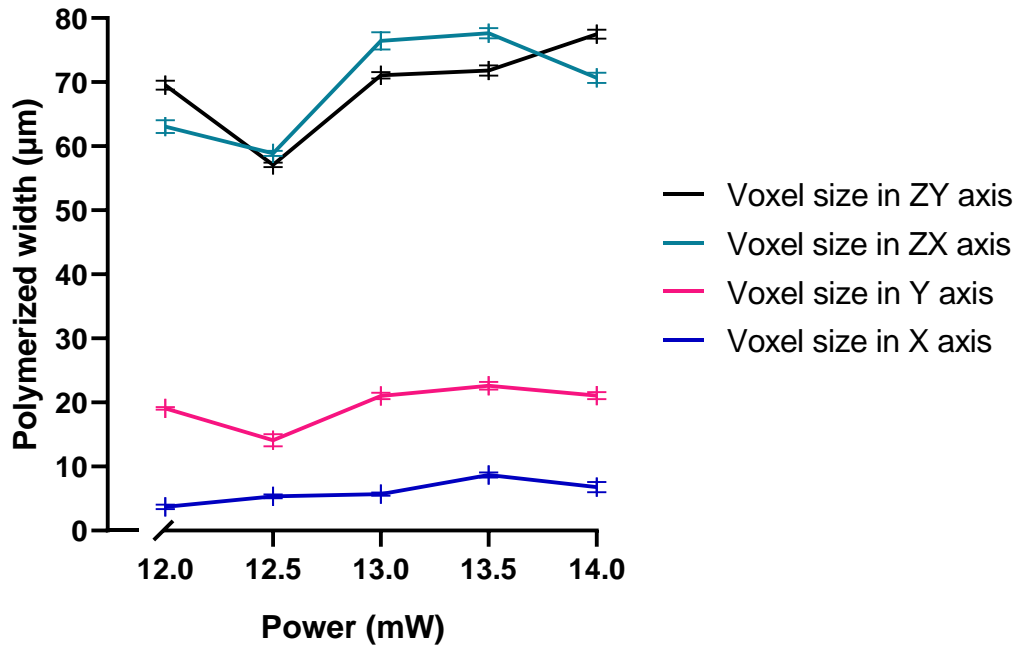


Figure 27 Voxel dimensions were recorded using a 100-pixel phase mask. The black and teal lines correspond to the ZY and ZX planes, while the blue and pink lines correspond to the X and Y axes. Error bars indicate the standard deviation of each data set.

Voxel size in X axis showed a mild increase correlating with the increase of laser power used during fabrication. However, it is the smallest increase in width compared to other voxel parameters generated with this phase mask. The smallest value was measured to be $3.72 \mu\text{m} \pm 0.38 \mu\text{m}$ while the biggest value was measured to be $8.67 \mu\text{m} \pm 0.41 \mu\text{m}$. Voxel size in Y axis was roughly two to three times bigger than observed in the X axis. The smallest width measured in Y axis consisted of $14.12 \mu\text{m} \pm 0.85 \mu\text{m}$, while the biggest width was measured to be $22.63 \mu\text{m} \pm 0.63 \mu\text{m}$. Overall, ZX and ZY parameters were both increasing as the laser power was increased during fabrication. The highest voxel value was observed in ZX configuration – $77.65 \mu\text{m} \pm 0.79 \mu\text{m}$, while the smallest measurement in ZX configuration reached $58.87 \mu\text{m} \pm 0.42 \mu\text{m}$. Voxel values in ZY configuration were observed to reach $77.47 \mu\text{m} \pm 0.71 \mu\text{m}$ at their height and $57.09 \mu\text{m} \pm 0.37 \mu\text{m}$ at their lowest point.

3.4.5. 200 px phase mask

Figure 28 summarizes the measurements taken from microstructures fabricated with an optimized 200-pixel phase mask. The measurement results reveal that voxel length grows sharply as laser power rises during fabrication, while voxel width remains essentially unchanged along the X and again has a sharp increase correlating with the used power in the Y direction. The resolution-bridge lines were produced using laser powers between 20.0 mW and 28.0 mW.

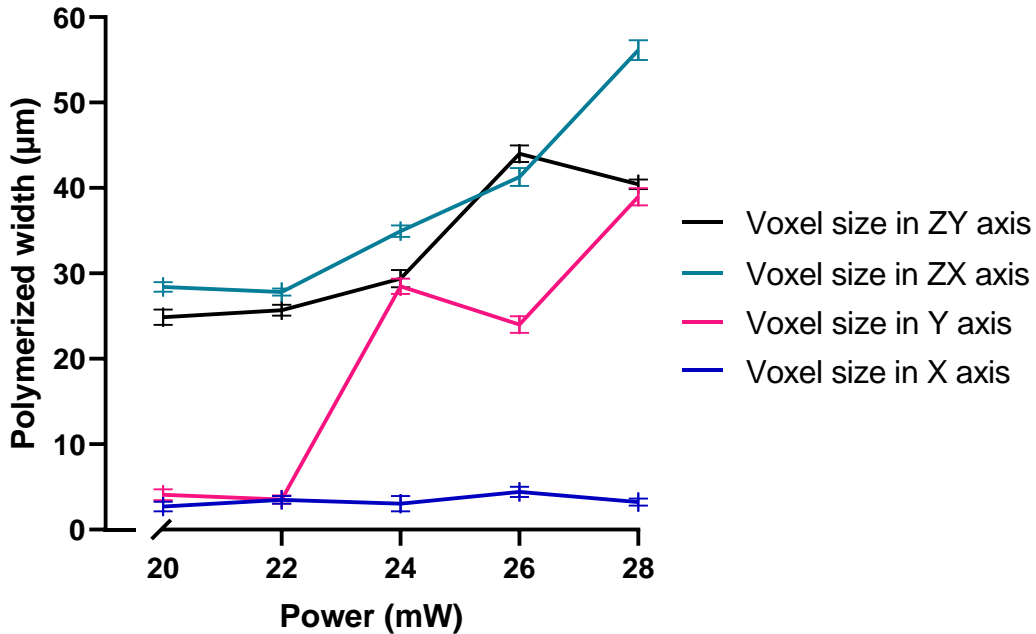


Figure 28 The 200pixel phase mask was used for voxel parameter generation. The ZY and ZX directions are charted in black and teal, whereas the X and Y directions appear in blue and pink. Error bars indicate the associated standard deviations.

Measurements taken in X axis show no correlation with the increasing laser power. The voxel size remains relatively consistent throughout the measurements reaching its maximum at $4.42 \mu\text{m} \pm 0.59 \mu\text{m}$ and minimum at $2.70 \mu\text{m} \pm 0.57 \mu\text{m}$. Measurements in Y axis show a steep increase at 22 mW mark. The voxel size increases from just $3.54 \mu\text{m} \pm 0.51 \mu\text{m}$ to $28.48 \mu\text{m} \pm 0.89 \mu\text{m}$ as the fabrication power increases. The maximum voxel size in Y axis reached $38.98 \mu\text{m} \pm 1.32 \mu\text{m}$. Voxel size in ZX and ZY also show an increase in size correlating with the increase of used power for microstructure fabrication. As the applied power increases the voxel size goes from $27.80 \mu\text{m} \pm 0.42 \mu\text{m}$ to $56.14 \mu\text{m} \pm 1.16 \mu\text{m}$ in ZX axis. At the same time, in ZY axis the voxel size expands from $24.88 \mu\text{m} \pm 0.82 \mu\text{m}$ to $43.99 \mu\text{m} \pm 0.93 \mu\text{m}$.

3.5. Scaffold printing for cell seeding

If the spheroidal model described in section 2.5. of the work was printed with the 1 px phase mask the entire structure would be completed in 2 days and 5 hours. Such print time is unacceptable and not compatible with the capacity that is needed for these structures to completely carry out cell seeding experiments. However, the voxel parameters that were obtained by printing the resolution bridges allowed to tune the used phase mask and printing parameters for spheroidal structure production. After measuring the voxel characterisation in 3D space a 200 px phase mask was picked for printing the spheroidal structure for cell seeding. Overall, the print time for spheroidal structures went from 2 days and 5 hours to just 30 minutes per spheroid. At hatching step of 1 μm and slicing step of 10 μm the print took 53 hours. When applied the 200 px phase mask a hatching step of 20 μm and a slicing step of 45 μm was applied, which shortened the printing time to about 30 minutes.

The spheroidal model was once trial printed to 30 % and 80 % completion to visualise the inner channels and pores to make sure that the finished structures features were up to standart. Later full sutructure was printed and used for cell seeding by the National Cancer Institute of Lithuania (Figure 29).

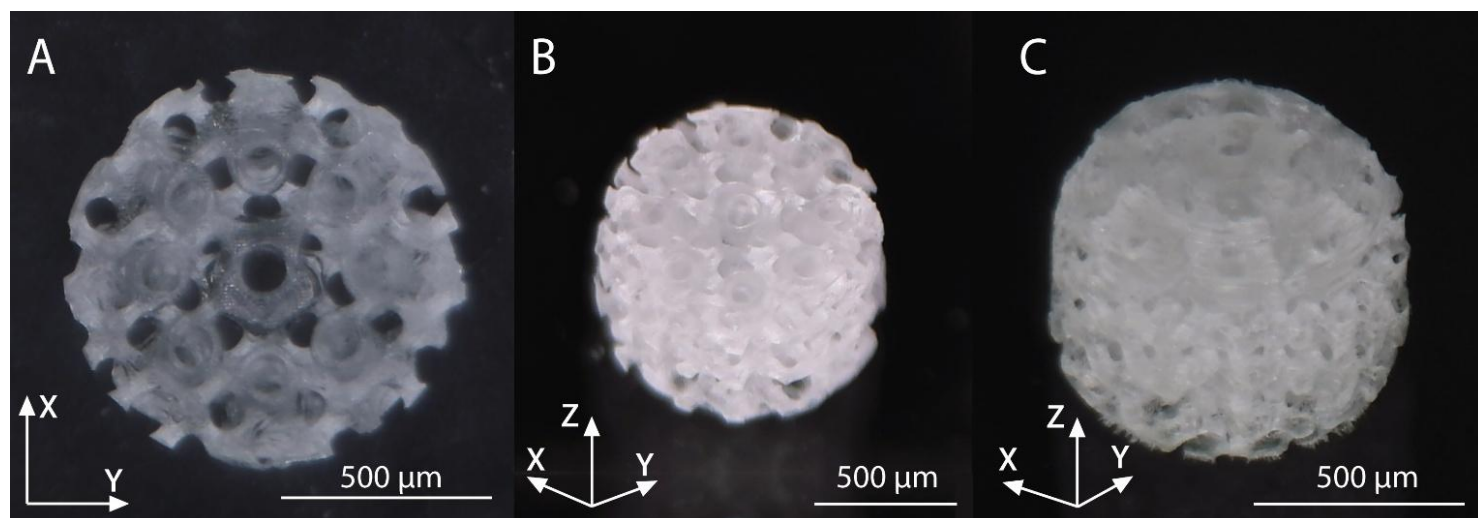


Figure 29 Printed spheroidal structures used for cell seeding. A – 1/3 of the spheroidal structure printed, with 100 μm pores. B – 2/3 of the spheroidal structure printed, with 100 μm pores. C – fully printed structure 1 cm in XYZ axes, with 100 μm pores.

4. Discussion

Results presented in this work showcase the current capabilities of phase mask generation software and how it can be applied for phase mask optimisation. The generated phase masks were analysed by using the Z-scan which allowed to determine their what actual intensity distributions they allow to achieve in 3D. Phase mask optimisation then took place by attempting to minimise the random elongated peaks present in data generated from Z-scan. Then the optimised phase masks were used during 2PP printing so that voxel parameters could be determined in 3D space. The phase mask with the best characteristics was used for organoid scaffold printing and the development process went from taking over 2 days to completion in just over 30 minutes. When determining which phase mask would be best suited to print the scaffolds for cell seeding the measured voxel parameters were compared in X, Y and Z planes. When comparing the voxel sizes in X axis it becomes apparent that despite the phase mask differences in length and applied modifications – the polymerized voxel width stays relatively similar (Figure 30).

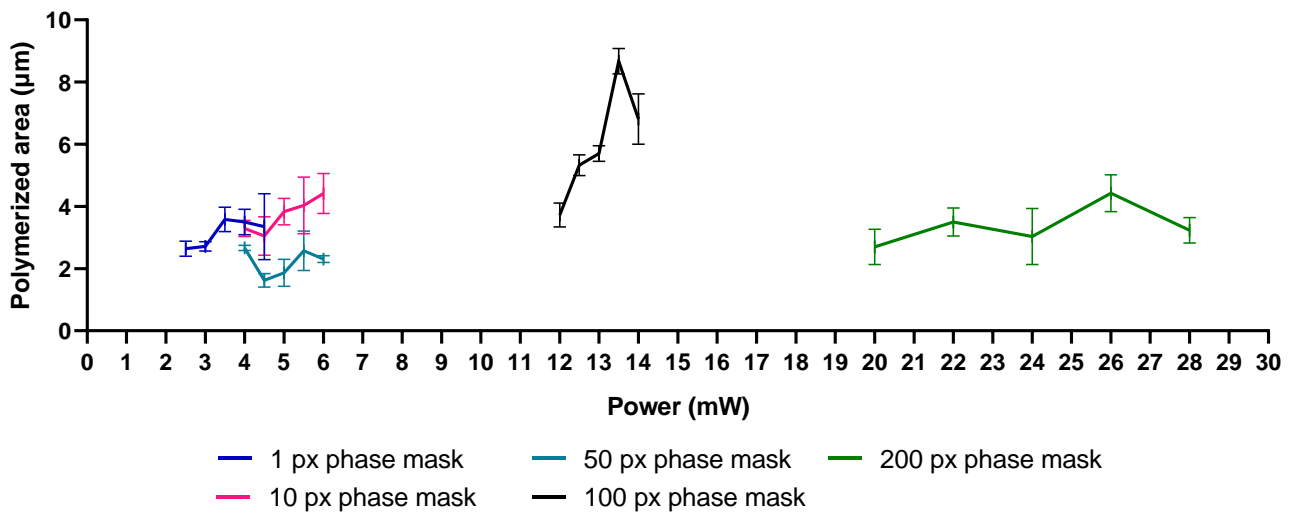


Figure 30 Voxel size comparison in the X axis. The blue line indicates a 1 px phase mask. Pink line indicates 10 px phase mask. Teal line indicates a 50 px phase mask. Black line indicates a 100 px phase mask. The green line indicates a 200 px phase mask.

1 px, 10 px, 50 px and 200 px phase mask on average generated a line 3.50 µm in width. However, it is important to note that the more pixels are used in a phase mask generation the bigger power output it requires to generate the polymerized lines of the same size. Every voxel must experience a peak intensity above the material's polymerization threshold to print a line. Therefore, when more pixels are used in phase mask generation the available pulse energy is divided among a larger set of diffraction orders, so the dose of power delivered to each voxel falls. This in turn explains why a 200 px phase mask

requires about $10\times$ more power to print a line of the same width as a 1 px, 10 px or 50 px phase mask. Jumping from the 10 px to the 200 px phase mask increases the threshold from 5 mW to 25 mW. Surprisingly the 50 px phase mask resulted in the smallest voxel width in X axis reaching only $2.20\ \mu\text{m}$. This can be attributed to the fact that this phase mask only reached the size of $0.66\ \text{cm}$ in the Z-scan and had the least amount of generated intensity peaks when compared to other phase masks. The intensity distribution generated for the 50 px phase mask was the most uniform compared with other generated phase masks. The polymerized area in X axis changed from $1.62\ \mu\text{m}$ to $8.67\ \mu\text{m}$.

When it comes to the Y axis 1 px, 10 px and 50 px phase mask on average generated a line $3.50\ \mu\text{m}$ in width. The measurements are nearly identical to the measurements of the X axis, which would mean that the voxel generated from these phase masks resembles a shape of a circle (Figure 31).

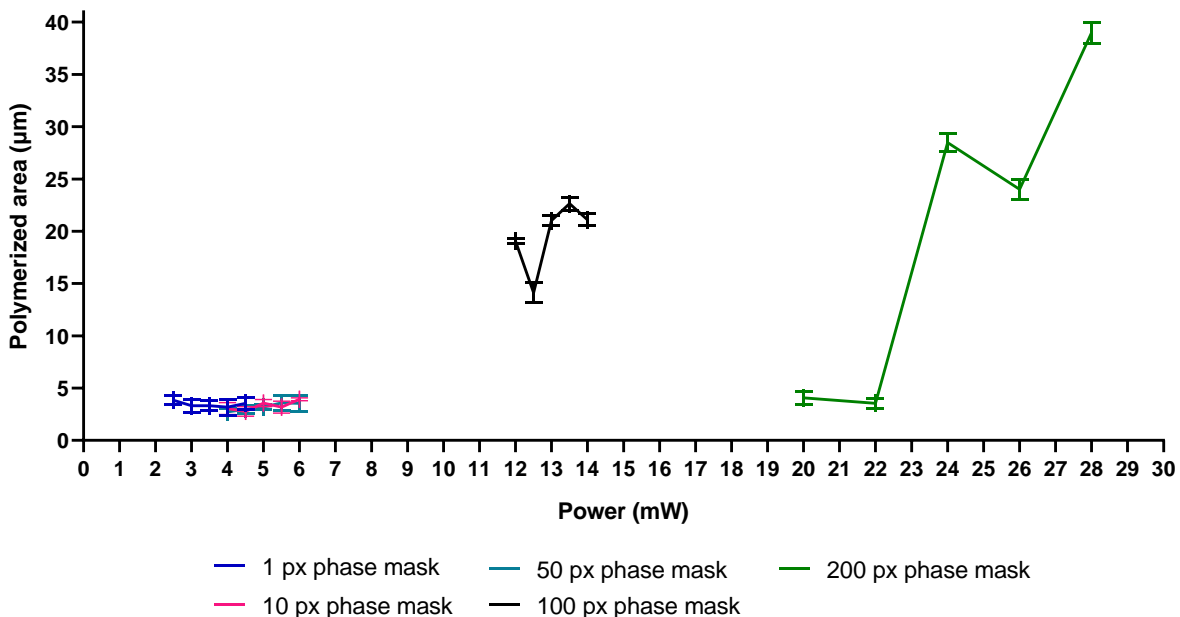


Figure 31 Voxel size comparison in the Y axis. The blue line indicates a 1 px phase mask. Pink line indicates 10 px phase mask. Teal line indicates a 50 px phase mask. Black line indicates a 100 px phase mask. The green line indicates a 200 px phase mask.

Additionally, this reinforces the claim in section 3.2. that modifications to the precursor phase masks of 1 px and 10 px do not generate any difference. The 50 px phase masks, although different from 1 px and 10 px phase masks still generates a line of similar parameters. This can be attributed to the fact that it concentrates energy in one dominant peak. That keeps the effective dose profile close to the single-Gaussian baseline, so the printed line width results in $3.50\ \mu\text{m}$. Additionally, 50 px phase mask operates in a similar power range during fabrication. However, the tendency of the bigger number of pixels in the phase masks the more power needed for fabrication - remains. Starting from 100 px there is an observable

increase of a polymerized area in fabrication going from 3.59 μm observed in 50 px phase mask to 22.63 μm , observed with a 100 px phase mask. On average 100 px phase mask reached 21.08 μm . A 200 px phase mask generates an even wider voxel on average reaching about 39.05 μm . In case of 200 px phase mask the voxel size went up from 3.54 μm to 38.98 μm . It is important to note that the 200 px phase mask began fabricating a wider voxel exhibited threshold-like behavior, starting to widen only after certain power was reached. At 20-22 mW the 200 px phase mask generated a voxel with the same width parameter as 1 px, 10 px or 50 px phase masks.

Figure 30 illustrates the comparison of voxel height in Z planes. There is a persistent correlation between an increasing amount of power used in fabrication and the increasing voxel size. 1 px and 10 px phase masks show that while using this phase mask the voxel grows nearly linearly with power. The 10 px phase mask expands at a similar rate to a 1 px phase mask. 1 px phase mask on average expands from 20.61 μm to 42.49 μm . However, the 10 px phase mask generates a voxel of a greater size than the 1 px phase mask expanding from 38.95 μm to 57.79 μm . The 1-pixel and 10-pixel phase masks draw relatively narrow lines in X and Y, but their voxels are tall in Z, so using them for printing tiny, precise features may be difficult. The 50 px phase mask, despite the higher pixel count, still polymerizes less area per watt — evidence that this mask concentrates light into a tighter, more uniform voxel, which positions the 50 px phase mask as the most optimal for fine feature printing. The 50 px phase mask expands from 14.86 μm to 41.26 μm . In the case of the 100 px phase mask a big jump in both threshold and printed size is observed going from 66.3 μm to 77.56 μm . Together with the voxel characteristics from X and Y planes it positions this phase mask as a valuable tool for large size structure generation. As the intensity distribution measurements suggested, the 200 px phase mask was overall shorter than the 100 px phase mask. In turn when applied experimentally the 200 px phase mask generated a smaller polymerized area in the Z axis when compared to the 100 px even at higher power going from 26.65 μm to 50.06 μm . Since the phase mask has 2 \times more pixels the same pulse energy is shared among more diffraction orders, therefore only a narrow region polymerizes (Figure 32).

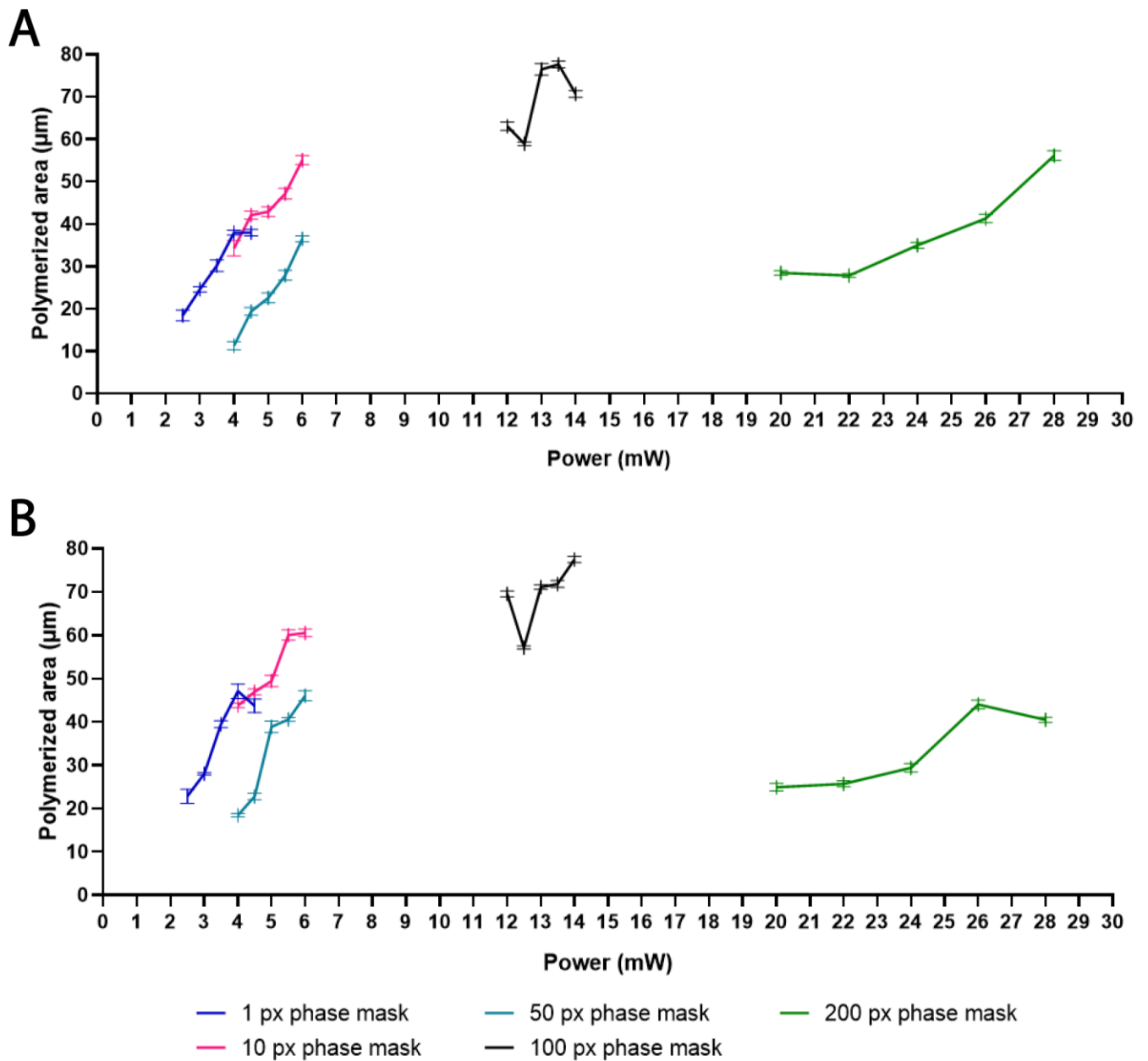


Figure 32 Voxel size comparison in the Z axis. A – illustrates the ZX plane. B – illustrates the ZY plane. The blue line indicates a 1 px phase mask. Pink line indicates a 10 px phase mask. Teal line indicates a 50 px phase mask. Black line indicates a 100 px phase mask. The green line indicates a 200 px phase mask.

Overall, low-threshold or heat-sensitive resins may be difficult to work with once you reach the 100- or 200-px phase masks, because the laser power needed to exceed threshold approaches levels that risk burning or ablation.

Voxel characterisation provided a necessary backbone to determine how the parameters for organoid scaffold should be modified to increase the efficiency of their fabrication. The originally used 1 px phase mask can only fabricate a voxel sizes of 3.15 µm in X axis, 3.43 µm in Y axis and 33.00 µm

in Z axis. While the 200 px phase mask can generate a voxel with parameters of 4.42 μm in X axis, 39.98 μm in Y axis and 56.14 μm in Z axis. The expanded voxel in the Y axis allowed to thin out the dense hatching of a printed spheroid model (Figure 33).

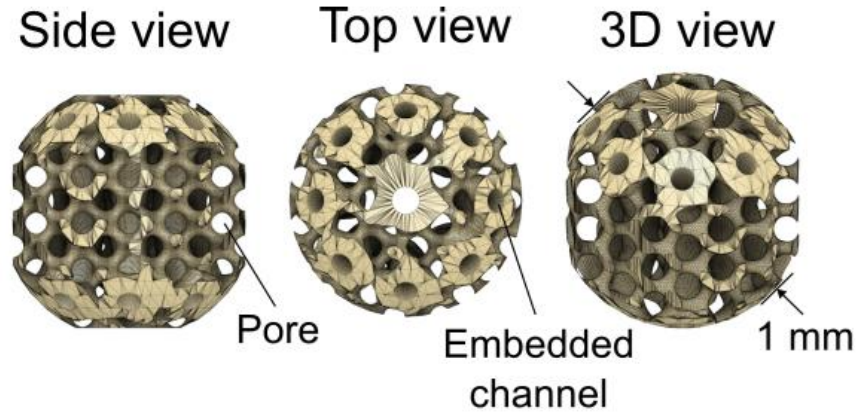


Figure 33 Cell seeding scaffolds showing main components and dimensions. Pore size – 100 μm (Vitkūnaitė et al., 2024).

The modified printing parameters allowed to fill the volume of the print much faster, which in turn greatly shortened the overall printing time. The spherical structure was being developed for cancer culture modeling and cancer cell seeding (Zhu et al., 2016). Scaffold-based 3D culture development models ensure that the cell cultures are formed uniformly if the used scaffold structure is optimized to the cell (Berens et al., 2015). Since there isn't a single standard diameter for a cancer cell, because cell sizes vary depending on the tumor type (e.g. small-cell lung carcinoma vs giant-cell sarcomas), cell cycle stage and ploidy and finally whether the cell culture line was developed from the primary - tumor tissue or circulating tumor cells. For most common cancers you can expect individual cells to be $\sim 12\text{--}20\ \mu\text{m}$ in diameter, roughly $1\frac{1}{2}\text{--}3$ times the size of a red blood cell ($6\text{--}8\ \mu\text{m}$) (Q. Li et al., 2015; Hao et al., 2018). Rare “giant” tumor cells or polyploid sub-populations can exceed $30\ \mu\text{m}$, while highly compact “small-cell” phenotypes can be below $10\ \mu\text{m}$, but those are exceptions rather than the norm (J. Liu et al., 2022). For the initial trials of the spheroidal structure it was decided to create a construct with consistent $100\ \mu\text{m}$ pores to ensure that the cells could move freely through it, interact with it, form colonies and hopefully to still have enough room to increase the metabolism of the 3D cell culture (Taniguchi et al., 2016; Han et al., 2021). The developed scaffolds were used to carry out a cell seeding study by Vitkūnaitė et al. (2024). Two human ovarian cancer cell lines (SKOV3 and A2780) were seeded on scaffolds printed from OrmoClear or PEGDA with 1 % w/v Irgacure 2959 photoinitiator. The main aim of the study was to analyze if the scaffold made a difference in cell culture development. The seeding experiment showed

that cells were quite receptive to the provided scaffold and the cell line A2780 that normally did not form organoid scaffolds, formed a uniform cell culture. Close to 150 scaffolds were produced to accommodate the experiment. (Figure 34). The used spherical scaffold was preferred by the cells in comparison to a cubic one used parallel in the study by Vitkūnaitė et al. (2024).

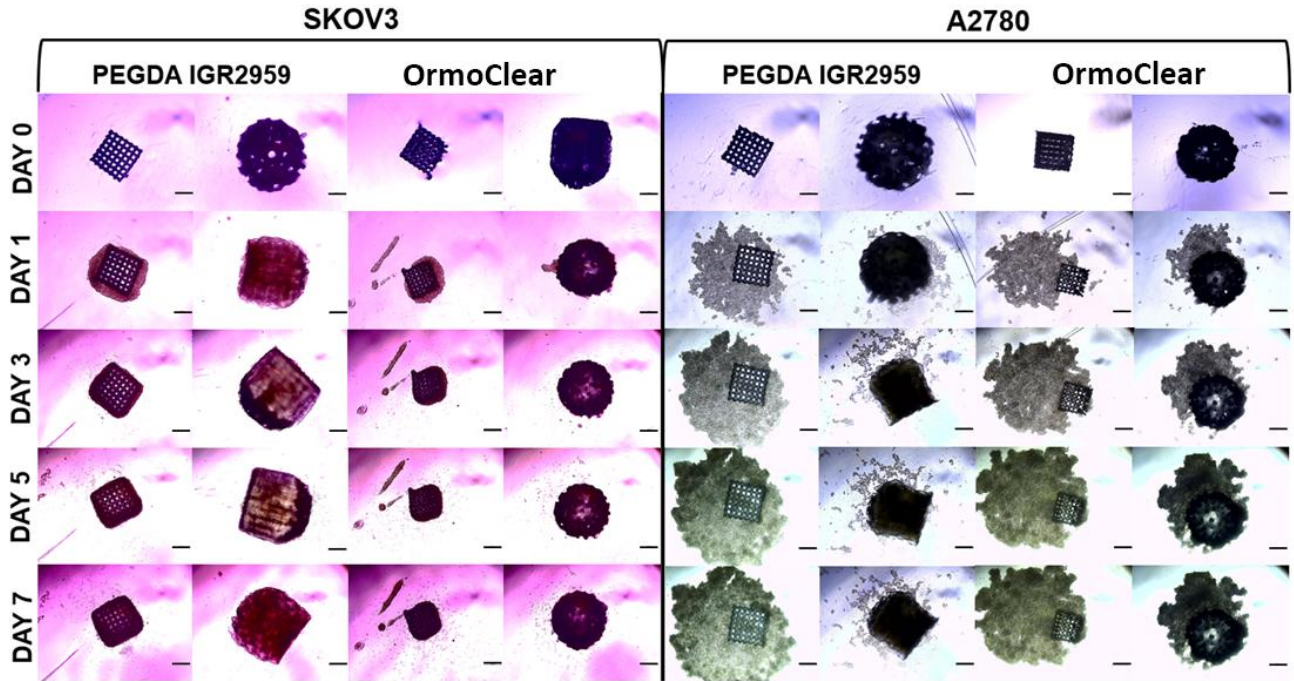


Figure 34 Images visualizing cell growth of the ovarian cancer cell lines SKOV3 and A2780. 3D cell cultures were grown on different scaffolds between 0 and 7 days. The scale bar represents 300 μm (Vitkūnaitė et al., 2024).

To get a better understanding of how scaffolds affect 3D cell culture formation an additional gene evaluation experiment was carried out. In SKOV3 cell line there were no noticeable differences when compared to the control group. However, the A2780 cell line showed heightened expression when it was grown on the printed scaffolds. The study revealed that the material used for scaffold printing made no impact on the 3D cell culture development as long as it was biocompatible and that the presence of scaffolds elevated 3D cell culture generating abilities for the cell lines that normally do not form that type of construct (Vitkūnaitė et al., 2024).

Developing 3D cell culture techniques that more accurately model cancer tumor microenvironment is a major focus area for many scientists. It has been shown that incorporating scaffolds for cell culture development results in more accurate tissue modeling (Campuzano & Pelling, 2019; Weisgrab et al., 2020; C. Li et al., 2023; Dozzo et al., 2023). Highly viscous scaffolds can enhance the stemness of cancer cell lines. Providing more insights into tumor development (Wu et al., 2023). Aside from cellular

behavior being affected by scaffolds, the tumor chemoresistance is also affected by the biochemical and physical properties of the material used for scaffold development. For example ovarian cancer cells grown on softer substrates were less sensitive to chemotherapeutic agents (Paradiso et al., 2022). Similarly, the usage of hyaluronic acid matrices reduced chemotherapy induced apoptosis by around 50 % in glioma and lung cancer models (Xiao et al., 2020). Scaffolds have also been used for self-mineralization of bone organoids *in vitro* (J. Wang et al., 2024) or even cortical organoids (Cadena et al., 2024). Additionally, an open porous architecture of the scaffold provides transport channels for cell migration, mass transport of cell nutrient and waste and support cell signaling. The range of pore sizes of the scaffold also influences cell behavior. Micro pores of 100 nm – 5 µm facilitate cell attachment, 5 µm – 250 µm pores allow cell infiltration and migration throughout the scaffold and finally large pores – over 250 µm support neo vascularization (Jackson et al., 2023). To create more physiologically accurate cell cultures, the developed scaffolds must be highly sophisticated and defined. Creating pore gradients that would mimic the natural progression of organ or tumor development.

Many scaffold development techniques have been developed over the years, however most of them have significant drawbacks when it comes to cell culture development, their development or scalability. Hydrogels, although closely match the native ECM and enable efficient nutrient, oxygen and waste transport have limited mechanical strength and are sensitive to sterilization protocols (Habanjar et al., 2021; Nerger et al., 2024). Electrospun scaffolds provide a high surface area for cellular attachment and are easily scalable. However, there is limited thickness and chaotic pore production (Piscitelli et al., 2024). Lyophilized scaffolds provide a complex interconnected microporous network. At the same time lyophilized scaffolds offer little to no control over pore sizes and are brittle (Anderson & Segura, 2022). Stereolithography provide highly reproducible scaffolds, however provide an overall low resolution in addition to being a slow process (Kumar & Kim, 2020). Scaffolds produced with 2PP can easily overcome these issues. This technology provides resolution up to 1.62 µm in X, 2.77 µm in Y and 11.25 µm in Z axes. 2PP can even reach resolutions of 100 nm, at the same time allowing to build centimeter-scale structures (Jonušauskas et al., 2018). True 3D freedom allowing to meticulously tune pore sizes or create structures specifically engineered for the needs of the cells (Jonušauskas et al., 2016; El-Tamer et al., 2020). Not to mention the vast range of biocompatible materials, that can be used for scaffold printing (Kufelt et al., 2015; Ežerskytė et al., 2022; Vitkūnaitė et al., 2024). Additionally, 2PP can be easily applied to bioprinting, since the printing process uses visible or infrared radiation, minimizing cellular damage via UV. Plus, 2PP is a cold process that further proves its adaptability for bioprinting applications (Kufelt et al., 2015). The main drawbacks of the 2PP process is possible

photoinitiator toxicity and the overall slow printing process. Photoinitiator toxicity can be mediated by using biocompatible photoinitiators like Irgacure 2959 and Lithium phenyl-2,4,6-trimethylbenzoyl-phosphinate (LAP). Finally, this work shows that by integrating spacial light modulation, the throughput of the printing process can be increased making the scaffold production a more scalable process.

Using polymer scaffolds for cell culture development not only provides a biomimetic environment of natural tissues but also recreates the ECM fostering cell proliferation and differentiation. All in all, this creates a versatile platform for studying complex cellular behavior and holds immense promise for individualized therapy development. Since 2PP is such a versatile tool, all that is really needed for cellular scaffold development is a clear liquid material and a biocompatible photo initiator. With further research multi-voxel printing can be developed to elevate the printing process even further and broaden the scaffold development capabilities even finally reaching true bioprinting.

Conclusions

1. 5 phase masks were optimized (1 px, 10 px, 50 px, 100 px, 200 px) and their respective voxels were characterized in X, Y, Z planes.
2. Gray scaling experiments showed no effect on intensity distributions of 1 px and 10 px phase mask.
3. Resolution bridge measurements proved that voxel can be horizontally elongated in one direction from 3.54 μm to 38.98 μm while maintaining comparatively similar voxel height at around 48.54 μm .
4. Organoid scaffold printing optimized to take only 30 minutes instead of 53 hours.
5. This work proved that while GS algorithm is sufficient for optimizing voxel shape for organoid scaffold printing, due to its inherent randomness further works should be pursued in the direction of creating more advanced mathematical algorithm for phase mask generation, especially towards greater control of uniformity in Z direction.

Supplementary

In this work an AI (Grammarly: <https://www.grammarly.com>) tool for grammar control and text editing was used in order to make the text more coherent and presentable.

References

- Abdul Samat, A., Abdul Hamid, Z. A., Jaafar, M., Ong, C. C., & Yahaya, B. H. (2023). Investigation of the In Vitro and In Vivo Biocompatibility of a Three-Dimensional Printed Thermoplastic Polyurethane/Polylactic Acid Blend for the Development of Tracheal Scaffolds. *Bioengineering (Basel, Switzerland)*, *10*(4), 394. <https://doi.org/10.3390/bioengineering10040394>
- Abuwatfa, W. H., Pitt, W. G., & Husseini, G. A. (2024). Scaffold-Based 3D Cell Culture Models in Cancer Research. *Journal of Biomedical Science*, *31*, 7. <https://doi.org/10.1186/s12929-024-00994-y>
- Additive Manufacturing Technology—An overview* | *ScienceDirect Topics*. (n.d.). Retrieved December 17, 2024, from <https://www.sciencedirect.com/topics/engineering/additive-manufacturing-technology>
- Alam, F., Shukla, V. R., Varadarajan, K. M., & Kumar, S. (2020). Microarchitected 3D Printed Polylactic Acid (PLA) Nanocomposite Scaffolds for Biomedical Applications. *J. Mech. Behav. Biomed. Mater.*, *103*, 103576.
- Alammar, A., Kois, J. C., Revilla-León, M., & Att, W. (2022). Additive Manufacturing Technologies: Current Status and Future Perspectives. *Journal of Prosthodontics*, *31*(S1), 4–12. <https://doi.org/10.1111/jopr.13477>
- Amin Yavari, S., Loozen, L., Paganelli, F. L., Bakhshandeh, S., Lietaert, K., Groot, J. A., Fluit, A. C., Boel, C. H. E., Alblas, J., Vogely, H. C., Weinans, H., & Zadpoor, A. A. (2016). Antibacterial Behavior of Additively Manufactured Porous Titanium with Nanotubular Surfaces Releasing Silver Ions. *ACS Appl. Mater. Interfaces*, *8*, 17080.
- Anderson, A. R., & Segura, T. (2022). Controlling Particle Fraction in Microporous Annealed Particle Scaffolds for 3D Cell Culture. *Journal of Visualized Experiments: JoVE*, *188*. <https://doi.org/10.3791/64554>

- Angulo-Pineda, C., Srirussamee, K., Palma, P., Fuenzalida, V. M., Cartmell, S. H., & Palza, H. (2020). Electroactive 3D Printed Scaffolds Based on Percolated Composites of Polycaprolactone with Thermally Reduced Graphene Oxide for Antibacterial and Tissue Engineering Applications. *Nanomaterials*, *10*, 428.
- Aqeilan, R. (2020). Engineering Organoids: A Promising Platform to Understand Biology and Treat Diseases. *Cell Death & Differentiation*, *28*. <https://doi.org/10.1038/s41418-020-00680-0>
- Balagangadharan, K., Dhivya, S., & Selvamurugan, N. (2017). Chitosan Based Nanofibers in Bone Tissue Engineering. *International Journal of Biological Macromolecules.*, *104*, 1372.
- Baldwin, P., Li, D. J., Auston, D. A., Mir, H. S., Yoon, R. S., & Koval, K. J. (2019). Autograft, Allograft, and Bone Graft Substitutes: Clinical Evidence and Indications for Use in the Setting of Orthopaedic Trauma Surgery. *J. Orthop. Trauma*, *33*, 203.
- Barnard, C. N. (1967). Human Cardiac Transplant: An Interim Report of a Successful Operation Performed at Groote Schuur Hospital, Cape Town. *South African Medical Journal*, *41*(48), 1271–1274. https://doi.org/10.10520/AJA20785135_34906
- Barner-Kowollik, C., Bastmeyer, M., Blasco, E., Delaittre, G., Müller, P., Richter, B., & Wegener, M. (2017). 3D Laser Micro- and Nanoprinting: Challenges for Chemistry. *Angewandte Chemie International Edition*, *56*(50), 15828–15845. <https://doi.org/10.1002/anie.201704695>
- Belaid, H., Nagarajan, S., Teyssier, C., Barou, C., Barés, J., Balme, S., Garay, H., Huon, V., Cornu, D., Cavallès, V., & Bechelany, M. (2020). Development of New Biocompatible 3D Printed Graphene Oxide-Based Scaffolds. *Mater. Sci. Eng., C*, *110*, 110595.
- Berens, E. B., Holy, J. M., Riegel, A. T., & Wellstein, A. (2015). A Cancer Cell Spheroid Assay to Assess Invasion in a 3D Setting. *Journal of Visualized Experiments : JoVE*, *105*, 53409. <https://doi.org/10.3791/53409>
- Bioprinting 3D microfibrinous scaffolds for engineering endothelialized myocardium and heart-on-a-*

chip—PubMed. (n.d.). Retrieved December 17, 2024, from
<https://pubmed.ncbi.nlm.nih.gov/27710832/>

- Bishop, E. S., Mostafa, S., Pakvasa, M., Luu, H. H., Lee, M. J., Wolf, J. M., Ameer, G. A., He, T. C., & Reid, R. R. (2017). 3-D Bioprinting Technologies in Tissue Engineering and Regenerative Medicine: Current and Future Trends. *Genes and Diseases.*, 4, 185.
- Bonanini, F., Kurek, D., Previdi, S., Nicolas, A., Hendriks, D., de Ruyter, S., Meyer, M., Clapés Cabrer, M., Dinkelberg, R., García, S. B., Kramer, B., Olivier, T., Hu, H., López-Iglesias, C., Schavemaker, F., Walinga, E., Dutta, D., Queiroz, K., Domansky, K., Vulto, P. (2022). *In vitro* Grafting of Hepatic Spheroids and Organoids on a Microfluidic Vascular bed. *Angiogenesis*, 25(4), 455–470. <https://doi.org/10.1007/s10456-022-09842-9>
- Boyer, C. J., Ballard, D. H., Barzegar, M., Winny Yun, J., Woerner, J. E., Ghali, G. E., Boktor, M., Wang, Y., & Steven Alexander, J. (2018). High-Throughput Scaffold-Free Microtissues Through 3D Printing. *3D Printing in Medicine*, 4, 9. <https://doi.org/10.1186/s41205-018-0029-4>
- Cadena, M. A., Sing, A., Taylor, K., Jin, L., Ning, L., Salar Amoli, M., Singh, Y., Lanjewar, S. N., Tomov, M. L., Serpooshan, V., & Sloan, S. A. (2024). A 3D Bioprinted Cortical Organoid Platform for Modeling Human Brain Development. *Advanced Healthcare Materials*, 13(27), 2401603. <https://doi.org/10.1002/adhm.202401603>
- Calandrini, C., & Drost, J. (2022). Normal and Tumor-Derived Organoids as a Drug Screening Platform for Tumor-Specific Drug Vulnerabilities. *STAR Protocols*, 3(1), 101079. <https://doi.org/10.1016/j.xpro.2021.101079>
- Campuzano, S., & Pelling, A. E. (2019). Scaffolds for 3D Cell Culture and Cellular Agriculture Applications Derived From Non-animal Sources. *Frontiers in Sustainable Food Systems*, 3. <https://doi.org/10.3389/fsufs.2019.00038>
- Cano-Vicent, A., Tambuwala, M. M., Hassan, S. S., Barh, D., Aljabali, A. A. A., Birkett, M., Arjunan,

- A., & Serrano-Aroca, Á. (2021). Fused Deposition Modelling: Current Status, Methodology, Applications and Future Prospects. *Additive Manufacturing*, 47, 102378.
- Castilho, M., de Ruijter, M., Beirne, S., Villette, C. C., Ito, K., Wallace, G. G., & Malda, J. (2020). Multitechnology Biofabrication: A New Approach for the Manufacturing of Functional Tissue Structures? *Trends in Biotechnology*, 38(12), 1316–1328.
<https://doi.org/10.1016/j.tibtech.2020.04.014>
- Castilho, M., Ruijter, M. de, Beirne, S., Villette, C. C., Ito, K., Wallace, G. G., & Malda, J. (2020). Multitechnology Biofabrication: A New Approach for the Manufacturing of Functional Tissue Structures? *Trends in Biotechnology*, 38(12), 1316–1328.
<https://doi.org/10.1016/j.tibtech.2020.04.014>
- Chen, K., Ma, Y., Zhong, X., Lan, J., Long, D., Tian, X., Yang, Y., & Yang, Y. (2024). Single-Cell Transcriptome Profiling of Primary Tumors and Paired Organoids of Pancreatobiliary Cancer. *Cancer Letters*, 582, 216586. <https://doi.org/10.1016/j.canlet.2023.216586>
- Chen, X., Chen, G., Wang, G., Zhu, P., & Gao, C. (2020). Recent Progress on 3D-Printed Polylactic Acid and Its Applications in Bone Repair. *Advanced Engineering Materials*, 22, 1901065.
- Cheng, A., Schwartz, Z., Kahn, A., Li, X., Shao, Z., Sun, M., Ao, Y., Boyan, B. D., & Chen, H. (2019). Advances in Porous Scaffold Design for Bone and Cartilage Tissue Engineering and Regeneration. *Tissue Engineering - Part B: Reviews*, 25, 14.
- Cheng, L., Wang, X., Liu, A., Zhu, Y., Cheng, H., Yu, J., Gong, L., Liu, H., Shen, G., & Liu, L. (2024). Phenylalanine Deprivation Inhibits Multiple Myeloma Progression by Perturbing Endoplasmic Reticulum Homeostasis. *Acta Pharmaceutica Sinica. B*, 14(8), 3493–3512.
<https://doi.org/10.1016/j.apsb.2024.04.021>
- Chimene, D., Miller, L., Cross, L. M., Jaiswal, M. K., Singh, I., & Gaharwar, A. K. (2020). Nanoengineered Osteoinductive Bioink for 3D Bioprinting Bone Tissue. *ACS Appl. Mater.*

Interfaces, 12, 15976.

Chimene, D., Peak, C. W., Gentry, J. L., Carrow, J. K., Cross, L. M., Mondragon, E., Cardoso, G. B., Kaunas, R., & Gaharwar, A. K. (2018). Nanoengineered Ionic-Covalent Entanglement (NICE) Bioinks for 3D Bioprinting. *ACS Appl. Mater. Interfaces*, 10, 9957.

Choe, G., Oh, S., Seok, J. M., Park, S. A., & Lee, J. Y. (2019). Graphene Oxide/Alginate Composites as Novel Bioinks for Three-Dimensional Mesenchymal Stem Cell Printing and Bone Regeneration Applications. *Nanoscale*, 11, 23275.

Chua, C. K., Leong, K. F., Sudarmadji, N., Liu, M. J. J., & Chou, S. M. (2011). Selective Laser Sintering of Functionally Graded Tissue Scaffolds. *MRS Bull.*, 36, 1006.

Colangelo, M. T., Elviri, L., Belletti, S., Mattarozzi, M., Govoni, P., Bergonzi, C., Careri, M., Bettini, R., Guizzardi, S., & Galli, C. (2020). 3D-Printed Chitosan Scaffolds Modified With D-(+) Raffinose and Enriched With Type IV Collagen to Improve Epithelial Cell Colonization. *Biomedical Materials (Bristol, England)*, 15(5), 055018. <https://doi.org/10.1088/1748-605X/ab9552>

Correia, T. R., Figueira, D. R., de Sá, K. D., Miguel, S. P., Fradique, R. G., Mendonça, A. G., & Correia, I. J. (2016). 3D Printed Scaffolds with Bactericidal Activity Aimed for Bone Tissue Regeneration. *Int. J. Biol. Macromol.*, 93, 1432.

Corrò, C., Novellademunt, L., & Li, V. S. (2020). A Brief History of Organoids. *American Journal of Physiology - Cell Physiology*, 319(1), C151. <https://doi.org/10.1152/ajpcell.00120.2020>

Cowan, C. S., Renner, M., Gennaro, M. D., Gross-Scherf, B., Goldblum, D., Hou, Y., Munz, M., Rodrigues, T. M., Krol, J., Szikra, T., Cuttat, R., Waldt, A., Papasaikas, P., Diggelmann, R., Patino-Alvarez, C. P., Galliker, P., Spirig, S. E., Pavlinic, D., Gerber-Hollbach, N., ... Roska, B. (2020). Cell Types of the Human Retina and Its Organoids at Single-Cell Resolution. *Cell*, 182(6), 1623. <https://doi.org/10.1016/j.cell.2020.08.013>

- Danilevicius, P., Rekstyte, S., Balciunas, E., Kraniauskas, A., Jarasiene, R., Sirmenis, R., Baltriukiene, D., Bukelskiene, V., Gadonas, R., & Malinauskas, M. (2012). Micro-Structured Polymer Scaffolds Fabricated by Direct Laser Writing for Tissue Engineering. *Journal of Biomedical Optics*, *17*(8), 081405–081401. <https://doi.org/10.1117/1.JBO.17.8.081405>
- Danilevicius, P., Rezende, R. A., Pereira, F. D. A. S., Selimis, A., Kasyanov, V., Noritomi, P. Y., da Silva, J. V. L., Chatzinikolaidou, M., Farsari, M., & Mironov, V. (2015). Burr-Like, Laser-Made 3D Microscaffolds for Tissue Spheroid Encagement. *Biointerphases*, *10*(2), 021011. <https://doi.org/10.1116/1.4922646>
- de Araújo, T. B. S., Nogueira, R. L. R., Siquara da Rocha, L. de O., Bastos, I. N., Dias, R. B., Souza, B. S. D. F., Lambert, D. W., Coletta, R. D., Silva, V. A. O., & Gurgel Rocha, C. A. (2024). Enhancing Scaffold-Free Spheroid Models: 3D Cell Bioprinting Method for Metastatic HSC3–Oral Squamous Carcinoma Cell Line. *SLAS Discovery*, *29*(4), 100158. <https://doi.org/10.1016/j.slasd.2024.100158>
- De Crignis, E., Hossain, T., Romal, S., Carofiglio, F., Moulos, P., Khalid, M. M., Rao, S., Bazrafshan, A., Verstegen, M. M., Pourfarzad, F., Koutsothanassis, C., Gehart, H., Kan, T. W., Palstra, R.-J., Boucher, C., IJzermans, J. N., Huch, M., Boj, S. F., Vries, R., Mahmoudi, T. (2021). Application of Human Liver Organoids as a Patient-Derived Primary Model for HBV Infection and Related Hepatocellular Carcinoma. *eLife*, *10*, e60747. <https://doi.org/10.7554/eLife.60747>
- Dissanayaka, W. L., Zhu, L., Hargreaves, K. M., Jin, L., & Zhang, C. (2014). Scaffold-free Prevascularized Microtissue Spheroids for Pulp Regeneration. *Journal of Dental Research*, *93*(12), 1296–1303. <https://doi.org/10.1177/0022034514550040>
- Dong, Q., Zhang, M., Zhou, X., Shao, Y., Li, J., Wang, L., Chu, C., Xue, F., Yao, Q., & Bai, J. (2021). 3D-Printed Mg-Incorporated PCL-Based Scaffolds: A Promising Approach for Bone Healing. *Mater. Sci. Eng., C*, *129*, 112372.

- Dong, X., Premaratne, I. D., Sariibrahimoglu, K., Limem, S., Scott, J., Gadjiko, M., Berri, N., Ginter, P., & Spector, J. A. (2022). 3D-printed poly-4-hydroxybutyrate Bioabsorbable Scaffolds for Nipple Reconstruction. *Acta Biomaterialia*, *143*, 333–343.
<https://doi.org/10.1016/j.actbio.2022.02.040>
- Dozzo, A., Chullipallyalil, K., McAuliffe, M., O’Driscoll, C. M., & Ryan, K. B. (2023). Nano-Hydroxyapatite/PLGA Mixed Scaffolds as a Tool for Drug Development and to Study Metastatic Prostate Cancer in the Bone. *Pharmaceutics*, *15*(1), 242.
<https://doi.org/10.3390/pharmaceutics15010242>
- Dubey, A., Vahabi, H., & Kumaravel, V. (2023). Antimicrobial and Biodegradable 3D Printed Scaffolds for Orthopedic Infections. *ACS Biomaterials Science & Engineering*, *9*(7), 4020–4044. <https://doi.org/10.1021/acsbomaterials.3c00115>
- Duval, K., Grover, H., Han, L.-H., Mou, Y., Pegoraro, A. F., Fredberg, J., & Chen, Z. (2017). Modeling Physiological Events in 2D vs. 3D Cell Culture. *Physiology*, *32*(4), 266–277.
<https://doi.org/10.1152/physiol.00036.2016>
- Elias, L., Taengua, R., Frígols, B., Serrano-Aroca, Á., & Salesa, B. (2019). Carbon Nanomaterials and LED Irradiation as Antibacterial Strategies against Gram-Positive Multidrug-Resistant Pathogens. *Int. J. Mol. Sci.*, *20*, 3603.
- El-Tamer, A., Hinze, U., & Chichkov, B. N. (2020). Two-Photon Polymerization in Optics, Microfluidics, and Biomedicine. In K. Sugioka (Ed.), *Handbook of Laser Micro- and Nano-Engineering* (pp. 1–44). Springer International Publishing. https://doi.org/10.1007/978-3-319-69537-2_35-1
- Ežerskytė, E., Vengris, M., Gineitis, K., Merkininkaitė, G., Leber, B., Vargalis, R., Stiegler, P., Schemmer, P., Šakirzanovas, S., Kielaitė-Gulla, A., Strupas, K., & Jonušauskas, L. (2022). Qualitative Comparison Between Different Biopolymers for Usage in Two-Photon

- Polymerization Towards Liver Regeneration. *Optical Materials Express*, 12(7), 2550.
<https://doi.org/10.1364/OME.459057>
- Fanhchaksai, K., Okada, F., Nagai, N., Pothacharoen, P., Kongtawelert, P., Hatano, S., Makino, S., Nakamura, T., & Watanabe, H. (2016). Host Stromal Versican is Essential for Cancer-Associated Fibroblast Function to Inhibit Cancer Growth. *International Journal of Cancer*, 138(3), 630–641. <https://doi.org/10.1002/ijc.29804>
- Ferrández-Montero, A., Lieblich, M., Benavente, R., González-Carrasco, J. L., & Ferrari, B. (2020). Study of the Matrix-Filler Interface in PLA/Mg Composites Manufactured by Material Extrusion Using a Colloidal Feedstock. *Addit. Manuf.*, 33, 101142.
- Ferreira, M., Rzhepishevskaya, O., Grenho, L., Malheiros, D., Gonçalves, L., Almeida, A. J., Jordão, L., Ribeiro, I. A., Ramstedt, M., Gomes, P., & Bettencourt, A. (2017). Levofloxacin-Loaded Bone Cement Delivery System: Highly Effective against Intracellular Bacteria and Staphylococcus Aureus Biofilms. *Int. J. Pharm.*, 532, 241.
- Fischer, J., Mueller, J. B., Kaschke, J., Wolf, T. J. A., Unterreiner, A.-N., & Wegener, M. (2013). Three-Dimensional Multi-Photon Direct Laser Writing With Variable Repetition Rate. *Optics Express*, 21(22), 26244–26260. <https://doi.org/10.1364/OE.21.026244>
- Fontoura, J. C., Viezzer, C., dos Santos, F. G., Ligabue, R. A., Weinlich, R., Puga, R. D., Antonow, D., Severino, P., & Bonorino, C. (2020). Comparison of 2D and 3D Cell Culture Models for Cell Growth, Gene Expression and Drug Resistance. *Materials Science and Engineering: C*, 107, 110264. <https://doi.org/10.1016/j.msec.2019.110264>
- Fu, H., Zhang, D., Zeng, J., Fu, Q., Chen, Z., Sun, X., Yang, Y., Li, S., & Chen, M. (2023). Application of 3D-Printed Tissue-Engineered Skin Substitute Using Innovative Biomaterial Loaded With Human Adipose-Derived Stem Cells in Wound Healing. *International Journal of Bioprinting*, 9(2), 674. <https://doi.org/10.18063/ijb.v9i2.674>

- Gao, B., Yang, Q., Zhao, X., Jin, G., Ma, Y., & Xu, F. (2016). 4D Bioprinting for Biomedical Applications. *Trends in Biotechnology.*, 34, 746.
- Georgantzinou, S. K., Giannopoulos, G. I., & Bakalis, P. A. (2021). Additive Manufacturing for Effective Smart Structures: The Idea of 6d Printing. *J. Compos. Sci.*, 5, 119.
- Gerli, M. F. M., Calà, G., Beesley, M. A., Sina, B., Tullie, L., Sun, K. Y., Panariello, F., Michielin, F., Davidson, J. R., Russo, F. M., Jones, B. C., Lee, D. D. H., Savvidis, S., Xenakis, T., Simcock, I. C., Straatman-Iwanowska, A. A., Hirst, R. A., David, A. L., O'Callaghan, C., De Coppi, P. (2024). Single Cell Guided Prenatal Derivation of Primary Fetal Epithelial Organoids From Human Amniotic and Tracheal Fluids. *Nature Medicine*, 30(3), 875–887.
<https://doi.org/10.1038/s41591-024-02807-z>
- Geurts, M. H., Gandhi, S., Boretto, M. G., Akkerman, N., Derks, L. L. M., van Son, G., Celotti, M., Harshuk-Shabso, S., Peci, F., Begthel, H., Hendriks, D., Schürmann, P., Andersson-Rolf, A., Chuva de Sousa Lopes, S. M., van Es, J. H., van Boxtel, R., & Clevers, H. (2023). One-Step Generation of Tumor Models by Base Editor Multiplexing in Adult Stem Cell-Derived Organoids. *Nature Communications*, 14(1), 4998. <https://doi.org/10.1038/s41467-023-40701-3>
- Gibson, I., Rosen, D., Stucker, B., & Khorasani, M. (2021). Introduction and Basic Principles. In I. Gibson, D. Rosen, B. Stucker, & M. Khorasani (Eds.), *Additive Manufacturing Technologies* (pp. 1–21). Springer International Publishing. https://doi.org/10.1007/978-3-030-56127-7_1
- Gillaspie, E. A., Matsumoto, J. S., Morris, N. E., Downey, R. J., Shen, K. R., Allen, M. S., & Blackmon, S. H. (2016). From 3-Dimensional Printing to 5-Dimensional Printing: Enhancing Thoracic Surgical Planning and Resection of Complex Tumors. *Ann. Thorac. Surg.*, 101, 1958.
- Gittard, S. D., Nguyen, A., Obata, K., Koroleva, A., Narayan, R. J., & Chichkov, B. N. (2011). Fabrication of Microscale Medical Devices by Two-Photon Polymerization With Multiple Foci Via a Spatial Light Modulator. *Biomedical Optics Express*, 2(11), 3167–3178.

<https://doi.org/10.1364/BOE.2.003167>

Grémare, A., Guduric, V., Bareille, R., Heroguez, V., Latour, S., L'heureux, N., Fricain, J. C., Catros, S., & Le Nihouannen, D. (2018). Characterization of Printed PLA Scaffolds for Bone Tissue Engineering. *J. Biomed. Mater. Res. - Part A*, *106*, 887.

Gruene, M., Deiwick, A., Koch, L., Schlie, S., Unger, C., Hofmann, N., Bernemann, I., Glasmacher, B., & Chichkov, B. (2011). Laser Printing of Stem Cells for Biofabrication of Scaffold-Free Autologous Grafts. *Tissue Engineering. Part C, Methods*, *17*(1), 79–87.

<https://doi.org/10.1089/ten.TEC.2010.0359>

Habanjar, O., Diab-Assaf, M., Caldefie-Chezet, F., & Delort, L. (2021). 3D Cell Culture Systems: Tumor Application, Advantages, and Disadvantages. *International Journal of Molecular Sciences*, *22*(22), 12200. <https://doi.org/10.3390/ijms222212200>

Haleem, A., Javaid, M., & Vaishya, R. (2018). 4D Printing and Its Applications in Orthopaedics. *Journal of Clinical Orthopaedics and Trauma.*, *9*, 275.

Haleem, A., Javaid, M., & Vaishya, R. (2019). 5D Printing and Its Expected Applications in Orthopaedics. *Journal of Clinical Orthopaedics and Trauma.*, *10*, 809.

Han, Y., Lian, M., Wu, Q., Qiao, Z., Sun, B., & Dai, K. (2021). Effect of Pore Size on Cell Behavior Using Melt Electrowritten Scaffolds. *Frontiers in Bioengineering and Biotechnology*, *9*.
<https://doi.org/10.3389/fbioe.2021.629270>

Hao, S.-J., Wan, Y., Xia, Y.-Q., Zou, X., & Zheng, S.-Y. (2018). Size-Based Separation Methods of Circulating Tumor Cells. *Advanced Drug Delivery Reviews*, *125*, 3–20.
<https://doi.org/10.1016/j.addr.2018.01.002>

Hardy, J. D., Eraslan, S., & Webb, W. R. (1964). Transplantation of the Lung. *Annals of Surgery*, *160*(3), 440.

Havel, S. L., & Griswold, M. D. (2024). Temporal Maturation of Sertoli Cells During the

- Establishment of the Cycle of the Seminiferous Epithelium. *Biology of Reproduction*, *111*(4), 959–974. <https://doi.org/10.1093/biolre/ioae115>
- He, H. Y., Zhang, J. Y., Mi, X., Hu, Y., & Gu, X. Y. (2015). Rapid Prototyping for Tissue-Engineered Bone Scaffold by 3D Printing and Biocompatibility Study. *Int. J. Clin. Exp. Med.*, *8*(7), 11777.
- Hendriks, S., Kascholke, C., Flath, T., Schumann, D., Gressenbuch, M., Schulze, F. P., Hacker, M. C., & Schulz-Siegmund, M. (2016). Indirect Rapid Prototyping of Sol-Gel Hybrid Glass Scaffolds for Bone Regeneration—Effects of Organic Crosslinker Valence, Content and Molecular Weight on Mechanical Properties. *Acta Biomaterialia*, *35*, 318–329. <https://doi.org/10.1016/j.actbio.2016.02.038>
- Hooper, R., Cummings, C., Beck, A., Vazquez-Armendariz, J., Rodriguez, C., & Dean, D. (2024). Sheet-Based Extrusion Bioprinting: A New Multi-Material Paradigm Providing Mid-Extrusion Micropatterning Control for Microvascular Applications. *Biofabrication*, *16*(2), 025032. <https://doi.org/10.1088/1758-5090/ad30c8>
- Hu, D., Cao, Y., Cai, C., Wang, G., Zhou, M., Peng, L., Fan, Y., Lai, Q., & Gao, Z. (2025). Establishment of Human Cerebral Organoid Systems to Model Early Neural Development and Assess the Central Neurotoxicity of Environmental Toxins. *Neural Regeneration Research*, *20*(1), 242–252. <https://doi.org/10.4103/NRR.NRR-D-23-00928>
- Huang, G., Zhao, Y., Chen, D., Wei, L., Hu, Z., Li, J., Zhou, X., Yang, B., & Chen, Z. (2024). Applications, Advancements, and Challenges of 3D Bioprinting in Organ Transplantation. *Biomaterials Science*, *12*(6), 1425–1448. <https://doi.org/10.1039/D3BM01934A>
- Huh, J., Moon, Y.-W., Park, J., Atala, A., Yoo, J. J., & Lee, S. J. (2021). Combinations of Photoinitiator and UV Absorber for Cell-Based Digital Light Processing (DLP) Bioprinting. *Biofabrication*, *13*(3). <https://doi.org/10.1088/1758-5090/abfd7a>
- Hussain, M., Askari Rizvi, S. H., Abbas, N., Sajjad, U., Shad, M. R., Badshah, M. A., & Malik, A. I.

- (2021). Recent Developments in Coatings for Orthopedic Metallic Implants. *Coatings.*, *11*, 791.
- Ino, K., Ozawa, F., Dang, N., Hiramoto, K., Hino, S., Akasaka, R., Nashimoto, Y., & Shiku, H. (2020). Biofabrication Using Electrochemical Devices and Systems. *Advanced Biosystems*, *4*(4), e1900234. <https://doi.org/10.1002/adbi.201900234>
- Ishiguro, Y., Iriguchi, S., Asano, S., Shinohara, T., Shiina, S., Arima, S., Kassai, Y., Sakai, Y., Obama, K., & Kaneko, S. (2023). Lineage Tracing of T Cell Differentiation From T-iPSC by 2D Feeder-Free Culture and 3D Organoid Culture. *Frontiers in Immunology*, *14*, 1303713. <https://doi.org/10.3389/fimmu.2023.1303713>
- Jackson, C. E., Ramos-Rodriguez, D. H., Farr, N. T. H., English, W. R., Green, N. H., & Claeysens, F. (2023). Development of PCL PolyHIPE Substrates for 3D Breast Cancer Cell Culture. *Bioengineering*, *10*(5), 522. <https://doi.org/10.3390/bioengineering10050522>
- Jaksa, L., Aryeetey, O. J., Hatamikia, S., Nägl, K., Buschmann, M., Dieter H, P., Kronreif, G., & Lorenz, A. (2023). 3D-Printed Multi-Material Liver Model With Simultaneous Mechanical and Radiological Tissue-Mimicking Features for Improved Realism. *International Journal of Bioprinting*, *9*(4), 721. <https://doi.org/10.18063/ijb.721>
- Jeibouei, S., Hojat, A., Mostafavi, E., Aref, A. R., Kalbasi, A., Niazi, V., Ajoudanian, M., Mohammadi, F., Saadati, F., Javadi, S. M., Shams, F., Moghaddam, M., Karami, F., Sharifi, K., Moradian, F., Akbari, M. E., & Zali, H. (2022). Radiobiological Effects of Wound Fluid on Breast Cancer Cell Lines and Human-Derived Tumor Spheroids in 2D and Microfluidic Culture. *Scientific Reports*, *12*, 7668. <https://doi.org/10.1038/s41598-022-11023-z>
- Ji, Y., Yang, Q., Huang, G., Shen, M., Jian, Z., Thoraval, M.-J., Lian, Q., Zhang, X., & Xu, F. (2019). Improved Resolution and Fidelity of Droplet-Based Bioprinting by Upward Ejection. *ACS Biomaterials Science & Engineering*, *5*. <https://doi.org/10.1021/acsbiomaterials.9b00400>
- Jiang, D., Ning, F., & Wang, Y. (2021). Additive Manufacturing of Biodegradable Iron-Based Particle

- Reinforced Polylactic Acid Composite Scaffolds for Tissue Engineering. *J. Mater. Process. Technol.*, 289, 116952.
- Jonušauskas, L., Baravykas, T., Andrijec, D., Gadišauskas, T., & Purlys, V. (2019). Stitchless Support-Free 3D Printing of Free-Form Micromechanical Structures With Feature Size On-Demand. *Scientific Reports*, 9(1), 17533. <https://doi.org/10.1038/s41598-019-54024-1>
- Jonušauskas, L., Juodkazis, S., & Malinauskas, M. (2018). Optical 3D printing: Bridging the gaps in the mesoscale. *Journal of Optics*, 20(5), 053001. <https://doi.org/10.1088/2040-8986/aab3fe>
- Jonušauskas, L., Lau, M., Gruber, P., Gökce, B., Barcikowski, S., Malinauskas, M., & Ovsianikov, A. (2016). Plasmon Assisted 3D Microstructuring of Gold Nanoparticle-Doped Polymers. *Nanotechnology*, 27(15), 154001. <https://doi.org/10.1088/0957-4484/27/15/154001>
- Kalirajan, C., Dukle, A., Nathanael, A. J., Oh, T.-H., & Manivasagam, G. (2021). A Critical Review on Polymeric Biomaterials for Biomedical Applications. *Polymers*, 13(17), Article 17. <https://doi.org/10.3390/polym13173015>
- Kanwar, S., & Vijayavenkataraman, S. (2021). Design of 3D Printed Scaffolds for Bone Tissue Engineering: A Review. *Bioprinting.*, 24, e00167.
- Kaplan, S. L. (2014). Recent Lessons for the Management of Bone and Joint Infections. *J. Infect.*, 68, S51.
- Karamat-Ullah, N., Demidov, Y., Schramm, M., Grumme, D., Auer, J., Bohr, C., Brachvogel, B., & Maleki, H. (2021). 3D Printing of Antibacterial, Biocompatible, and Biomimetic Hybrid Aerogel-Based Scaffolds with Hierarchical Porosities via Integrating Antibacterial Peptide-Modified Silk Fibroin with Silica Nanostructure. *ACS Biomater. Sci. Eng.*, 7, 4545.
- Kawasaki, Y., & Sendo, T. (2021). Three Photoinitiators Induce Breast Tumor Growth in Mouse Xenografts With MCF-7 Breast Cancer Cells. *Current Research in Toxicology*, 2, 322–328. <https://doi.org/10.1016/j.crttox.2021.08.004>

- Keiser, G. (2021). Nonlinear Processes in Optical Fibers. In G. Keiser (Ed.), *Fiber Optic Communications* (pp. 477–506). Springer. https://doi.org/10.1007/978-981-33-4665-9_12
- Kerslake, R., Belay, B., Panfilov, S., Hall, M., Kyrou, I., Randeva, H. S., Hyttinen, J., Karteris, E., & Sisu, C. (2023). Transcriptional Landscape of 3D vs. 2D Ovarian Cancer Cell Models. *Cancers*, *15*(13), 3350. <https://doi.org/10.3390/cancers15133350>
- Kiefer, P., Hahn, V., Kalt, S., Sun, Q., Eggeler, Y. M., & Wegener, M. (2024). A Multi-Photon (7×7)-Focus 3D Laser Printer Based on a 3D-Printed Diffractive Optical Element and a 3D-Printed Multi-Lens Array. *Light: Advanced Manufacturing*, *4*(1), 28–41. <https://doi.org/10.37188/lam.2024.003>
- Kim, H. I., Raja, N., Kim, J., Sung, A., Choi, Y. J., Yun, H.-S., & Park, H. (2022). A 3D Calcium-Deficient Hydroxyapatite-Based Scaffold with Gold Nanoparticles Effective against *Micrococcus Luteus* as an Artificial Bone Substitute. *Mater. Des.*, *219*, 110793.
- Kim, J., & Choi, H. (2024). Review on Principal and Applications of Temporal and Spatial Beam Shaping for Ultrafast Pulsed Laser. *Photonics*, *11*, 1140. <https://doi.org/10.3390/photonics11121140>
- Kleinman, H. K., Philp, D., & Hoffman, M. P. (2003). Role of the Extracellular Matrix in Morphogenesis. *Current Opinion in Biotechnology*, *14*(5), 526–532. <https://doi.org/10.1016/j.copbio.2003.08.002>
- Kotlarz, M., Ferreira, A. M., Gentile, P., Russell, S. J., & Dalgarno, K. (2022). Droplet-Based Bioprinting Enables the Fabrication of Cell–Hydrogel–Microfibre Composite Tissue Precursors. *Bio-Design and Manufacturing*, *5*(3), 512–528. <https://doi.org/10.1007/s42242-022-00192-5>
- Kufelt, O., El-Tamer, A., Sehring, C., Meißner, M., Schlie-Wolter, S., & Chichkov, B. N. (2015). Water-Soluble Photopolymerizable Chitosan Hydrogels for Biofabrication via Two-Photon

- Polymerization. *Acta Biomaterialia*, 18, 186–195. <https://doi.org/10.1016/j.actbio.2015.02.025>
- Kumar, H., & Kim, K. (2020). Stereolithography 3D Bioprinting. In J. M. Crook (Ed.), *3D Bioprinting: Principles and Protocols* (pp. 93–108). Springer US. https://doi.org/10.1007/978-1-0716-0520-2_6
- Kumaravel, V., Nair, K. M., Mathew, S., Bartlett, J., Kennedy, J. E., Manning, H. G., Whelan, B. J., Leyland, N. S., & Pillai, S. C. (2021). Antimicrobial TiO₂ Nanocomposite Coatings for Surfaces, Dental and Orthopaedic Implants. *Chem. Eng. J.*, 416, 129071.
- Kunwar, P., Aryal, U., Poudel, A., Fougner, D., Geffert, Z. J., Xie, R., Li, Z., & Soman, P. (2024). Droplet Bioprinting of Acellular and Cell-Laden Structures at High-Resolutions. *Biofabrication*, 16(3). <https://doi.org/10.1088/1758-5090/ad4c09>
- Lee, A., Hudson, A. R., Shiwarski, D. J., Tashman, J. W., Hinton, T. J., Yerneni, S., Bliley, J. M., Campbell, P. G., & Feinberg, A. W. (2019). 3D Bioprinting of Collagen to Rebuild Components of the Human Heart. *Science*, 365(6452), 482–487. <https://doi.org/10.1126/science.aav9051>
- Lee, J. H., Baik, J. M., Yu, Y. S., Kim, J. H., Ahn, C. B., Son, K. H., Kim, J. H., Choi, E. S., & Lee, J. W. (2020). Development of a Heat Labile Antibiotic Eluting 3D Printed Scaffold for the Treatment of Osteomyelitis. *Sci. Rep.*, 10, 7554.
- Lee, M., Bae, K., Levinson, C., & Zenobi-Wong, M. (2020). Nanocomposite Bioink Exploits Dynamic Covalent Bonds between Nanoparticles and Polysaccharides for Precision Bioprinting. *Biofabrication*, 12, 025025.
- Lee, S. H., Kang, M. S., Jeon, S., Jo, H. J., Hong, S. W., Kim, B., & Han, D.-W. (2023). 3D Bioprinting of Human Mesenchymal Stem Cells-Laden Hydrogels Incorporating MXene for Spontaneous Osteodifferentiation. *Heliyon*, 9(3), e14490. <https://doi.org/10.1016/j.heliyon.2023.e14490>

- Levato, R., Lim, K. S., Li, W., Asua, A. U., Peña, L. B., Wang, M., Falandt, M., Bernal, P. N., Gawlitta, D., Zhang, Y. S., Woodfield, T. B. F., & Malda, J. (2021). High-Resolution Lithographic Biofabrication of Hydrogels With Complex Microchannels From Low-Temperature-Soluble Gelatin Bioresins. *Materials Today Bio*, *12*, 100162. <https://doi.org/10.1016/j.mtbio.2021.100162>
- Lewis-Israeli, Y. R., Wasserman, A. H., Gabalski, M. A., Volmert, B. D., Ming, Y., Ball, K. A., Yang, W., Zou, J., Ni, G., Pajares, N., Chatzistavrou, X., Li, W., Zhou, C., & Aguirre, A. (2021). Self-Assembling Human Heart Organoids for the Modeling of Cardiac Development and Congenital Heart Disease. *Nature Communications*, *12*(1), 5142. <https://doi.org/10.1038/s41467-021253295>
- Li, C., Fleck, J. S., Martins-Costa, C., Burkard, T. R., Themann, J., Stuempflen, M., Peer, A. M., Vertesy, Á., Littleboy, J. B., Esk, C., Elling, U., Kasprian, G., Corsini, N. S., Treutlein, B., & Knoblich, J. A. (2023). Single-Cell Brain Organoid Screening Identifies Developmental Defects in Autism. *Nature*, *621*(7978), 373. <https://doi.org/10.1038/s41586-023-06473-y>
- Li, J., Li, L., Zhou, J., Zhou, Z., Wu, X.-L., Wang, L., & Yao, Q. (2019). 3D Printed Dual-Functional Biomaterial with Self-Assembly Micro-Nano Surface and Enriched Nano Silver for Antibacterial and Bone Regeneration. *Appl. Mater. Today*, *17*, 206.
- Li, M. L., Aggeler, J., Farson, D. A., Hatier, C., Hassell, J., & Bissell, M. J. (1987). Influence of a Reconstituted Basement Membrane and its Components on Casein Gene Expression and Secretion in Mouse Mammary Epithelial Cells. *Proceedings of the National Academy of Sciences of the United States of America*, *84*(1), 136–140. <https://doi.org/10.1073/pnas.84.1.136>
- Li, P., Fu, L., Liao, Z., Peng, Y., Ning, C., Gao, C., Zhang, D., Sui, X., Lin, Y., Liu, S., Hao, C., & Guo, Q. (2021). Chitosan Hydrogel/3D-printed Poly(ϵ -caprolactone) Hybrid Scaffold Containing Synovial Mesenchymal Stem Cells for Cartilage Regeneration Based on Tetrahedral

- Framework Nucleic Acid Recruitment. *Biomaterials*, 278, 121131.
<https://doi.org/10.1016/j.biomaterials.2021.121131>
- Li, Q., Rycaj, K., Chen, X., & Tang, D. G. (2015). Cancer Stem Cells and Cell Size: A Causal Link? *Seminars in Cancer Biology*, 35, 191–199. <https://doi.org/10.1016/j.semcancer.2015.07.002>
- Li, X., Wang, Y., Guo, M., Wang, Z., Shao, N., Zhang, P., Chen, X., & Huang, Y. (2018). Degradable Three Dimensional-Printed Polylactic Acid Scaffold with Long-Term Antibacterial Activity. *ACS Sustain. Chem. Eng.*, 6, 2047.
- Li, Y. C., Zhang, Y. S., Akpek, A., Shin, S. R., & Khademhosseini, A. (2017). 4D Bioprinting: The next-Generation Technology for Biofabrication Enabled by Stimuli-Responsive Materials. *Biofabrication.*, 9, 012001.
- Li, Y., Yang, W., Li, X., Zhang, X., Wang, C., Meng, X., Pei, Y., Fan, X., Lan, P., Wang, C., Li, X., & Guo, Z. (2015). Improving Osteointegration and Osteogenesis of Three-Dimensional Porous Ti6Al4V Scaffolds by Polydopamine-Assisted Biomimetic Hydroxyapatite Coating. *ACS Appl. Mater. Interfaces*, 7, 5715.
- Lin, Y.-N., Nasir, A., Camacho, S., Berry, D. L., Schmidt, M. O., Pearson, G. W., Riegel, A. T., & Wellstein, A. (2020). Monitoring Cancer Cell Invasion and T-cell Cytotoxicity in 3D culture. *Journal of Visualized Experiments : JoVE*, 160, 10.3791/61392. <https://doi.org/10.3791/61392>
- Liu, J., Erenpreisa, J., & Sikora, E. (2022). Polyploid Giant Cancer Cells: An Emerging New Field of Cancer Biology. *Seminars in Cancer Biology*, 81, 1–4.
<https://doi.org/10.1016/j.semcancer.2021.10.006>
- Liu, J., Ye, S., Guo, H., Yao, Y., Zhou, X., Nie, H., Wang, R., Yang, K., He, J., & Zhang, B. (2023). Enhanced Ultrafast Dynamics and Saturable Absorption Response of Nb₂SiTe₄/graphene Heterostructure for Femtosecond Mode-Locked Bulk Lasers. *Optics & Laser Technology*, 166, 109635. <https://doi.org/10.1016/j.optlastec.2023.109635>

- Liu, W., Li, Z., Zheng, L., Zhang, X., Liu, P., Yang, T., & Han, B. (2016). Electrospun Fibrous Silk Fibroin/poly(L-lactic acid) Scaffold for Cartilage Tissue Engineering. *Tissue Engineering and Regenerative Medicine*, 13(5), 516–526. <https://doi.org/10.1007/s13770-016-9099-9>
- Liu, W., Zuo, R., Zhu, T., Zhu, M., Zhao, S., & Zhu, Y. (2021). Forsterite-Hydroxyapatite Composite Scaffolds with Photothermal Antibacterial Activity for Bone Repair. *J. Adv. Ceram.*, 10, 1095.
- Liu, X., Gao, J., Cui, X., Nie, S., Wu, X., Zhang, L., Tang, P., Liu, J., & Li, M. (2023). Functionalized 3D-Printed PLA Biomimetic Scaffold for Repairing Critical-Size Bone Defects. *Bioengineering (Basel, Switzerland)*, 10(9), 1019. <https://doi.org/10.3390/bioengineering10091019>
- Liu, Z., Wang, Y., Wu, B., Cui, C., Guo, Y., & Yan, C. (2019). A Critical Review of Fused Deposition Modeling 3D Printing Technology in Manufacturing Polylactic Acid Parts. *International Journal of Advanced Manufacturing Technology.*, 102, 2877.
- Llorens-Gámez, M., Salesa, B., & Serrano-Aroca, Á. (2020). Physical and Biological Properties of Alginate/Carbon Nanofibers Hydrogel Films. *Int. J. Biol. Macromol.*, 151, 499.
- Lu, Y., Aimetti, A. A., Langer, R., & Gu, Z. (2017). Bioresponsive Materials. *Nature Reviews Materials.*, 2, 16075.
- Mačiulaitis, J., Deveikytė, M., Rekštytė, S., Bratchikov, M., Darinskas, A., Šimbelytė, A., Daunoras, G., Laurinavičienė, A., Laurinavičius, A., Gudas, R., Malinauskas, M., & Mačiulaitis, R. (2015). Preclinical Study of SZ2080 Material 3D Microstructured Scaffolds for Cartilage Tissue Engineering Made by Femtosecond Direct Laser Writing Lithography. *Biofabrication*, 7(1), 015015. <https://doi.org/10.1088/1758-5090/7/1/015015>
- Maibohm, C., Silvestre, O. F., Borme, J., Sinou, M., Heggarty, K., & Nieder, J. B. (2020). Multi-Beam Two-Photon Polymerization for Fast Large Area 3D Periodic Structure Fabrication for Bioapplications. *Scientific Reports*, 10(1), 8740. <https://doi.org/10.1038/s41598-020-64955-9>
- Malinauskas, M., Žukauskas, A., Bičkauskaitė, G., Gadonas, R., & Juodkazis, S. (2010). Mechanisms

- of Three-Dimensional Structuring of Photo-Polymers by Tightly Focussed Femtosecond Laser Pulses. *Optics Express*, 18(10), 10209–10221. <https://doi.org/10.1364/OE.18.010209>
- Marks, W. H., Yang, S. C., Dombi, G. W., & Bhatia, S. K. (2012). Carbon Nanobrush-Containing Poloxamer Hydrogel Composites For Tissue Regeneration. *Journal of Long-Term Effects of Medical Implants*, 22(3), 229–236. <https://doi.org/10.1615/jlongtermeffmedimplants.2013006208>
- Martin, V., Ribeiro, I. A., Alves, M. M., Gonçalves, L., Claudio, R. A., Grenho, L., Fernandes, M. H., Gomes, P., Santos, C. F., & Bettencourt, A. F. (2019). Engineering a Multifunctional 3D-Printed PLA-Collagen-Minocycline-NanoHydroxyapatite Scaffold with Combined Antimicrobial and Osteogenic Effects for Bone Regeneration. *Mater. Sci. Eng., C*, 101, 15.
- Martínez-Espuga, M., Mata, A., & Ordóñez-Morán, P. (2023). Intestinal Cell Differentiation and Phenotype in 2D and 3D Cell Culture Models. In P. Ordóñez-Morán (Ed.), *Intestinal Differentiated Cells: Methods and Protocols* (pp. 235–243). Springer US. https://doi.org/10.1007/978-1-0716-3076-1_18
- Masters, E. A., Trombetta, R. P., de Mesy Bentley, K. L., Boyce, B. F., Gill, A. L., Gill, S. R., Nishitani, K., Ishikawa, M., Morita, Y., Ito, H., Bello-Irizarry, S. N., Ninomiya, M., Brodell, J. D., Lee, C. C., Hao, S. P., Oh, I., Xie, C., Awad, H. A., Daiss, J. L., Muthukrishnan, G. (2019). Evolving Concepts in Bone Infection: Redefining “Biofilm”, “Acute vs. Chronic Osteomyelitis”, “the Immune Proteome” and “Local Antibiotic Therapy. *Bone Research*, 7, 20.
- Mazzoli, A., Ferretti, C., Gigante, A., Salvolini, E., & Mattioli-Belmonte, M. (2015). Selective Laser Sintering Manufacturing of Polycaprolactone Bone Scaffolds for Applications in Bone Tissue Engineering. *Rapid Prototyp. J.*, 21, 386.
- Mehrpouya, M., Vahabi, H., Barletta, M., Laheurte, P., & Langlois, V. (2021). Additive Manufacturing of Polyhydroxyalkanoates (PHAs) Biopolymers: Materials, Printing Techniques, and

- Applications. *Materials Science and Engineering C*, 127, 112216.
- Mehrpouya, M., Vahabi, H., Janbaz, S., Darafsheh, A., Mazur, T. R., & Ramakrishna, S. (2021). 4D Printing of Shape Memory Polylactic Acid (PLA). *Polymer.*, 230, 124080.
- Melo, S. F., Neves, S. C., Pereira, A. T., Borges, I., Granja, P. L., Magalhães, F. D., & Gonçalves, I. C. (2020). Incorporation of Graphene Oxide into Poly(ϵ -Caprolactone) 3D Printed Fibrous Scaffolds Improves Their Antimicrobial Properties. *Mater. Sci. Eng., C*, 109, 110537.
- Merkininkaitė, G., Gailevičius, D., Šakirzanovas, S., & Jonušauskas, L. (2019). Polymers for Regenerative Medicine Structures Made via Multiphoton 3D Lithography. *International Journal of Polymer Science*, 2019(1), 3403548. <https://doi.org/10.1155/2019/3403548>
- Moncal, K. K., Ozbolat, V., Datta, P., Heo, D. N., & Ozbolat, I. T. (2019). Thermally Controlled Extrusion-Based Bioprinting of Collagen. *Journal of Materials Science: Materials in Medicine*, 30(5), 55. <https://doi.org/10.1007/s10856-019-6258-2>
- Mueller, J. B., Fischer, J., Mange, Y. J., Nann, T., & Wegener, M. (2013). *In-situ* Local Temperature Measurement During Three-Dimensional Direct Laser Writing. *Applied Physics Letters*, 103(12), 123107. <https://doi.org/10.1063/1.4821556>
- Mun, S. J., Ryu, J.-S., Lee, M.-O., Son, Y. S., Oh, S. J., Cho, H.-S., Son, M.-Y., Kim, D.-S., Kim, S. J., Yoo, H. J., Lee, H.-J., Kim, J., Jung, C.-R., Chung, K.-S., & Son, M. J. (2019). Generation of Expandable Human Pluripotent Stem Cell-Derived Hepatocyte-Like Liver Organoids. *Journal of Hepatology*, 71(5), 970–985. <https://doi.org/10.1016/j.jhep.2019.06.030>
- Murphy, C. M., Haugh, M. G., & O'Brien, F. J. (2010). The Effect of Mean Pore Size on Cell Attachment, Proliferation and Migration in Collagen-Glycosaminoglycan Scaffolds for Bone Tissue Engineering. *Biomaterials*, 31, 461.
- Murphy, S. V., & Atala, A. (2014). 3D Bioprinting of Tissues and Organs. *Nat. Biotechnol.*, 32, 773.
- Murray, J. E., Merrill, J. P., Dammin, G. J., Dealy, J. B. J., Alexandre, G. W., & Harrison, J. H. (1962).

- Kidney Transplantation in Modified Recipients. *Annals of Surgery*, 156(3), 337.
- Nerger, B. A., Sinha, S., Lee, N. N., Cheriyan, M., Bertsch, P., Johnson, C. P., Mahadevan, L., Bonventre, J. V., & Mooney, D. J. (2024). 3D Hydrogel Encapsulation Regulates Nephrogenesis in Kidney Organoids. *Advanced Materials (Deerfield Beach, Fla.)*, 36(14), e2308325. <https://doi.org/10.1002/adma.202308325>
- Ngo, T. D., Kashani, A., Imbalzano, G., Nguyen, K. T. Q., & Hui, D. (2018). Additive Manufacturing (3D Printing): A Review of Materials, Methods, Applications and Challenges. *Composites Part B: Engineering*, 143, 172.
- Nguyen, A. K., & Narayan, R. J. (2017). Two-Photon Polymerization for Biological Applications. *Materials Today*, 20(6), 314–322. <https://doi.org/10.1016/j.mattod.2017.06.004>
- Nie, R., Sun, Y., Lv, H., Lu, M., Huangfu, H., Li, Y., Zhang, Y., Wang, D., Wang, L., & Zhou, Y. (2022). 3D Printing of MXene Composite Hydrogel Scaffolds for Photothermal Antibacterial Activity and Bone Regeneration in Infected Bone Defect Models. *Nanoscale*, 14, 8112.
- Nieto, D., Marchal Corrales, J. A., Jorge de Mora, A., & Moroni, L. (2020). Fundamentals of Light-Cell–Polymer Interactions in Photo-Cross-Linking Based Bioprinting. *APL Bioengineering*, 4(4), 041502. <https://doi.org/10.1063/5.0022693>
- Nordham, K. D., & Ninokawa, S. (n.d.). The History of Organ Transplantation. *Proceedings (Baylor University. Medical Center)*, 35(1), 124–128. <https://doi.org/10.1080/08998280.2021.1985889>
- Norrie, J. L., Nityanandam, A., Lai, K., Chen, X., Wilson, M., Stewart, E., Griffiths, L., Jin, H., Wu, G., Orr, B., Tran, Q., Allen, S., Reilly, C., Zhou, X., Zhang, J., Newman, K., Johnson, D., Brennan, R., & Dyer, M. A. (2021). Retinoblastoma From Human Stem Cell-Derived Retinal Organoids. *Nature Communications*, 12(1), 4535. <https://doi.org/10.1038/s41467-021-24781-7>
- O’Halloran, S., Pandit, A., Heise, A., & Kellett, A. (2023). Two-Photon Polymerization: Fundamentals, Materials, and Chemical Modification Strategies. *Advanced Science*, 10(7), 2204072.

<https://doi.org/10.1002/advs.202204072>

Organ Donation Statistics | *organdonor.gov*. (2024). Retrieved December 2, 2024, from

<https://www.organdonor.gov/learn/organ-donation-statistics>

Ovsianikov, A., Gruene, M., Pflaum, M., Koch, L., Maiorana, F., Wilhelmi, M., Haverich, A., &

Chichkov, B. (2010). Laser printing of cells into 3D scaffolds. *Biofabrication*, 2(1), 014104.

<https://doi.org/10.1088/1758-5082/2/1/014104>

Paradiso, F., Lenna, S., Gazze, S. A., Garcia Parra, J., Murphy, K., Margarit, L., Gonzalez, D., Francis,

L., & Taraballi, F. (2022). Mechanomimetic 3D Scaffolds as a Humanized In Vitro Model for

Ovarian Cancer. *Cells*, 11(5), 824. <https://doi.org/10.3390/cells11050824>

Paris, J. L., Lafuente-Gómez, N., Cabañas, M. V., Román, J., Peña, J., & Vallet-Regí, M. (2019).

Fabrication of a Nanoparticle-Containing 3D Porous Bone Scaffold with Proangiogenic and

Antibacterial Properties. *Acta Biomater.*, 86, 441.

Park, J. S., Lee, S. J., Jo, H. H., Lee, J. H., Kim, W. D., Lee, J. Y., & Park, S. A. (2017). Fabrication

and Characterization of 3D-Printed Bone-like β -Tricalcium Phosphate/Polycaprolactone

Scaffolds for Dental Tissue Engineering. *J. Ind. Eng. Chem.*, 46, 175.

Pascual-González, C., de la Vega, J., Thompson, C., Fernández-Blázquez, J. P., Herráez-Molinero, D.,

Biurrun, N., Lizarralde, I., del Río, J. S., González, C., & LLorca, J. (2022). Processing and

Mechanical Properties of Novel Biodegradable Poly-Lactic Acid/Zn 3D Printed Scaffolds for

Application in Tissue Regeneration. *J. Mech. Behav. Biomed. Mater.*, 132(May), 105290.

Pascual-González, C., Thompson, C., de la Vega, J., Biurrun Churruca, N., Fernández-Blázquez, J. P.,

Lizarralde, I., Herráez-Molinero, D., González, C., & LLorca, J. (2022). Processing and

Properties of PLA/Mg Filaments for 3D Printing of Scaffolds for Biomedical Applications.

Rapid Prototyp. J., 28, 884.

Piscitelli, E., Maya, I. C., Cocola, C., Martino, V., Abeni, E., Pelucchi, P., Angeli, E., Guida, P.,

- Consiglio, A., Grillo, G., Karnavas, T., Gritzapis, A., Palizban, M., Missitzis, I., Götte, M., Luini, S., Kehler, J., Balbino, C., Guarino, V., Reinbold, R. (2024). Long-term Culture of Patient-Derived Mammary Organoids in Non-Biogenic Electrospun Scaffolds for Identifying Metalloprotein and Motor Protein Activities in Aging and Senescence. *Advances in Protein Chemistry and Structural Biology*, *141*, 331–360. <https://doi.org/10.1016/bs.apcsb.2024.03.008>
- Putnam, N. E., Fulbright, L. E., Curry, J. M., Ford, C. A., Petronglo, J. R., Hendrix, A. S., & Cassat, J. E. (2019). MyD88 and IL-1R Signaling Drive Antibacterial Immunity and Osteoclast-Driven Bone Loss During Staphylococcus Aureus Osteomyelitis. *PLoS Pathog.*, *15*, e1007744.
- Qi, F., Li, Y., Guo, H., Yang, H., & Gong, Q. (2004). Wavy Lines in Two-Photon Photopolymerization Microfabrication. *Optics Express*, *12*(20), 4725–4730. <https://doi.org/10.1364/OPEX.12.004725>
- Radhakrishnan, S., Nagarajan, S., Belaid, H., Farha, C., Iatsunskyi, I., Coy, E., Soussan, L., Huon, V., Bares, J., Belkacemi, K., Teyssier, C., Balme, S., Miele, P., Cornu, D., Kalkura, N., Cavallès, V., & Bechelany, M. (2021). Fabrication of 3D Printed Antimicrobial Polycaprolactone Scaffolds for Tissue Engineering Applications. *Mater. Sci. Eng., C*, *118*, 111525.
- Ratner, B. D., Hoffman, A. S., Schoen, F. J., & Lemons, J. E. (2004). *Biomaterials Science: An Introduction to Materials in Medicine*.
- Rederer, A., Rose, V., Krüger, R., Schmittutz, L., Swierzy, I., Fischer, L., Thievessen, I., Bauer, J., Friedrich, O., Schiffer, M., & Müller-Deile, J. (2023). Partner, Neighbor, Housekeeper and Dimension: 3D versus 2D Glomerular Co-Cultures Reveal Drawbacks of Currently Used Cell Culture Models. *International Journal of Molecular Sciences*, *24*(12), 10384. <https://doi.org/10.3390/ijms241210384>
- Redlich, K., & Smolen, J. S. (2012). Inflammatory Bone Loss: Pathogenesis and Therapeutic Intervention. *Nature Reviews Drug Discovery*, *11*, 234.
- Remuzzi, A., Bonandrini, B., Tironi, M., Longaretti, L., Figliuzzi, M., Conti, S., Zandrini, T.,

- Osellame, R., Cerullo, G., & Raimondi, M. T. (2020). Effect of the 3D Artificial Nichoid on the Morphology and Mechanobiological Response of Mesenchymal Stem Cells Cultured In Vitro. *Cells*, 9(8), 1873. <https://doi.org/10.3390/cells9081873>
- Richter, B., Hahn, V., Bertels, S., Claus, T. K., Wegener, M., Delaittre, G., Barner-Kowollik, C., & Bastmeyer, M. (2017). Guiding Cell Attachment in 3D Microscaffolds Selectively Functionalized with Two Distinct Adhesion Proteins. *Advanced Materials*, 29(5), 1604342. <https://doi.org/10.1002/adma.201604342>
- Rivera-Briso, A. L., Aachmann, F. L., Moreno-Manzano, V., & Serrano-Aroca, Á. (2020). Graphene Oxide Nanosheets versus Carbon Nanofibers: Enhancement of Physical and Biological Properties of Poly(3-Hydroxybutyrate-Co-3-Hydroxyvalerate) Films for Biomedical Applications. *Int. J. Biol. Macromol.*, 143, 1000.
- Rivera-Briso, A. L., Aparicio-Collado, J. L., Serra, R. S. I., & Serrano-Aroca, Á. (2022). Graphene Oxide versus Carbon Nanofibers in Poly(3-Hydroxybutyrate-Co-3-Hydroxyvalerate) Films: Degradation in Simulated Intestinal Environments. *Polymers (Basel)*, 14, 348.
- Rivera-Briso, A. L., & Serrano-Aroca, Á. (2018). Poly(3-Hydroxybutyrate-Co-3-Hydroxyvalerate): Enhancement Strategies for Advanced Applications. *Polymers*, 10, 732.
- Rolver, M. G., Elingaard-Larsen, L. O., & Pedersen, S. F. (2019). Assessing Cell Viability and Death in 3D Spheroid Cultures of Cancer Cells. *Journal of Visualized Experiments: JoVE*, 148. <https://doi.org/10.3791/59714>
- Roversi, K., Orimi, H. E., Erfanian, M., Talbot, S., & Boutopoulos, C. (2022). LIST: A Newly Developed Laser-assisted Cell Bioprinting Technology. *Bio-Protocol*, 12(19), e4527. <https://doi.org/10.21769/BioProtoc.4527>
- Saleem, M. A., O'Hare, M. J., Reiser, J., Coward, R. J., Inward, C. D., Farren, T., Xing, C. Y., Ni, L., Mathieson, P. W., & Mundel, P. (2002). A Conditionally Immortalized Human Podocyte Cell

- Line Demonstrating Nephrin and Podocin Expression. *Journal of the American Society of Nephrology: JASN*, 13(3), 630–638. <https://doi.org/10.1681/ASN.V133630>
- Salinas Vera, Y., Valdes, J., Pérez-Navarro, Y., Mandujano-Lázaro, G., Marchat, L., Ramos Payan, R., Nuñez-Olvera, S., Perez-Plasencia, C., & Lopez-Camarillo, C. (2022). Three-Dimensional 3D Culture Models in Gynecological and Breast Cancer Research. *Frontiers in Oncology*, 12, 826113. <https://doi.org/10.3389/fonc.2022.826113>
- Sánchez-Salcedo, S., Shruti, S., Salinas, A. J., Malavasi, G., Menabue, L., & Vallet-Regí, M. (2014). In Vitro Antibacterial Capacity and Cytocompatibility of SiO₂-CaO-P₂O₅ Meso-Macroporous Glass Scaffolds Enriched with ZnO. *J. Mater. Chem. B*, 2, 4836.
- Sanmartín-Santos, I., Gandía-Llop, S., Salesa, B., Martí, M., Aachmann, F. L., & Serrano-Aroca, Á. (2021). Enhancement of Antimicrobial Activity of Alginate Films with a Low Amount of Carbon Nanofibers (0.1% w/W). *Appl. Sci.*, 11, 2311.
- Saraiva, A. S., Ribeiro, I. A. C., Fernandes, M. H., Cerdeira, A. C., Vieira, B. J. C., Waerenborgh, J. C., Pereira, L. C. J., Cláudio, R., Carnezim, M. J., Gomes, P., Gonçalves, L. M., Santos, C. F., & Bettencourt, A. F. (2021). 3D-Printed Platform Multi-Loaded with Bioactive, Magnetic Nanoparticles and an Antibiotic for Re-Growing Bone Tissue. *Int. J. Pharm.*, 593, 120097.
- Senatov, F. S., Niaza, K. V., Zadorozhnyy, M. Y., Maksimkin, A. V., Kaloshkin, S. D., & Estrin, Y. Z. (2016). Mechanical Properties and Shape Memory Effect of 3D-Printed PLA-Based Porous Scaffolds. *J. Mech. Behav. Biomed. Mater.*, 57, 139.
- Shinozawa, T., Kimura, M., Cai, Y., Saiki, N., Yoneyama, Y., Ouchi, R., Koike, H., Maezawa, M., Zhang, R.-R., Dunn, A., Ferguson, A., Togo, S., Lewis, K., Thompson, W. L., Asai, A., & Takebe, T. (2021). High-Fidelity Drug-Induced Liver Injury Screen Using Human Pluripotent Stem Cell-Derived Organoids. *Gastroenterology*, 160(3), 831-846.e10. <https://doi.org/10.1053/j.gastro.2020.10.002>

- Shirshneva-Vashchenko, E., Mohammadian, N., Divliansky, I., & Glebov, L. (2023). Modeling of Laser Beam Shaping by Volume Holographic Phase Masks. *Components and Packaging for Laser Systems IX, 12402*, 58–70. <https://doi.org/10.1117/12.2651281>
- Shoval, H., Karsch-Bluman, A., Brill-Karniely, Y., Stern, T., Zamir, G., Hubert, A., & Benny, O. (2017). Tumor Cells and Their Crosstalk With Endothelial Cells in 3D spheroids. *Scientific Reports, 7*, 10428. <https://doi.org/10.1038/s41598-017-10699-y>
- Shuai, C., Guo, W., Gao, C., Yang, Y., Wu, P., & Feng, P. (2018). An NMgO Containing Scaffold: Antibacterial Activity, Degradation Properties and Cell Responses. *Int. J. Bioprinting, 4*(1), 120.
- Shuai, C., Guo, W., Wu, P., Yang, W., Hu, S., Xia, Y., & Feng, P. (2018). A Graphene Oxide-Ag Co-Dispersing Nanosystem: Dual Synergistic Effects on Antibacterial Activities and Mechanical Properties of Polymer Scaffolds. *Chem. Eng. J., 347*, 322.
- Silva, A. C., Matthys, O. B., Joy, D. A., Kauss, M. A., Natarajan, V., Lai, M. H., Turaga, D., Blair, A. P., Alexanian, M., Bruneau, B. G., & McDevitt, T. C. (2021). Co-Emergence of Cardiac and Gut Tissues Promotes Cardiomyocyte Maturation Within Human iPSC-Derived Organoids. *Cell Stem Cell, 28*(12), 2137-2152.e6. <https://doi.org/10.1016/j.stem.2021.11.007>
- Sivarajah, I. (2023, May 15). *A Guide to Laser Beam Shaping Techniques*. AZoOptics. <https://www.azooptics.com/Article.aspx?ArticleID=2432>
- Sokocevic, D., Bonenfant, N. R., Wagner, D. E., Borg, Z. D., Lathrop, M. J., Lam, Y. W., Deng, B., Desarno, M. J., Ashikaga, T., Loi, R., Hoffman, A. M., & Weiss, D. J. (2013). The Effect of Age and Emphysematous and Fibrotic Injury on the Re-Cellularization of De-Cellularized Lungs. *Biomaterials, 34*(13), 3256–3269. <https://doi.org/10.1016/j.biomaterials.2013.01.028>
- Starzl, T. E., & Demetris, A. J. (1990). Liver transplantation: A 31-year perspective part I. *Current Problems in Surgery, 27*(2), 55–116. [https://doi.org/10.1016/0011-3840\(90\)90021-V](https://doi.org/10.1016/0011-3840(90)90021-V)

- Sun, H., Hu, C., Zhou, C., Wu, L., Sun, J., Zhou, X., Xing, F., Long, C., Kong, Q., Liang, J., Fan, Y., & Zhang, X. (2020). 3D Printing of Calcium Phosphate Scaffolds with Controlled Release of Antibacterial Functions for Jaw Bone Repair. *Mater. Des.*, *189*, 108540.
- Suryavanshi, P., Kudtarkar, Y., Chaudhari, M., & Bodas, D. (2023). Fabricating a Low-Temperature Synthesized Graphene-Cellulose Acetate-Sodium Alginate Scaffold for the Generation of Ovarian Cancer Spheroid and its Drug Assessment. *Nanoscale Advances*, *5*(18), 5045–5053. <https://doi.org/10.1039/d3na00420a>
- Taniguchi, N., Fujibayashi, S., Takemoto, M., Sasaki, K., Otsuki, B., Nakamura, T., Matsushita, T., Kokubo, T., & Matsuda, S. (2016). Effect of Pore Size on Bone Ingrowth into Porous Titanium Implants Fabricated by Additive Manufacturing: An in Vivo Experiment. *Mater. Sci. Eng., C*, *59*, 690.
- Temple, J. P., Hutton, D. L., Hung, B. P., Huri, P. Y., Cook, C. A., Kondragunta, R., Jia, X., & Grayson, W. L. (2014). Engineering Anatomically Shaped Vascularized Bone Grafts with HASCs and 3D-Printed PCL Scaffolds. *J. Biomed. Mater. Res. - Part A*, *102*(12), 4317.
- Tian, L., Zhang, Z., Tian, B., Zhang, X., & Wang, N. (2020). Study on Antibacterial Properties and Cytocompatibility of EPL Coated 3D Printed PCL/HA Composite Scaffolds. *RSC Adv.*, *10*, 4805.
- Turtaev, S., Leite, I. T., Mitchell, K. J., Padgett, M. J., Phillips, D. B., & Čížmár, T. (2017). Comparison of Nematic Liquid-Crystal and DMD Based Spatial Light Modulation in Complex Photonics. *Optics Express*, *25*(24), 29874–29884. <https://doi.org/10.1364/OE.25.029874>
- Tytgat, L., Dobos, A., Markovic, M., Van Damme, L., Van Hoorick, J., Bray, F., Thienpont, H., Ottevaere, H., Dubruel, P., Ovsianikov, A., & Van Vlierberghe, S. (2020). High-Resolution 3D Bioprinting of Photo-Cross-linkable Recombinant Collagen to Serve Tissue Engineering Applications. *Biomacromolecules*, *21*(10), 3997–4007.

<https://doi.org/10.1021/acs.biomac.0c00386>

- Ulery, B. D., Nair, L. S., & Laurencin, C. T. (2011). Biomedical Applications of Biodegradable Polymers. *Journal of Polymer Science, Part B: Polymer Physics*, *49*, 832.
- Urciuolo, A., Giobbe, G. G., Dong, Y., Michielin, F., Brandolino, L., Magnussen, M., Gagliano, O., Selmin, G., Scattolini, V., Raffa, P., Caccin, P., Shibuya, S., Scaglioni, D., Wang, X., Qu, J., Nikolic, M., Montagner, M., Galea, G. L., Clevers, H., ... Elvassore, N. (2023). Hydrogel-in-Hydrogel Live Bioprinting for Guidance and Control of Organoids and Organotypic Cultures. *Nature Communications*, *14*, 3128. <https://doi.org/10.1038/s41467-023-37953-4>
- Vařák, P., Mrázek, J., Blanc, W., Aubrecht, J., Kamrádek, M., & Podrazky, O. (2020). Preparation and Properties of Tm-doped SiO₂-ZrO₂ Phase Separated Optical Fibers for Use in Fiber Lasers. *Optical Materials Express*, *10*. <https://doi.org/10.1364/OME.394068>
- Vidler, C., Halwes, M., Kolesnik, K., Segeritz, P., Mail, M., Barlow, A. J., Koehl, E. M., Ramakrishnan, A., Caballero Aguilar, L. M., Nisbet, D. R., Scott, D. J., Heath, D. E., Crozier, K. B., & Collins, D. J. (2024). Dynamic Interface Printing. *Nature*, *634*(8036), 1096–1102. <https://doi.org/10.1038/s41586-024-08077-6>
- Vidyasekar, P., Shyamsunder, P., Sahoo, S. K., & Verma, R. S. (2016). Scaffold-Free and Scaffold-Assisted 3D Culture Enhances Differentiation of Bone Marrow Stromal Cells. *In Vitro Cellular & Developmental Biology. Animal*, *52*(2), 204–217. <https://doi.org/10.1007/s11626-015-9971-2>
- Vincent-Chong, V. K., & Seshadri, M. (2020). Development and Radiation Response Assessment in A Novel Syngeneic Mouse Model of Tongue Cancer: 2D Culture, 3D Organoids and Orthotopic Allografts. *Cancers*, *12*(3), 579. <https://doi.org/10.3390/cancers12030579>
- Vitkūnaitė, E., Žymantaitė, E., Mlynska, A., Andrijec, D., Limanovskaja, K., Kaszynski, G., Matulis, D., Šakalys, V., & Jonušauskas, L. (2024). Advancing 3D Spheroid Research through 3D Scaffolds Made by Two-Photon Polymerization. *Bioengineering*, *11*(9), 902.

<https://doi.org/10.3390/bioengineering11090902>

- Vizsnyiczai, G., Kelemen, L., & Ormos, P. (2014). Holographic Multi-Focus 3D Two-photon Polymerization With Real-Time Calculated Holograms. *Optics Express*, 22(20), 24217–24223. <https://doi.org/10.1364/OE.22.024217>
- Vu, B., Souza, G. R., & Dengjel, J. (2021). Scaffold-free 3D Cell Culture of Primary Skin Fibroblasts Induces Profound Changes of the Matrisome. *Matrix Biology Plus*, 11, 100066. <https://doi.org/10.1016/j.mbplus.2021.100066>
- Wang, J., Wu, Y., Li, G., Zhou, F., Wu, X., Wang, M., Liu, X., Tang, H., Bai, L., Geng, Z., Song, P., Shi, Z., Ren, X., & Su, J. (2024). Engineering Large-Scale Self-Mineralizing Bone Organoids with Bone Matrix-Inspired Hydroxyapatite Hybrid Bioinks. *Advanced Materials*, 36(30), 2309875. <https://doi.org/10.1002/adma.202309875>
- Wang, M., Li, H., Yang, Y., Yuan, K., Zhou, F., Liu, H., Zhou, Q., Yang, S., & Tang, T. (2021). A 3D-Bioprinted Scaffold with Doxycycline-Controlled BMP2-Expressing Cells for Inducing Bone Regeneration and Inhibiting Bacterial Infection. *Bioact. Mater.*, 6, 1318.
- Wang, S., Wang, X., Tan, Z., Su, Y., Liu, J., Chang, M., Yan, F., Chen, J., Chen, T., Li, C., Hu, J., & Wang, Y. (2019). Human ESC-derived Expandable Hepatic Organoids Enable Therapeutic Liver Repopulation and Pathophysiological Modeling of Alcoholic Liver Injury. *Cell Research*, 29(12), 1009–1026. <https://doi.org/10.1038/s41422-019-0242-8>
- Wehrli, M., Guinn, S., Birocchi, F., Kuo, A., Sun, Y., Larson, R. C., Almazan, A. J., Scarfò, I., Bouffard, A. A., Bailey, S. R., Anekal, P. V., Montero Llopis, P., Nieman, L. T., Song, Y., Xu, K. H., Berger, T. R., Kann, M. C., Leick, M. B., Silva, H., Maus, M. V. (2024). Mesothelin CAR T Cells Secreting Anti-FAP/Anti-CD3 Molecules Efficiently Target Pancreatic Adenocarcinoma and its Stroma. *Clinical Cancer Research: An Official Journal of the American Association for Cancer Research*, 30(9), 1859–1877. <https://doi.org/10.1158/1078->

- Weisgrab, G., Guillaume, O., Guo, Z., Heimel, P., Slezak, P., Poot, A., Grijpma, D., & Ovsianikov, A. (2020). 3D Printing of Large-Scale and Highly Porous Biodegradable Tissue Engineering Scaffolds From Poly(Trimethylene-Carbonate) Using Two-Photon-Polymerization. *Biofabrication*, *12*(4), 045036. <https://doi.org/10.1088/1758-5090/abb539>
- Wen, H., Zhu, S., Li, C., & Xu, Y. (2020). Bone Transport versus Acute Shortening for the Management of Infected Tibial Bone Defects: A Meta-Analysis. *BMC Musculoskelet. Disord*, *21*, 80.
- Wilson, J., Rahul, V. G., Thomas, L. V., & Nair, P. D. (2022). Three-Dimensional Wet Electrospun Scaffold System for the Differentiation of Adipose-Derived Mesenchymal Stem Cells to Islet-Like Clusters. *Journal of Tissue Engineering and Regenerative Medicine*, *16*(12), 1276–1283. <https://doi.org/10.1002/term.3366>
- Wu, G. H., & Hsu, S. H. (2015). Review: Polymeric-Based 3D Printing for Tissue Engineering. *J. Med. Biol. Eng.*, *35*, 285.
- Wu, P., Hu, S., Liang, Q., Guo, W., Xia, Y., Shuai, C., & Li, Y. (2020). A Polymer Scaffold with Drug-Sustained Release and Antibacterial Activity. *Int. J. Polym. Mater. Polym. Biomater.*, *69*, 398.
- Wu, Y., Liang, H., Luo, A., Li, Y., Liu, Z., Li, X., Li, W., Liang, K., Li, J., Liu, Z., & Du, Y. (2023). Gelatin-based 3D Biomimetic Scaffolds Platform Potentiates Culture of Cancer Stem Cells in Esophageal Squamous Cell Carcinoma. *Biomaterials*, *302*, 122323. <https://doi.org/10.1016/j.biomaterials.2023.122323>
- Xiao, W., Wang, S., Zhang, R., Sohrabi, A., Yu, Q., Liu, S., Ehsanipour, A., Liang, J., Bierman, R. D., Nathanson, D. A., & Seidlits, S. K. (2020). Bioengineered Scaffolds for 3D Culture Demonstrate Extracellular Matrix-Mediated Mechanisms of Chemotherapy Resistance in

- Glioblastoma. *Matrix Biology: Journal of the International Society for Matrix Biology*, 85–86, 128–146. <https://doi.org/10.1016/j.matbio.2019.04.003>
- Xin, Q., Shah, H., Nawaz, A., Xie, W., Akram, M. Z., Batool, A., Tian, L., Jan, S. U., Boddula, R., Guo, B., Liu, Q., & Gong, J. R. (2019). Antibacterial Carbon-Based Nanomaterials. *Adv. Mater.*, 31, 1804838.
- Xu, C., & Pu, K. (2021). Second Near-Infrared Photothermal Materials for Combinational Nanotheranostics. *Chemical Society Reviews.*, 50, 1111.
- Yang, L., Li, J., Hu, Y., Zhang, C., Lao, Z., Huang, W., & Chu, J. (2014). Projection two-photon polymerization using a spatial light modulator. *Optics Communications*, 331, 82–86. <https://doi.org/10.1016/j.optcom.2014.05.051>
- Yang, Y., Chu, L., Yang, S., Zhang, H., Qin, L., Guillaume, O., Eglin, D., Richards, R. G., & Tang, T. (2018). Dual-Functional 3D-Printed Composite Scaffold for Inhibiting Bacterial Infection and Promoting Bone Regeneration in Infected Bone Defect Models. *Acta Biomater.*, 79, 265.
- Yang, Y., Yang, S., Wang, Y., Yu, Z., Ao, H., Zhang, H., Qin, L., Guillaume, O., Eglin, D., Richards, R. G., & Tang, T. (2016). Anti-Infective Efficacy, Cytocompatibility and Biocompatibility of a 3D-Printed Osteoconductive Composite Scaffold Functionalized with Quaternized Chitosan. *Acta Biomater.*, 46, 112.
- Yu, C., Schimelman, J., Wang, P., Miller, K. L., Ma, X., You, S., Guan, J., Sun, B., Zhu, W., & Chen, S. (2020). Photopolymerizable Biomaterials and Light-Based 3D Printing Strategies for Biomedical Applications. *Chemical Reviews*, 120(19), 10695–10743. <https://doi.org/10.1021/acs.chemrev.9b00810>
- Zarrintaj, P., Vahabi, H., Gutiérrez, T. J., Mehrpouya, M., Ganjali, M. R., & Saeb, M. R. (2020). *Handbook of Polymer Nanocomposites for Industrial Applications*.
- Zhang, J., Tong, D., Song, H., Ruan, R., Sun, Y., Lin, Y., Wang, J., Hou, L., Dai, J., Ding, J., & Yang,

- H. (2022). Osteoimmunity-Regulating Biomimetically Hierarchical Scaffold for Augmented Bone Regeneration. *Advanced Materials (Deerfield Beach, Fla.)*, 34(36), e2202044.
<https://doi.org/10.1002/adma.202202044>
- Zhang, J., Wang, L., Song, Q., Xiao, M., Gao, J., Cao, X., & Zheng, W. (2022). Organoids in recapitulating tumorigenesis driven by risk factors: Current trends and future perspectives. *International Journal of Biological Sciences*, 18(7), 2729–2743.
<https://doi.org/10.7150/ijbs.70406>
- Zhang, L., Yang, G., Johnson, B. N., & Jia, X. (2019). Three-Dimensional (3D) Printed Scaffold and Material Selection for Bone Repair. *Acta Biomaterialia.*, 84, 16.
- Zhang, Y. S., Arneri, A., Bersini, S., Shin, S.-R., Zhu, K., Goli-Malekabadi, Z., Aleman, J., Colosi, C., Busignani, F., Dell’Erba, V., Bishop, C., Shupe, T., Demarchi, D., Moretti, M., Rasponi, M., Dokmeci, M. R., Atala, A., & Khademhosseini, A. (2016). Bioprinting 3D microfibrillar scaffolds for engineering endothelialized myocardium and heart-on-a-chip. *Biomaterials*, 110, 45–59. <https://doi.org/10.1016/j.biomaterials.2016.09.003>
- Zhang, Y., Zhai, D., Xu, M., Yao, Q., Zhu, H., Chang, J., & Wu, C. (2017). 3D-Printed Bioceramic Scaffolds with Antibacterial and Osteogenic Activity. *Biofabrication*, 9, 025037.
- Zhao, S., Xie, K., Guo, Y., Tan, J., Wu, J., Yang, Y., Fu, P., Wang, L., Jiang, W., & Hao, Y. (2020). Fabrication and Biological Activity of 3D-Printed Polycaprolactone/Magnesium Porous Scaffolds for Critical Size Bone Defect Repair. *ACS Biomater. Sci. Eng.*, 6, 5120.
- Zheng, L., Kurselis, K., El-Tamer, A., Hinze, U., Reinhardt, C., Overmeyer, L., & Chichkov, B. (2019). Nanofabrication of High-Resolution Periodic Structures with a Gap Size Below 100 nm by Two-Photon Polymerization. *Nanoscale Research Letters*, 14(1), 134.
<https://doi.org/10.1186/s11671-019-2955-5>
- Zheng, Z., Eglin, D., Alini, M., Richards, G. R., Qin, L., & Lai, Y. (2021). Visible Light-Induced 3D

- Bioprinting Technologies and Corresponding Bioink Materials for Tissue Engineering: A Review. *Engineering*, 7(7), 966–978. <https://doi.org/10.1016/j.eng.2020.05.021>
- Zhongxing, L., Shaohong, W., Jinlong, L., Limin, Z., Yuanzheng, W., Haipeng, G., & Jian, C. (2021). Three-Dimensional Printed Hydroxyapatite Bone Tissue Engineering Scaffold with Antibacterial and Osteogenic Ability. *J. Biol. Eng.*, 15(1), 21.
- Zhou, W., Dong, X., He, Y., Zheng, W., & Leng, J. (2022). In-Vitro and in-Vivo Studies of 4D Printed Shape Memory Scaffolds with Bioactive Fillers and Coating for Enhanced Bone Tissue Regeneration. *Smart Mater. Struct.*, 31(10), 105002.
- Zhou, Z., Yao, Q., Li, L., Zhang, X., Wei, B., Yuan, L., & Wang, L. (2018). Antimicrobial Activity of 3D-Printed Poly(ϵ -Caprolactone) (PCL) Composite Scaffolds Presenting Vancomycin-Loaded Polylactic Acid-Glycolic Acid (PLGA) Microspheres. *Med. Sci. Monit.*, 24, 6934.
- Zhu, W., Holmes, B., Glazer, R. I., & Zhang, L. G. (2016). 3D Printed Nanocomposite Matrix For the Study of Breast Cancer Bone Metastasis. *Nanomedicine: Nanotechnology, Biology and Medicine*, 12(1), 69–79. <https://doi.org/10.1016/j.nano.2015.09.010>

Karolina Limanovskaja

Master's thesis

Rapid Manufacturing of 3D Organoid Scaffolds Using Femtosecond Laser

ABSTRACT

Around the world, organ-donor shortages leave thousands of patients without lifesaving treatment available to them creating an always present strain in the medical system. Bioprinting, the highly promising technology for the assembly of living tissues, could provide a sustainable alternative, to solve this issue. However, currently available technologies still struggle to recreate the fine architecture of real organs. Three-dimensional cell cultures and organoids come forward as invaluable tools for organ and tissue development studies and disease modeling. Biocompatible scaffolds are one of the tools specifically designed to improve organoid culture development. Unfortunately, due to the lack of easily reproducible and highly tunable scaffold fabrication, organoid research still leans on labor-intensive, low-throughput methods.

Two-photon polymerization (2PP) offers the sub-micron resolution needed to print intricate biocompatible scaffolds that could elevate 3D cultures and streamline the overall development process. Integrating a spatial-light modulator (SLM) can improve the relatively slow 2PP technology by changing the shape of the volumized pixel (voxel). For that process SLM uses phase masks. A phase mask is a gray-scale image that recreates the desired voxel in 3D space. While effective, the process of phase mask generation and voxel modification is complicated and hard to control deterministically. This in turn limits applicability and proliferation of SLM enhanced 2PP in biofabrication and bioprinting.

This study aims to determine the current capabilities of phase mask generation and voxel optimization in order to make the process of organoid scaffold printing more efficient.

Karolina Limanovskaja

Magistro baigiamasis darbas

Greita 3D organoidinių karkasų gamyba naudojant femtosekundinį lazerį

SANTRAUKA

Dėl organų donorų trūkumo visame pasaulyje tūkstančiai pacientų negali gauti gyvybę gelbstinčio gydymo, taip nuolat sukuriant apkrovimą medicinos sistemai. Biospausdinimas tampa vis populiarėjanti audinių inžinerijos kryptis galinti suteikti inovacijų audinių persodinimo ar regeneracijos sferoje. Tačiau šiuo metu turimomis technologijomis vis dar sunku atkurti smulkią tikrų organų struktūrą sąlyginai dideliose audinių tūriuose. Dėl šios prižasties trimatės ląstelių kultūros ir organoidai yra neįkainojamos priemonės organų ir audinių vystymosi tyrimams bei ligų modeliavimui, kadangi suteikia reikalingų išvalgų audinių inžinerijos srityje. 3D karkasai ląstelėms spausdinamos iš biosuderinamų medžiagų yra viena iš priemonių, specialiai sukurtų organoidų kultūrų kūrimui pagerinti. Organoidų eksperimentams vis dar taikomos daug laiko reikalaujančios, riboto našumo procedūros, daugiausia dėl to, kad universalių karkasų gamyba dar nėra paprasta.

Dviejų fotonų polimerizacija (2PP) užtikrina submikroninę skiriamąją gebą, reikalingą sudėtingoms biosuderinamoms matricų formoms spausdinti, o tai galėtų pagerinti 3D kultūrų kokybę ir supaprastinti visą jų naudojimo procesą. Integravus erdvinį šviesos moduliatorių (SLM) galima patobulinti palyginti lėtą 2PP technologiją keičiant tūrinio pikselio (vokselio) formą. Šiam procesui SLM naudoja fazines kaukes. Fazinė kaukė - tai pilkosios skalės atvaizdas, kuris atkuria norimą vokselį 3D erdvėje. Nors šis metodas yra veiksmingas, fazinės kaukės generavimo procesas yra ribotas. Tai savo ruožtu suteikia labai ribotą kontrolę ir mažai atskleidžia, kaip tiksliai kaukė atkuria intensyvumą išilgai optinės ašies.

Šiuo tyrimu siekiama iširti dabartines fazių kaukės generavimo ir vokselių optimizavimo galimybes, kad organoidinių matricų spausdinimo procesas taptų veiksmingesnis.

Author's personal contribution

The research planning and the formulation of the research thesis was carried out by Dr. Linas Jonušauskas, Technical Director of Vital3D Technologies UAB.

The research planning, execution, analysis of results and formulation of conclusions were carried out by Karolina Limanosvskaja, a second year student of molecular biotechnology, who is writing her master's thesis.